UNIVERSITÀ DEGLI STUDI DI MILANO

SCUOLA DI DOTTORATO

Medicina sperimentale e biotecnologie mediche

DIPARTIMENTO

Biotecnologie mediche e medicina traslazionale

CURRICULUM /CORSO DI DOTTORATO

Endocrinologico-metabolico / XXX ciclo

TESI DI DOTTORATO DI RICERCA

New insights in bone biology from exome sequencing of rare skeletal diseases

DOTTORANDO: **Eleonora Palagano**

Matricola R11067

TUTOR: Prof. Domenico Mavilio

SUPERVISOR: Dr. Cristina Sobacchi

COORDINATORE DEL DOTTORATO: Prof. Massimo Locati

A.A. 2016/2017

ABSTRACT

Whole exome sequencing (WES) is a powerful tool to identify new molecules involved in skeletal homeostasis. In particular we used WES to establish the molecular diagnosis of two particular skeletal diseases: osteopetrosis and the acrofrontofacionasal dysostosis 1 (AFFND1).

The osteopetroses are a group of rare bone diseases characterized by increased bone density due to the failure in bone resorption. Due to their genetic heterogeneity, WES represents a valuable strategy to identify the genetic defect. We analyzed osteopetrotic patients with autosomal dominant osteopetrosis (ADO) and autosomal recessive osteopetrosis (ARO), which is the most severe form. In our cohort we performed molecular diagnosis of 4 ADOI or ADOII patients that carried mutations in the *LRP5* and *CLCN7* genes, respectively. The analysis of ARO patients confirmed *TCIRG1* as the most frequently mutated gene, identified mutations in the other known ARO genes and in genes very rarely associated with osteopetrosis, namely *FERMT3* and *USB1*. Of note, we demonstrated the causative role of four deep intronic mutations in *TCIRG1* gene and two different synonymous changes in the *TCIRG1* and *CLCN7* genes in the pathogenesis of the disease. In addition, WES helped in the differential diagnosis in a patient who was found to bear a mutation in the *FAM20C* gene, known to cause Raine syndrome.

Regarding AFFND1, this is an extremely rare syndrome, comprising facial and skeletal abnormalities, short stature and intellectual disability. WES found a novel truncating mutation in the neuroblastoma-amplified sequence (NBAS) gene in two Indian patients (c.6237-3C>G). This mutation impaired NBAS functions in HEK293T cells overexpressing the truncated NBAS protein. Furthermore, we demonstrated that NBAS expression in mouse embryos was compatible with a role in bone and brain development and that the depletion of endogenous z-nbas in fish embryos resulted in defective morphogenesis of chondrogenic cranial skeletal elements. Overall, we provided evidence supporting the hypothesis of a causative role of the mutated *NBAS* gene in the pathogenesis of AFFND1.

In conclusion, we effectively exploited WES in the genetic diagnosis of rare skeletal diseases. We also highlighted potential limitations of this approach, specifically with respect to deep intronic mutations and synonymous changes, and underlined the importance to complement WES with analysis at the transcript level and functional validation, when possible.

INDEX

1. ACRONYMS AND ABBREVIATIONS

$1,25(OH)_2D_3$: 1,25 dihydroxy vitamin D_3

ADO: autosomal dominant osteopetrosis

AFFND1: acrofrontofacionasal dysostosis 1

AKT: protein kinase B

ALP: alkaline phosphatase

AP1: activator protein 1

APC: adenomatous polyposis coli

ARL8: ADP-ribosylation factor-like protein 8

ARO: autosomal recessive osteopetrosis

ATF4: activating transcription factor 4

Atp6v0d2: d2 isoform of vacuolar ATPase V0 domain

Bcl6: B-cell lymphoma 6

BD: basolateral domain

BGLAP: bone gamma-carboxyglutamate protein

BLCs: bone lining cells

BLIMP1: B lymphocyte-induced maturation protein 1

BMP: bone morphogenetic protein

BMU: basic multicellular unit

BSP: bone sialoprotein

CA2: carbonic anhydrase type II

CBS: cystathionine-beta-synthase

cDNA: complementary DNA

CE: capillary electrophoresis

Ch: ceratohyale

CHIP: chromatin immunoprecipitation

CHKA: choline kinase alpha

CLCN7: chloride voltage-gated channel 7

COLIA1: collagen type I alpha 1

COMMAD: coloboma, osteopetrosis, microphthalmia, macrocephaly, albinism, and deafness

CT: computed tomography

CTLA4: cytotoxic T-lymphocyte protein 4

CTSK: cathepsin K

DAB: 3,3'-diaminobenzidine

DAP12: DNAX-activating protein 12

DC-STAMP: dendritic cell-specific transmembrane protein

DKK1: dickkopf-related protein 1

DLX3: distal-less homeobox 3

DMP1: dentin matrix protein 1

dNTPs: deoxyribonucleotide triphosphates

Dpf: days post fertilization

DSH: disheveled

DSS: dysosteosclerosis

E: embryonic day

ERK: extracellular signal-regulated kinase

ERRα: estrogen-related receptor α

ESID: european society for immunodeficiences

FcRγ: Fc receptor common γ subunit

FERMT3: fermitin family member 3

FGF23: fibroblast growth factor 23

FSD: functional secretory domain

FZD: frizzled

GAGs: glycosaminoglycans

GATK: genome analysis toolkit

GH: growth hormone

GRB2: growth-factor-receptor-bound protein 2

GSK3: glycogen synthase kinase 3

GTP: guanosine triphosphate

HLA: human leukocyte antigen

Hpf: hours post fertilization

HSCs: hematopoietic stem cells

HSCT: hematopoietic stem cell transplantation

IEWP-EBMT: inborn errors working party of the EBMT

IFNγ: interferon γ

IGF I: insulin-like growth factor I

IHH: indian hedgehog

IKBKG: inhibitor of nuclear factor kappa B kinase subunit gamma

IKK: IκB kinase

IL-17: interleukin 17

InDel: insertion/deletion

IQ: intelligence quotient

IRF8: interferon regulatory factor 8

ITAM: immunoglobulin tyrosine-based activation motif

JNK: c-Jun N-terminal kinase

LAD-III: leukocyte adhesion deficiency

LEF: lymphoid enhancing factor

LGR4/5/6: leucine-rich repeat containing G-protein-coupled receptors

LIR: LC3-interacting region

LRP5/6: low-density lipoprotein co-receptors

MAFB: v-Maf musculoaponeurotic fibrosarcoma oncogene family homolog B

MAPK: mitogen activated protein kinase

Mck: meckel's cartilage

M-CSF: macrophage-colony stimulating factor

MGP: matrix gla protein

MITF: microphthalmia-associated transcription factor

MMP9: matrix metalloprotease 9

MOs: morpholino oligonucleotides

MRI: magnetic resonance imaging

mRNA: messenger RNA

MSCs: mesenchymal stem cells

MSX1: msh homeobox 1

MVs: matrix vesicles

NBAS/NAG: neuroblastoma amplified sequence/neuroblastoma amplified gene

NCC: neural crest cells

NEMO: NF-*k*B essential modulator

NFATc1: nuclear factor of activated T cell c1

NF-*k*B : nuclear factor kappa B

NGS: next generation sequencing

NIK: NF-*k*B-inducing kinase

NMD: nonsense-mediated decay

OCN: osteocalcin

OC-STAMP: osteoclast stimulatory transmembrane protein

OFC: orbitofrontal cortex

OI: osteogenesis imperfecta

OL-HED-ID: osteopetrosis, lymphoedema, hypohidrotic ectodermal dysplasia and immunodeficiency

OPG: osteoprotegerin

OPN: osteopontin

OSCAR: osteoclast-associated receptor

OSTM1: osteopetrosis associated transmembrane protein 1

OSX: osterix

PBMCs: peripheral blood mononuclear cells

PBS: dulbecco's phosphate buffer saline

PBST: PBS 0,05% Tween 20

PCR: polymerase chain reaction

PFA: paraformaldehyde

PGs: proteoglycans

PH: pleckstrin homology

PI3K: phosphatidylinositol 3-kinase

PLEKHM1: pleckstrin homology domain-containing family M (with RUN domain) member 1

PN: poikiloderma with neutropenia

PN2: post-natal day 2

PPARγ: peroxisome proliferator-activated receptor gamma

Pq: palatoquadrate

PTH: parathyroid hormone

PTHrP: parathyroid hormone-related protein

RAB7: ras-related protein Rab 7

RAG1: recombination activating gene 1

RALF: recurrent acute liver failure

RANK: receptor activator of nuclear kappa B

RANKL: receptor activator of nuclear kappa B ligand

RB: ruffled border

RH: rubicon homology

RHOA: ras homolog family member A

RNA-seq: RNA-sequencing

RNF43: ring finger 43

RSK2: ribosomal S6 kinase 2

RSPO: roof plate-specific spondin

RT-PCR: reverse transcriptase-polymerase chain reaction

RUNX2: runt-related transcription factor 2

S1P: sphingosine 1 phosphate

SCID: severe combined immunodeficiency

Scr: scrambled

SDF1 or CXCL12: stromal-derived factor 1

sFRP: frizzled related proteins

SIBLING: small integrin-binding ligand N-linked glycoprotein

SLC19A1: solute carrier family 19 (folate transporter) member 1

SLC29A3: solute carrier family 29 (nucleoside transporter), member 3

SNAREs: N-ethylmaleimide-sensitive factor attachment protein (SNAP) receptors

SNPs: single-nucleotide polymorphisms

SNX10: sorting nexin 10

SOPH: syndrome, presenting with short stature, facial dysmorphisms, optic nerve atrophy and Pelger-Huet anomaly of the neutrophils

SPARC: secreted protein acidic and rich in cysteine

SPP1: secreted phosphoprotein 1

SS: splice site

SYK: tyrosine-protein kinase

SZ: sealing zone

T3: thyroid hormones

TB: translation block

TBST: tris-buffered saline, 0.1% Tween 20

TCF: T-cell factor

TCIRG1: T cell immune regulator 1

TGFβ: transforming growth factor beta

TNFα: tumor necrosis factor α

TNFRSF11A: TNF receptor superfamily member 11a

TNFSF11: TNF superfamily member 11

TNMD: tenomodulin

TRAF6: TNF receptor-associated factor 6

TRAIL: TNF-related apoptosis inducing ligand

TRAP: tartrate resistant acid phosphatase

TREM 2: triggering receptor expressed in myeloid cells 2

TWISTNB: TWIST Neighbor

UPF2: regulator of nonsense transcripts 2

UTR: untranslated regions

VCAM1: vascular cell adhesion molecule 1

VEGF: vascular endothelial growth factor

VLA4: very late antigen 4

WES: whole exome sequencing

WGS: whole genome sequencing

WIF1: Wnt inhibitor factor 1

ZNRF3: transmembrane E3 ubiquitin ligase zinc and ring finger 3

2. LIST OF FIGURES AND TABLES

3. INTRODUCTION

3.1 General aspects of bone biology

The skeleton is a dynamic tissue exerting different functions: it provides support and protection to soft tissues, aids locomotion serving as lever for muscular action, stores calcium and phosphate contributing to their homeostasis, and harbors the bone marrow [1-3].

The dynamic nature of the skeleton is achieved through a process of modeling and remodeling in response to mechanical and metabolic influences [4]. Bone modeling is a hallmark of skeletal development and growth, but it can occur also in adult life as an adaptation to permanent changes in mechanical strain or in response to hormonal or genetic factors, ultimately resulting in changes in bone size and shape [5]. During the modeling process, osteoblast and osteoclast activities (bone deposition and resorption, respectively) are not necessarily coupled; on the contrary, by definition, in bone remodeling osteoclasts and osteoblasts sequentially work in the same basic multicellular unit (BMU) [6].

Bone remodeling is a highly complex cyclic process, which can be divided in three phases:

1) Initiation phase (duration: about 2 weeks): osteoclast precursors are recruited to the bone surface, differentiate and start resorbing bone.
2) Transition or reversal phase (duration: about 1 month): osteoclasts undergo apoptosis, while osteoblast precursors are recruited and differentiate into mature osteoblasts.
3) Termination or formation phase (duration: several months): it ensures that the resorbed lacuna is refilled with new bone produced by the osteoblasts. When this phase is completed, flattened lining cells cover the surface, which enters a resting period [7].

The balance between bone formation and resorption is crucial to maintain bone homeostasis; indeed an imbalance may result in bone diseases. For example, unrestrained resorption leads to bone loss and osteoporosis [8], on the contrary the lack of osteoclast activity may result in osteopetrosis [9].

The bone tissue is a composite environment: in addition to bone-specific cells, several other cell types are present, such as mesenchymal stem cells (MSCs) and hematopoietic

stem cells (HSCs), their derivatives at different stage of differentiation and, moreover, blood vessels and peripheral nerve fibers that all together contribute to generate a dynamic compartment. As an additional layer of complexity, several local and systemic factors (hormones, cytokines, biomechanical stimulation) contribute to modify cell behavior [10, 11].

3.1.1 Bone composition

The bone tissue is a mineralized connective tissue formed by a dense extracellular matrix and a cellular component, which comprises "skeletal-specific" cell types (osteoblasts, osteocytes, osteoclasts, bone lining cells and chondrocytes) and also other cells, such as immune cells, hematopoietic stem and progenitor cells at different stages of lineage commitment, endothelial cells and adipocytes.

3.1.1.1 Osteoblasts

Osteoblasts (4-6% of total resident bone cells) are cuboidal-shaped cells covering the bone surface as a single cells row. They are polarized, rich in alkaline phosphatase (ALP, the enzyme responsible for pyrophosphate hydrolysis) on the basolateral membrane, while no or little expression on the membrane facing the osteoid (non-mineralized bone matrix). In addition, osteoblasts possess abundant rough endoplasmic reticulum, large Golgi apparatus and numerous vesicles, which are typical features of secretory cells; in particular, the Golgi complex is filled with fibrillar structures, containing procollagen and proteoglycans [12]. Osteoblasts establish different types of interactions with other cells: they form focal, non-continuous tight junctions and gap junctions, mainly composed of connexin 43 and involved in ion and micromolecules exchange. Adherens junction, based on cadherins and important to transduce differentiation, activation and survival signals are also present. Moreover, osteoblasts bind type I collagen through β1 integrins; this interaction activates mitogen activated protein kinase (MAPK) and is crucial for osteoblast differentiation and function. These cells are responsible for the deposition of bone matrix, and contribute to the regulation of osteoclasts functionality and to the development and maintenance of the hematopoietic stem cell niche [2, 13, 14].

Osteoblast differentiation

Osteoblasts derive from MSCs, which are multipotent stem cells that can differentiate towards osteogenic, adipogenic and chondrogenic lineages under different stimuli (Figure 1) [10]. Specific transcription factors drive the differentiation towards one or the other lineage: SOX5, 6 and 9 guide chondrogenic differentiation, peroxisome proliferator-activated receptor gamma (PPARγ) the adipocytic one, runt-related transcription factor 2 (RUNX2) and osterix (OSX) regulate the osteogenic differentiation and in fact their absence completely block skeletal mineralization [15, 16]. Besides RUNX2 and OSX, a plethora of transcription factors have been involved in the regulation of osteoblast differentiation and function [17]; among them, TWIST proteins provide a transient block during early skeletogenesis through interaction of their Twist box with RUNX2 DNA binding domain [18]. Homeobox factors, such as msh homeobox 1 ad 2 (MSX1, MSX2), distal-less homeobox 3 and 5 (DLX3, DLX5), orchestrate skeletal patterning *via* intricate regulatory loops [19]. Activating transcription factor 4 (ATF4) mediates some aspects of RUNX2-driven transcriptional program and intervenes in the control of mature osteoblast function after phosphorylation by the growth factor-regulated kinase ribosomal S6 kinase 2 (RSK2) [20].

Overall, these transcriptional regulatory systems result in increased expression of cell lineage markers, such as collagen type I alpha 1 (COLIA1), ALP, bone sialoprotein (BSP) and bone gamma-carboxyglutamate protein (BGLAP), morphological changes (cells become large and cuboidal) and high secretion of bone matrix proteins [13, 21]. The activation of bone morphogenetic protein (BMP) and Wnt pathways is a crucial event in promoting MSCs commitment towards osteoprogenitors [22, 23]. Other factors regulating osteogenic differentiation are hormones, such as 1,25 dihydroxy vitamin D_3 ($1,25(OH)_2D_3$), parathyroid hormone (PTH) and estrogens, and cytokines.

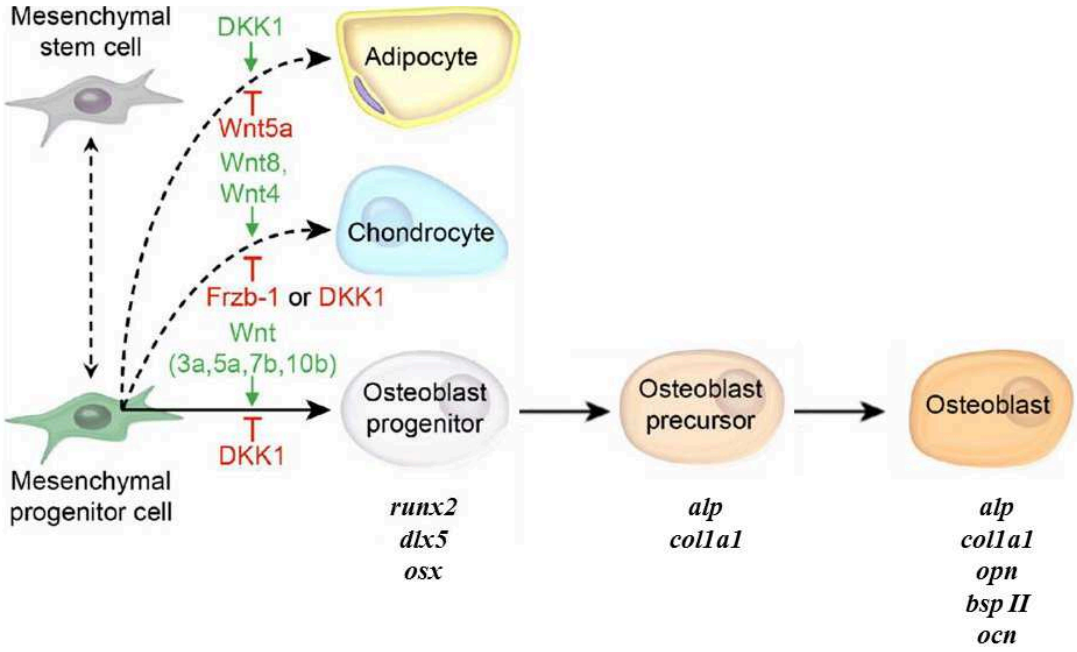

Figure 1: Schematic representation of MSCs commitment towards different cell fates. Adapted from Pinzone et al., 2009.

Main pathways in osteoblast differentiation: Wnt and BMP signaling

There are two main pathways involved in osteoblast differentiation: the Wnt and the BMP signaling pathways.

Wnt ligands constitute a family of secreted glycoproteins that bind a co-receptor complex, including the seven-pass transmembrane G-protein coupled receptor frizzled (FZD) and the low-density lipoprotein co-receptors LRP5/6. The elicited intracellular signaling may occur either via β-catenin activation (canonical) or via a calcium-dependent or planar-cell polarity pathway (non-canonical); however, the former has been better characterized. The hallmark of Wnt pathway activation is the inhibition of glycogen synthase kinase 3 (GSK3) activity and the resulting increase of β-catenin, an integral E-cadherin cell-cell adhesion adaptor protein and transcriptional coregulator [24]. More in detail, in the absence of Wnt ligands, the inhibitory complex composed of adenomatous polyposis coli (APC), axin and GSK3 binds and phosphorylates β-catenin, thus targeting it to degradation by the proteasome [25]. Instead, when Wnt ligands bind FZD and LRP5/6, the destruction complex is disrupted: axin is recruited by the cytoplasmic tail of LRP5/6 and de-phosphorylated, disheveled (DSH) is activated by

sequential phosphorylation, poly-ubiquitination and polymerization and inhibits GSK3. Therefore β-catenin is stabilized and translocates into the nucleus, where it drives the expression of Wnt target genes in collaboration with TCF/LEF (T-cell factor/lymphoid enhancing factor) transcription factors. For example, Wnt5a and Wnt10b not only promote osteoblast differentiation, but also prevent the expression of transcription factors responsible for MSCs commitment towards adipogenesis [26].

A number of molecules negatively regulate the Wnt pathway. The dickkopf-related protein 1 (DKK1) binds LRP5/6 receptor and kremen, inducing internalization of the receptor and reduced availability for Wnt ligands [27-29]. Sclerostin acts similarly to DKK1, i.e. it binds LRP5 and inhibits the Wnt pathway activation.

On the other hand, secreted frizzled related proteins (sFRP) and Wnt inhibitor factor 1 (WIF1) act by directly binding Wnt ligands, thus reducing their availability for the functional receptors (Figure 2) [30].

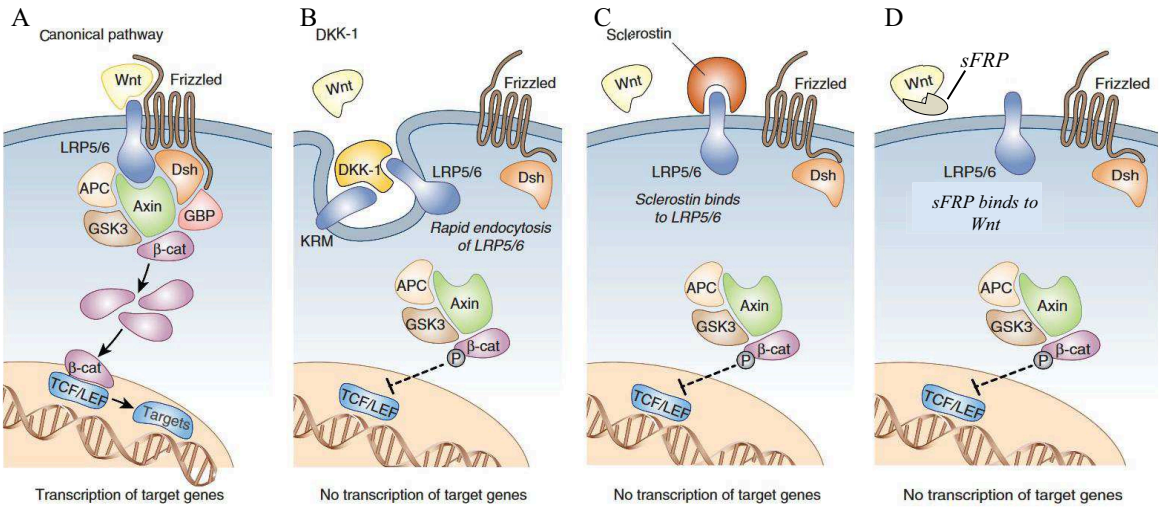

Figure 2: Schematic representation of Wnt signaling pathway and regulatory mechanisms. (A) The association between Wnt ligands, FZD and LRP5/6 receptors results in the stabilization and nuclear translocation of β-catenin, and activation of transcription. (B) DKK1 binds LRP5/6 and Kremen (KRM), and triggers endocytosis of the receptor. (C) Similarly sclerostin binds the LRP5/6 receptors, thereby favoring β-catenin degradation. (D) sFRP binds Wnt ligands and prevents the activation of the functional receptors. Adapted from Evenepoel et al., 2015.

Moreover, the transmembrane E3 ubiquitin ligase zinc and ring finger 3 (ZNRF3) associates with the Wnt ligand/receptors complex and promotes turnover of the receptors.

On the contrary, leucine-rich repeat containing G-protein-coupled receptors (LGR4/5/6) and R-spondins (roof plate-specific spondin, RSPO) potentiate Wnt pathway [31]. R-spondins are potent stem cell growth factors, whose role in bone metabolism has been only recently highlighted. They form a complex with their LGR receptors, ZNRF3 and its homologue ring finger 43 (RNF43), and lead to β-catenin stabilization, ultimately promoting osteoblast differentiation and bone formation. In particular, LGR4 signals through the cAMP-PKA-ATF4 pathway and is important for BMP induced osteoblastic differentiation [32].

BMPs comprise at least 20 molecules that belong to the transforming growth factor beta (TGFβ) family and act in several biological processes such as embryogenesis, skeletal formation, hematopoiesis and neurogenesis. Among different BMPs, BMP-2, 4, 5, 6 and 7 are clearly implicated in osteogenesis: for example, BMP-2 increases osteocalcin (OCN) expression and induces bone formation; BMP-7 stimulates the expression of ALP and other osteoblastic differentiation markers and increases calcium mineralization. BMPs are implicated in many steps during endochondral bone development; indeed, BMP signaling promotes chondrocyte proliferation and differentiation by sustaining SOX9 expression, fundamental for chondrogenic commitment and differentiation. In particular, BMP-2 and BMP-4 are essential for osteoblastogenesis as well as chondrocyte proliferation, differentiation and apoptosis during skeletal development [33].

BMPs bind their receptors on MSCs surface and form a heterotetrameric complex composed of type I and type II serine/threonine kinase receptors. The activated type II receptor transphosphorylates the type I receptor which, in turn, phosphorylates the SMAD1/5/8 complex. This associates to SMAD4 and translocates to the nucleus, stimulating the expression of the transcription factors RUNX2 and OSX [13].

BMP signaling pathway is regulated by various BMP antagonists, such as noggin, chordin, follistatin, twisted gastrulation and DAN family members (Dan, Cerberus, Sclerostin), that prevent specific binding of BMPs to their cell surface receptors [34].

Osteoblast functions

Osteoblasts are specialized cells primarily responsible for bone matrix synthesis. This process is characterized by deposition of organic matrix and subsequent mineralization.

In the first step, osteoblasts secrete collagen, non-collagen proteins and proteoglycans (PGs), which form the osteoid. In the second step, osteoblasts secrete matrix vesicles (MVs) by budding and shedding of specific regions of the outer plasma membrane. The MVs contain hydroxyapatite crystals preformed in the osteoblasts; in the extracellular environment mineral crystals are released from the MVs, further grow thanks to the presence of Ca^{2+} and $PO_4^{(3-)}$ in the extracellular fluids and serve as template for the formation of new crystals [35]. At the end of the bone formation phase, osteoblasts can become embedded in the bone as osteocytes, or become bone-lining cells or undergo apoptosis.

In addition, osteoblasts carry out an intense crosstalk with osteoclasts through different molecular mechanisms. The best known is represented by the macrophage-colony stimulating factor (M-CSF)/C-FMS and receptor activator of nuclear kappa B ligand (RANKL)/RANK/OPG signaling axis. M-CSF and RANKL interact with their receptors (C-FMS and RANK respectively) on osteoclast precursors surface to promote their proliferation and differentiation [10, 36]. On the contrary, osteoprotegerin (OPG) is a soluble factor acting as a decoy receptor for RANKL preventing its interaction with the functional receptor RANK. OPG itself is controlled by many ligands, such as TNF-related apoptosis inducing ligand (TRAIL), von Willebrand factor and glycosaminoglycans (GAGs), which impacts on the overall inhibitory effect of OPG on RANKL [37-39].

Other molecules for osteoblasts-osteoclasts communication are semaphorins, a large family of secreted and membrane-bound glycoproteins characterized by the presence of the “sema” domain. In particular, SEMA3A, mainly produced by cells of the osteoblast lineage, reduces the differentiation and migration of osteoclast precursors by suppressing immunoglobulin tyrosine-based activation motif (ITAM) signaling and ras homolog family member A (RHOA) activation; on the contrary, it increases osteoblast differentiation by activating Wnt/β-catenin signaling [40].

Moreover, osteoblasts are important for the development and maintenance of the HSC niche [14]. They favor HSC homing in the marrow and self-renewal. Different ligand-receptor pairs are exploited for this function; the best characterized are the stromal-derived factor 1 (SDF1 or CXCL12)/CXCR4 and the vascular cell adhesion molecule

1/very late antigen 4 (VCAM1/VLA4) systems. Homotypic interactions between N-cadherins on osteoblasts and HSC plasma membrane are also involved.

3.1.1.2 Osteocytes

Osteocytes are the most abundant cells in bone (90-95% of the total cells). They derive from terminal differentiation of osteoblasts which remain embedded in the bone matrix during bone formation, undergo morphological and ultrastructural changes (i.e. rough endoplasmic reticulum and Golgi apparatus decrease in volume and the nucleus/cytoplasm ratio increases), modify their gene expression profile (e.g. the expression of osteoblast markers such as OCN, BSPII, collagen type I and ALP decreases, while the expression of osteocyte markers such as dentine matrix protein 1 and sclerostin increases) and reduce their synthetic and secretory functions [41]. Osteocytes have up to 50 long and branched processes, which elongate through tiny tunnels originating from the lacuna space (canaliculi). Thanks to these cytoplasmic processes, osteocytes are connected to other osteocytes, osteoblasts and bone lining cells, which facilitates the exchange of signaling molecules (Figure 3). The cell-cell communication is also achieved by means of the interstitial fluid flowing in the canaliculi [2].

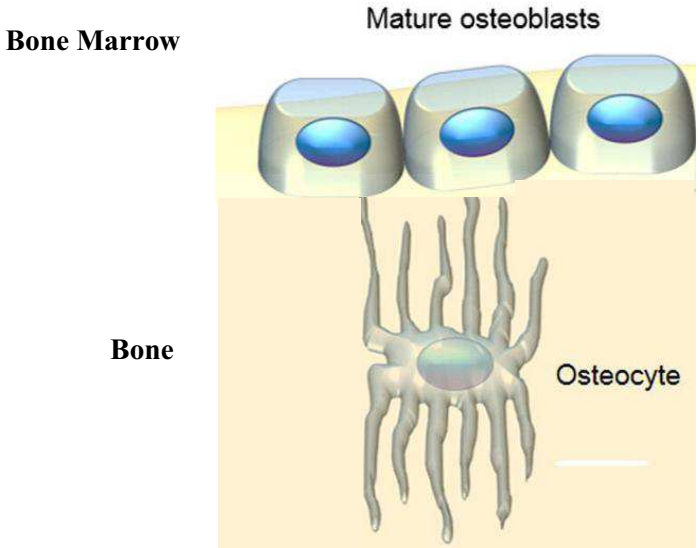

Figure 3: Osteocytes differentiate from osteoblasts that become trapped in the bone matrix during bone deposition. They develop dendritic-like cell processes that connect them to other osteocytes and to cells on the bone surface. Adapted from Capulli et al., 2014.

The canalicular structure allows osteocytes to respond to mechanical and biological signals [2, 13]. Even though the underlying mechanism is not completely clear, the involvement of protein complexes composed of a cilium and cilia-associated proteins, and of cytoskeletal elements activated by changes in the fluid flow deriving from mechanical load, has been proposed to mediate the conversion of the mechanical signal into a chemical one. As a result, different factors such as nitric oxide, prostaglandins, and sclerostin are produced by osteocytes and modulate bone resorption and formation [42].

Osteocytes are an essential source of RANKL which is required to stimulate osteoclasts during bone remodeling in cancellous bone [43], under the control of PTH [42]. Changes in the RANKL/OPG ratio, together with increased vascular endothelial growth factor (VEGF) production from cells neighboring apoptotic osteocytes and release of pro-inflammatory chemotactic signal for osteoclasts from dying osteocytes, are probably some of the mechanisms linking osteocyte apoptosis and increased bone resorption [44].

Another essential osteocytic factor is fibroblast growth factor 23 (FGF23), which is a hormone regulating mineralization and phosphate homeostasis. In fact, FGF23 reduces the expression of the sodium-phosphate transporters (type IIa and IIc) in the kidney proximal tubule and increases phosphate excretion; in addition, it inhibits the expression of 1-α-hydroxylase and promotes 24-hydroxylase in the kidney, thus diminishing $1,25(OH)_2D$ levels and phosphate absorption from the gut and bone [45].

Finally, osteocytes can remodel the lacuna where they are located, thus changing its shape. This process is called osteocytic osteolysis and, even though debated, is probably limited to situations requiring increased release of mineral from the skeleton, such as pregnancy or lactation [46].

3.1.1.3 Bone Lining Cells

Bone lining cells (BLCs) are quiescent osteoblasts on bone surfaces where neither bone resorption nor bone formation occurs [2, 47]. BLCs are flat-shaped with thin and flat nuclear profile; their cytoplasm extends on bone surface and is characterized by few cytoplasmic organelles. Thanks to gap junctions and processes that extend into

canaliculi, BLCs interact with each other and with osteocytes into bone matrix, respectively.

Depending on bone physiological status, BLCs can display a secretory activity and change their size, adopting a cuboidal appearance [48]. Their function is not completely understood, but they have been demonstrated to produce OPG and RANKL, thus participating in osteoclast differentiation, and to prevent the direct interaction between osteoclasts and bone matrix when bone resorption should not occur [49, 50].

3.1.1.4 Osteoclasts

Osteoclasts are large multinucleated cells originating from hematopoietic progenitors of the monocyte/macrophage lineage, responsible for bone resorption. To perform this activity, they contain many mitochondria and lysosomes and display a unique morphology, organelle distribution and plasma membrane domain organization [51]. They move by extending membrane protrusions called lamellipodia at their leading edge and retracting the plasma membrane at the opposite side; during this phase they are flattened cells. At the site of resorption, the osteoclasts are dome-shaped and their plasma membrane is polarized. Four specialized domains can be distinguished: the sealing zone, which is a large F-actin ring structure anchoring the osteoclast to the bone surface by peculiar adhesions called podosomes; the ruffled border, which is a highly convoluted membrane region delimited by the sealing zone and facing the resorption lacuna; the functional secretory domain, located at the opposite side of the cell with respect to the ruffled border; and the basolateral membrane (Figure 4) [52]. This polarization allows vesicular trafficking from the basolateral membrane to the ruffled border and from this latter to the functional secretory domain.

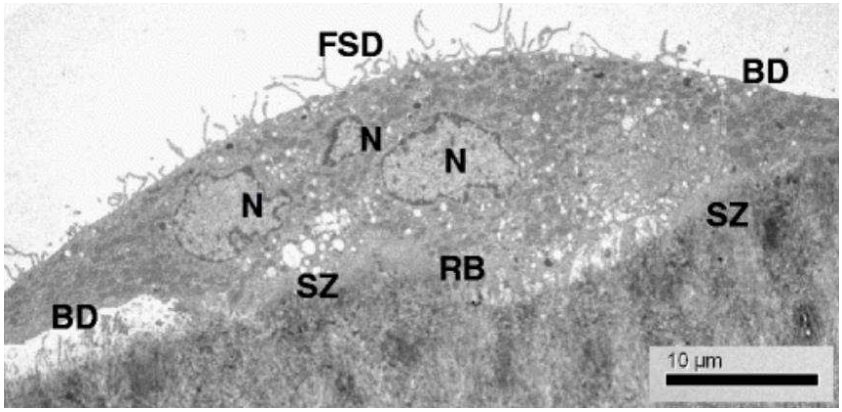

Figure 4: Electron microscopy image of an osteoclast showing the four functional domains: the. ruffled border (RB), the sealing zone (SZ), the basolateral domain (BD) and the functional secretory domain (FSD). N: nucleus. Adapted from Crockett et al., 2011.

Through bone resorption, osteoclasts participate in the regulation of calcemia and phosphatemia under the control of PTH. In addition, they are involved in the formation and maintenance of the HSC niche in the bone (even though this is debated) and in HSC mobilization from the bone marrow. This is achieved by cleaving factors present in the matrix and important for the HSC niche and by producing TGFβ and bFGF that direct HSC fate [53, 54]. Osteoclasts influence osteoblast differentiation by releasing potent anabolic agents, such as BMPs, insulin-like growth factor I (IGF I) and TGFβ, from the bone matrix and secreting so-called clastokines, such as a sphingosine 1 phosphate (S1P), BMP6 and Wnt10b, with a similar anabolic effect. Through the production of VEGF and other angiogenic factors, osteoclasts play a role in the regulation of blood supply to bone. Finally, they are extremely sensitive and responsive to stimuli coming from the immune system such as RANKL, tumor necrosis factor α (TNFα) and interferon γ (IFNγ); the recognition of the complex interactions between osteoclasts and immune cells fuelled a specific research field, named osteoimmunology [55]. Osteoclasts themselves have been suggested to act as innate immune cells, based on several evidence, such as the production of a variety of cytokines, the expression of immune receptors and the capacity to process and present antigens [56, 57].

Molecular control of osteoclast differentiation

Osteoclast differentiation takes place through the activation of different pathways comprising an ever-growing number of molecules either directly or indirectly involved. In the early stage of the process, the commitment of hematopoietic cells towards the osteoclast lineage is regulated by the transcription factors PU.1 and microphthalmia-associated transcription factor (MITF)/Tfe3, which induce the expression of the M-CSF receptor C-FMS [58]. Then, M-CSF promotes RANK expression by myeloid precursors, thus priming them to respond to RANKL, and enhances proliferation, differentiation and survival of osteoclast precursors *via* the signaling complexes DNAX-activating protein 12/tyrosine-protein kinase (DAP12/SYK), extracellular signal-regulated kinase/growth-factor-receptor-bound protein 2 (ERK/GRB2) and protein kinase B/phosphatidylinositol 3-kinase (AKT/PI3K) [55].

RANKL binding to its receptor RANK induces trimerization of the receptor and recruitment of different adaptor molecules; among them, TNF receptor-associated factor 6 (TRAF6) appears to be the most important. TRAF6 recruitment leads to the activation of several signaling pathways such as c-Jun N-terminal kinase/activator protein 1 (JNK/AP1), nuclear factor kappa B (NF-*k*B) and nuclear factor of activated T cell c1 (NFATc1) during osteoclast formation; SRC and p38/MITF in the resorption phase; SRC and ERK to promote osteoclast survival [59, 60].

More in detail, the most important regulator is NF-*k*B that comprises a family of transcription factors, such as p65, p50 and p52, which during basal/unstimulated conditions are inhibited by proteins called IκBs. After the initiation of osteoclast differentiation, TRAF6 activates NF-*k*B-inducing kinase (NIK) and then a complex consisting of IκB kinase (IKK) α, IKKβ and IKKγ (IKBKG, hereafter called NF-*k*B essential modulator, NEMO). IKK phosphorylates and degrades IκBα, thus releasing the p65/p50 heterodimer, which translocates into the nucleus and mediates a key event, which is the up-regulation of NFATc1 [61]. NFATc1 is the master regulator of osteoclast differentiation; its promoter contains NFAT binding sites that allow transient autoamplification during osteoclastogenesis, resulting in a robust induction of NFATc1. After NFATc1 activation, the expression of genes essential for osteoclast fusion (such as dendritic cell-specific transmembrane protein, DC-STAMP; osteoclast stimulatory transmembrane protein, OC-STAMP; and the d2 isoform of vacuolar ATPase V0

domain, Atp6v0d2) and for osteoclast function (tartrate resistant acid phosphatase, TRAP and cathepsin K, CTSK) is induced (Figure 5) [62].

In parallel to RANKL/RANK axis, co-stimulatory signaling contributes to induce osteoclast formation and activation. Basically, Immunoglobulin-like receptors, such as triggering receptor expressed in myeloid cells-2 (TREM 2) and osteoclast-associated receptor (OSCAR), after binding to as yet poorly defined ligands, recruit adaptor molecules, including Fc receptor common γ subunit (FcRγ) and DAP12. The phosphorylation of ITAMs in these adaptors stimulates downstream pathways, comprising also phospholipase Cγ and calcium-calmodulin signaling, resulting in potentiation of NFATc1 signal via a calcium-dependent mechanism [55].

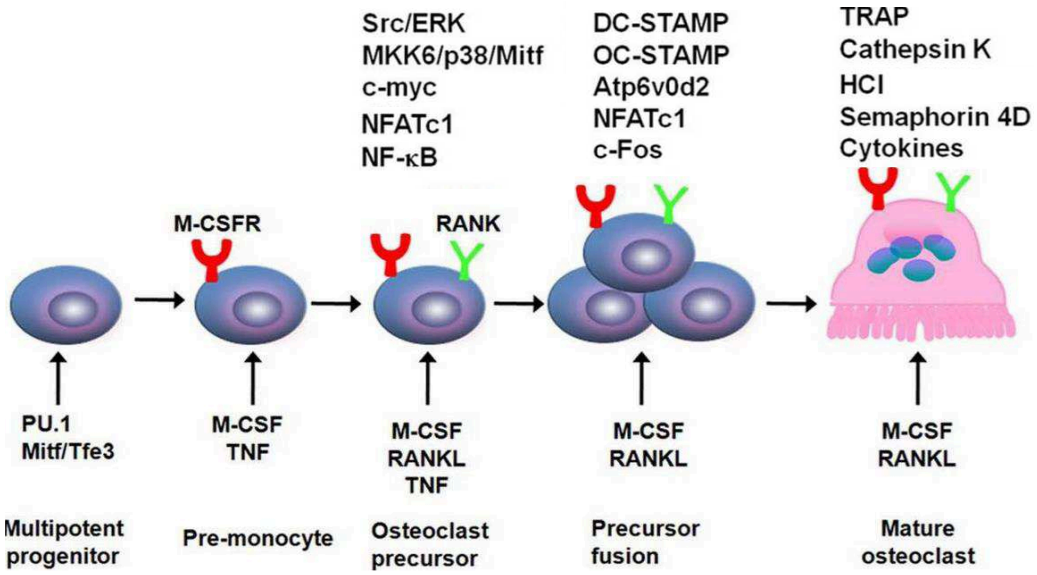

Figure 5: Principal molecules involved in osteoclast differentiation and function. PU.1 and M-CSF with its receptor C-FMS act in the early stage regulating HSC differentiation into osteoclast precursors, which form multinucleated cells by cell-cell fusion. RANKL-RANK binding stimulates the activation of downstream molecules that lead to the formation of mature and functional osteoclast. Adapted from Boyce, 2013.

In this framework, the transcription factor c-MYC has been proposed as the key upstream regulator of the metabolic reprogramming occurring upon RANKL/RANK signal activation. c-MYC expression would be activated downstream of RANKL/RANK binding through an as yet undefined mechanism, and this would directly enhance the expression of the estrogen-related receptor α (ERRα), ultimately

resulting in increased osteoclastogenesis via enhanced mitochondrial respiration. Of note, c-MYC would also act upstream NFATc1 [63].

Another important transcription factor downstream activation of the RANKL/RANK signaling axis is the B lymphocyte-induced maturation protein 1 (BLIMP1), which mediates the transcriptional repression of anti-osteoclastogenic genes, such as B-cell lymphoma 6 (Bcl6), interferon regulatory factor 8 (IRF8), and v-Maf musculoaponeurotic fibrosarcoma oncogene family homolog B (MAFB) [64].

In addition, LGR4 has recently been demonstrated to prevent RANKL binding to its functional receptor RANK. LGR4 binding to RANKL activates the GSK3 pathway suppressing the expression of NFATc1 during osteoclastogenesis, thus reducing osteoclast differentiation [65].

Osteoclast physiology

Osteoclasts' main function is the degradation of the bone matrix; to this end, they form the sealing zone, through which they firmly attach to bone thanks to integrin expression (in particular $\alpha_v\beta_3$ integrin). The binding process results in actin ring formation and deployment of adhesive proteins into a ring-shaped structure, so that a seal is formed [66, 67].

The adherent osteoclasts are polarized and form the ruffled border, a series of fingerlike processes that increase the surface area of the plasma membrane facing the resorption lacuna. The ruffled border is enriched in vacuolar H^+-ATPase proton pumps, multisubunit complexes which allow establishing the low pH required for the dissolution of bone mineral matrix and degradation of the organic matrix by a number of secreted lysosomal enzymes. Several acid hydrolases are present in the osteoclast lysosomes and in the resorption lacuna, for example the cysteine protease cathepsin K, matrix metalloprotease 9 (MMP9) and TRAP [68].

The protons extruded by the V-ATPase originate in the cytoplasm by the activity of the enzyme carbonic anhydrase type 2 (CA2), which accelerates the hydration of CO_2 in H_2CO_3, soon dissociated into HCO_3^- and H^+. The generated HCO_3^- is taken up by a Cl^-/HCO_3^- anion exchanger located in the basolateral membrane, which prevents cytoplasmic alkalinization and provides the Cl^- ions required by the chloride voltage-

gated channel 7/osteopetrosis associated transmembrane protein 1 (CLCN7/OSTM1) $2Cl^-/H^+$ antiporter complex in order to electrically shunt the resorption lacuna [69].

Two distinct subdomains of the ruffled border, the fusion zone and the uptake zone, have been implicated in vesicular fusion and uptake of bone degradation products, respectively; both subdomains would take part also in vesicular trafficking, membrane recycling and re-uptake of lysosomal enzymes. Intricate mechanisms involving also small guanosine triphosphate (GTP)-binding proteins and microtubule-based protein complexes, allow efficient delivery of osteolytic cargos and transport of products of bone matrix degradation through the cell and their release at the functional secretory domain into the extracellular space [51].

3.1.1.5 Other cells in bone

In the bone tissue, several other cells are present besides those above described. Here we will provide just few examples in order to give a flavor of the complexity of bone tissue composition and of the cellular interactions taking place therein.

MSCs can be found in the bone marrow, periosteum, endosteum and in the mineralized tissue itself. In addition to osteoblasts, they give rise to other cell types, in particular adipocytes and chondrocytes. Adipogenic differentiation is specifically important for bone homeostasis, because in many physiopathological conditions (such as aging, estrogen loss) differentiation occurs towards either lineage as mutually exclusive cell fate decision [70]. Moreover, bone marrow adipocytes secrete a spectrum of biologically active signaling molecules, such as resistin, leptin and adiponectin, that have been reported to influence the development and function of osteoblasts and osteoclasts [71].

HSC residing in the bone marrow establish complex interactions with their microenvironment, which can direct their fate. On one hand, osteoblasts and osteoclasts produce molecules able to affect HSC localization and function, whereas the activation of osteoclasts leads to HSC egress from the bone marrow [72]. On the other, HSCs themselves express factors, such as angiopoietin1, able to modulate the properties of their niche [73] and, more in general, of the bone tissue, particularly in pathological conditions [74].

Immune cells are important components of the bone microenvironment playing a role in health and disease. For example, in physiological bone turnover B and T lymphocytes have been shown to participate in the maintenance of tissue homeostasis by regulating the RANKL/OPG ratio (of note, B cells are a key source of OPG in the bone marrow) and by directly modulating osteoclastogenesis via cytotoxic T-lymphocyte protein 4 (CTLA4) [75]. In pathological conditions, activated immune cells drive systemic bone loss by producing TNFα and RANKL. Moreover, Th17 cells produce interleukin 17 (IL-17) that induces RANK expression on osteoclast precursors as well as RANKL production, further supporting osteoclasts formation [76].

3.1.1.6 Bone matrix

Bone matrix is composed of an organic phase (20%), an inorganic one (70%) and water (10%); the relative amount of each component varies depending on age, gender, site, and in general physiopathological conditions [77].

The organic component is also called osteoid; the most abundant protein in this part is type I collagen (90%), which is a heterotrimer of two type I alpha 1 chains [α1(I)] and one type I alpha 2 chain [α2(I)]. Other types of collagen are also present in bone in a lower amount, such as type II, IX and XI. Collagen is synthetized as a procollagen molecule, in which an N-terminal and a C-terminal globular domain flank the helical domain. These propeptides are required for folding, which starts at the C-terminal and proceeds towards the N-terminal, and are cleaved by specific proteases after secretion. The basic feature of the helical domain is the presence of an uninterrupted series of triplets Gly-X-Y, in which the glycine residue in the first position is mandatory, while in the second and third position a proline and hydroxyproline, respectively, are often found. The small side chain of the glycine residue in the triplet can be easily accommodated in the inner part of the helix, thus is essential for collagen structural integrity [78]. The helical structure undergoes posttranslational modifications, mainly hydroxylation at proline and lysine residues in specific positions, glycosylation of hydroxylysine and isomerization of peptidyl prolyl bonds. These modifications, occuring mainly in the rough endoplasmic reticulum, require the activity of several enzymes and are essential for proper folding. The folded collagen is then transferred to the Golgi and released in the extracellular space, where it undergoes a maturation

process consisting in the removal of the propeptides and in the spontaneous assembly in microfibrils. These latter grow in longitudinal and axial directions by forming crosslinks between each other and generating long, thin and elastic mature fibers (Figure 6) [79].

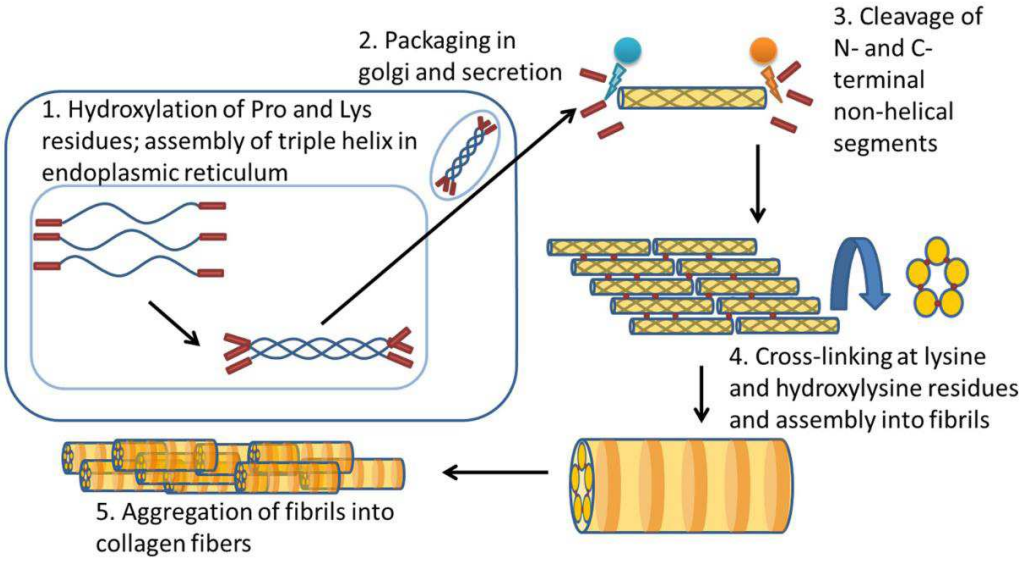

Figure 6: Schematic representation of collagen synthesis. The process starts in the rough endoplasmic reticulum with the translation of pro-collagen α chains. These chains form a triple helix and are secreted from the cell, where they undergo further processing and aggregation into fibrils and fibers. Adapted from McKleroy et al., 2013.

The organic matrix of the bone tissue contains also non-collagenous proteins, such as PGs, osteonectin, osteocalcin and proteins of the small integrin-binding ligand N-linked glycoprotein (SIBLING) family, such as BSP, osteopontin (OPN) and dentin matrix protein 1 (DMP1).

Proteoglycans are molecules composed of a proteic core covalently bound by one or more sulfated GAG chains, i.e. linear polymers formed by repeated disaccharidic units produced in the Golgi. Based on the disaccharide, GAGs can be divided in glucosaminoglycans (comprising heparin/heparan sulfate and keratan sulfate) and galactosaminoglycans (comprising chondroitin sulfate and dermatan sulfate); a peculiar GAG is hyaluronic acid, which is not sulfated and not bound to a protein. In general, PGs are involved in the organization of the bone matrix structure; in addition, they bind several growth factors, such as TGFβ, FGFs and VEGF, thus modulating their availability in the bone microenvironment. Recent evidence suggests that PGs may also interfere with the RANKL/RANK signaling axis by binding osteoprotegerin [see below

for detailed description of this pathway] and modulate cathepsin K activity, thus indirectly influencing osteoclast function [80]; in parallel, PGs may inhibit osteoblast proliferation [81].

Osteonectin (also named secreted protein acidic and rich in cysteine, SPARC) is a calcium-binding protein; it contains two distinct domains for the interaction with collagen and hydroxyapatite, respectively. Osteonectin is highly expressed during bone formation, while its production decreases in mature bone. It has been proposed to facilitate procollagen processing by limiting its interaction with the cell surface collagen receptors discoidin domain receptors 1 and 2 [82].

Osteocalcin is abundantly deposited in the extracellular matrix thanks to the high affinity for the mineral component conferred by three carboxylated glutamate residues. Osteocalcin is also present in the general circulation, where its levels are measured as a bone turnover marker. Of note, recent advances have identified osteocalcin as a bone-derived hormone able to influence energy metabolism and reproductive functions [83].

The SIBLING proteins have been implicated in cell attachment/signaling processes due to the presence of an Arg-Gly-Asp (RGD) motif mediating their interaction with integrins; moreover, they have been implicated in matrix mineralization. In particular, BSP is expressed at the early stage of bone formation during embryogenesis, suggesting that it might have a role in mineral nucleation. On the contrary, OPN (also termed secreted phosphoprotein 1, SPP1), originally described as a bridge between cells and mineral, has been shown to inhibit hydroxyapatite formation and growth. Finally, DMP1 seems to perform opposite functions: it inhibits the mineralization process as a native protein, while it initiates this process when cleaved or dephosphorylated, through the activation of an intracellular signaling cascade downstream $\alpha_v\beta_3$ integrin resulting in the release of Ca^{2+} stored in the osteoblasts. Interestingly, BSP has been also implicated in bone remodeling and in particular in osteoclast adhesion to bone [84, 85].

Of note, the bone organic matrix contains also many growth factors, like TGFβ, BMPs, IGF I and II [33], which are produced by osteoblasts, stored in the matrix and made available by osteoclast resorbing activity promoting the osteoclast-osteoblast crosstalk.

The inorganic component of the bone matrix is the mineral phase. It contributes to the mechanical properties of the matrix, such as strength in compression and stiffness in tension, while it reduces toughness. Bone crystals are small (20-50 nm long, 15 nm

wide and 2-5 nm thick), plate-shaped and often quite closely packed, with their long axes almost parallel to the axes of the collagen fibrils [86]. The primary constituent of the mineral phase is hydroxyapatite ($Ca_{10}(PO_4)_6(OH)_2$), since calcium and phosphate are the most abundant ions; amorphous calcium phosphate is present, too. The mineral phase is also rich in carbonate ions, which form carbonate hydroxyapatite; other ions, such as citrate, magnesium, sodium, potassium and fluoride, are present in a lower amount. Mineralization is a biphasic process; in the initial phase, crystal number and size rapidly increase within the gaps inside collagen fibrils, then a slower phase lasting months to years allows mineral interaction with local ions, crystal growth towards the overlapping zones and matrix maturation [86].

Finally, another important component of the bone matrix is water, which binds collagen and mineral particles and allows their relative movement and deformation during loading. Therefore, the amount of water in the bone tissue can importantly impact on bone mechanical properties. In particular, the mineralization process allows mineral crystals to replace water within collagen fibers and to lose their diffusion capacity; this results in reduced collagen fiber diameter and loss of toughness and elasticity [87].

3.1.2 Bone material pattern

At microscopic level, two types of bone can be distinguished based on its composition: woven bone and lamellar bone.

Woven bone is characterized by irregular disposition of collagen fibers and mineral crystals. This type of bone is a transient tissue, typical of young fetal bones, but is present also in adults during very rapid bone remodeling and fractures repair. It is quickly laid down and displays similar mechanical properties in all directions.

On the other hand, almost all adult bones have a lamellar structure, which means they are composed of a series of 3-7 μm thick lamellae forming circumferential layers at the outer (periosteal) and inner (endosteal) surfaces. The greatest portion of lamellae forms osteons, which represent the basic units of cortical bone; the estimated number of osteons in the adult skeleton is 21 million [88]. The osteons are characterized by the presence of neurovascular channels (termed Haversian canals) surrounded by concentric cylinders of lamellae with a final diameter ranging from 100 to 400 μm (Figure 7). They

contain osteocytes in confined spaces called lacunae, and are crossed by canaliculi, which are crossed by the cytoplasmic processes connecting the cells one to another and allow the diffusion of nutrients, gases and other diverse molecules. The central Haversian canals communicate with each other and with the bone marrow cavity *via* channels called Volkmann's canals, which run obliquely to the long axes of the osteons. This three dimensional structure and the main direction of the collagen fibers within osteons of long bone shafts can vary: the fibers are predominantly longitudinal at sites mostly subjected to tension, and more oblique at sites subjected to compression.

The trabecular bone (also called cancellous or spongy bone) does not contain osteons and is less dense as compared to cortical bone, which makes it more flexible and suitable for metabolic activities [89]. It is typically found at the ends of long bones, is highly vascularized and hosts bone marrow cells. The trabeculae, thin plates of bone, are its primary anatomical and functional unit and are aligned towards the mechanical load distribution (Figure 2).

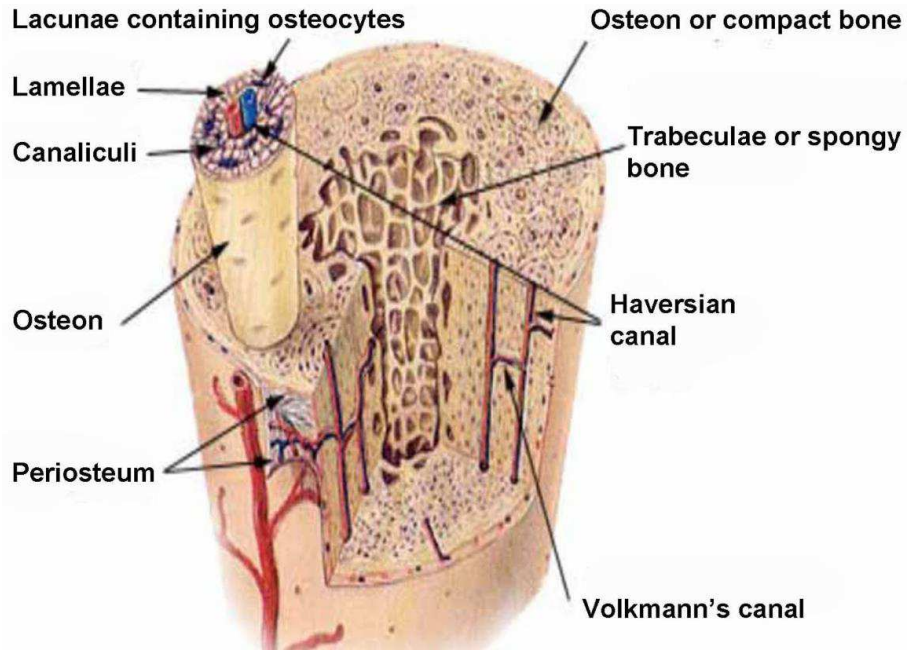

Figure 7: Schematic section of a long bone showing cortical and trabecular bone tissue. Adapted from Cowin et al., 2015.

3.2 Bone development

Bone development takes place through two different processes: endochondral and intramembranous ossification. During the former, ossification is preceded by the formation of a cartilaginous template; this mechanism gives rise to all the axial (vertebral column and ribs) and appendicular (limb) bones of the body.
On the other hand, the majority of the face and skull bones (called dermal or membrane bones) directly originate by intramembranous ossification of the mesenchyme, from neural crest cells or unsegmented paraxial mesoderm [90].
Fine temporal and spatial regulation of the commitment to the chondrogenic and osteogenic lineages is essential for both embryonic and adult bone development and is determined, at a molecular level, by distinct transcription factors. In particular, SOX9 is a key regulator of the differentiation towards the chondrogenic lineage acting on collagen type II expression, whose protein product is the main constituent of the early cartilaginous matrix. On the other hand, commitment to the osteoblastic lineage requires the transcription factor RUNX2 (as already described in 3.1.1.1 chapter) [91]. Accordingly, loss of SOX9 in mice affects the early development of all cartilaginous bones, whereas gene inactivation of *Runx2* in mice results in ossification defects due to lack of osteoblasts [92, 93].

3.2.1 Endochondral ossification

Endochondral ossification begins as mesenchymal cells condense. In response to growth factors, chondrocytes differentiate within the mesenchyme, become hypertrophic and start to secrete molecules of the cartilaginous extracellular matrix mainly composed of collagen type II and PGs (Figure 8A). Afterwards, osteoblasts differentiate from the cells of the perichondrium, that is the layer surrounding the cartilaginous area, and form a primary bone collar around the circumference of the bone in the diaphysis, whereas hypertrophic chondrocytes attract blood vessels and then undergo apoptosis (Figure 8B) [94, 95]. The ossification process starts in the primary ossification center in the middle of the long bone, when the developing bone is invaded by multiple blood vessels and proceeds towards the epiphyses (i.e. each of the two extremities of a long bone). The establishment of the vasculature recruits preosteoblastic cells that differentiate into

osteoblasts and replace hypertrophic chondrocytes. Osteoblasts of the primary spongiosa produce the trabecular bone, while those of the bone collar produce the cortical bone; in the meantime, chondrocyte proliferation results in bone elongation (Figure 8C). Osteoclast precursors migrated in the spongiosa through blood vessels, which differentiate and remove cartilage matrix, while osteoblasts use the remaining of this matrix as a scaffold for the deposition of bone; overall, these processes achieve modeling of the growing bone.

At birth, the diaphyses are completely ossified, whereas the epiphyses are still cartilaginous and ossify after birth during the secondary ossification. However, a layer of cartilage (epiphyseal growth plate) persists between the epiphysis and the growing end of the diaphysis (metaphysis) (Figure 8D) [95]. Finally, when the growth of the body is complete (around 20 years of age), the epiphyseal growth plate completely ossifies.

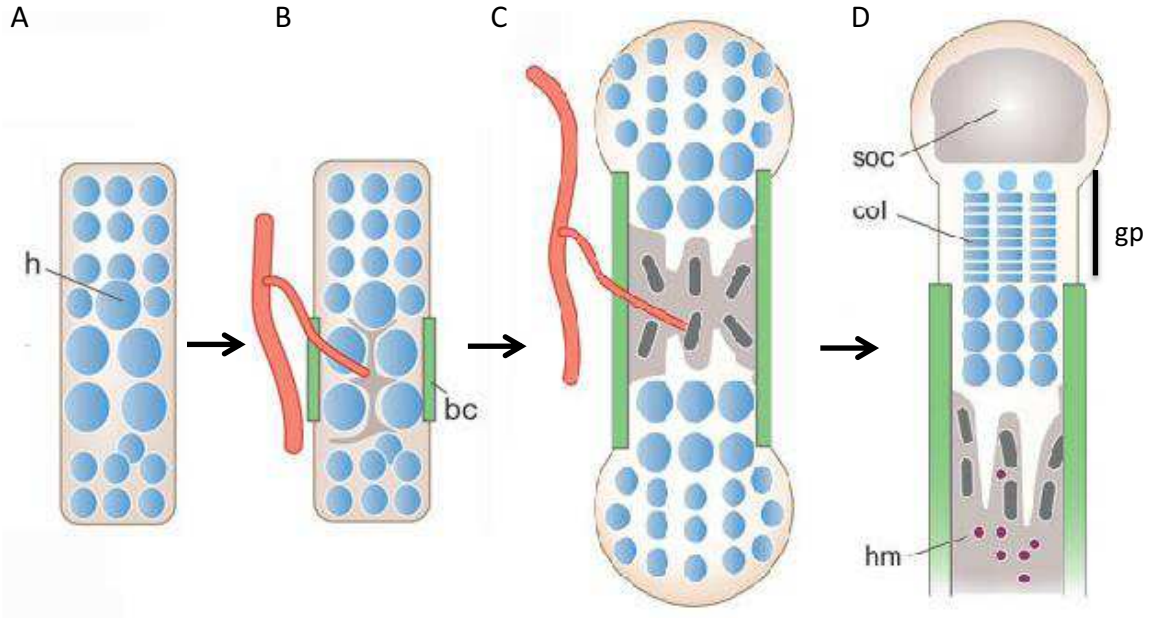

Figure 8: Schematic representation of long bone development. h = hypertrophic chondrocytes. bc = bone collar. soc = secondary ossification center. col = columns of proliferating chondrocytes. hm = hematopoietic marrow. gp = growth plate. Adapted from Kronenberg, 2003.

In all these processes chondrocytes play a pivotal role. In order to accomplish their functions, they undergo morphological and functional changes (from resting to proliferating, then hypertrophic and lastly apoptotic) under the control of systemic factors such as growth hormone (GH) and thyroid hormones (T3), and of locally

secreted factors, such IGFs, Indian hedgehog (IHH), parathyroid hormone-related protein (PTHrP), BMPs, Wnts and FGFs [96, 97]. These extracellular factors control a number of transcription factors and signaling pathways, including the already mentioned SOX9 and RUNX2 transcription factors and the BMP and Wnt (canonical and non-canonical) signaling pathways (Figure 9) [97].

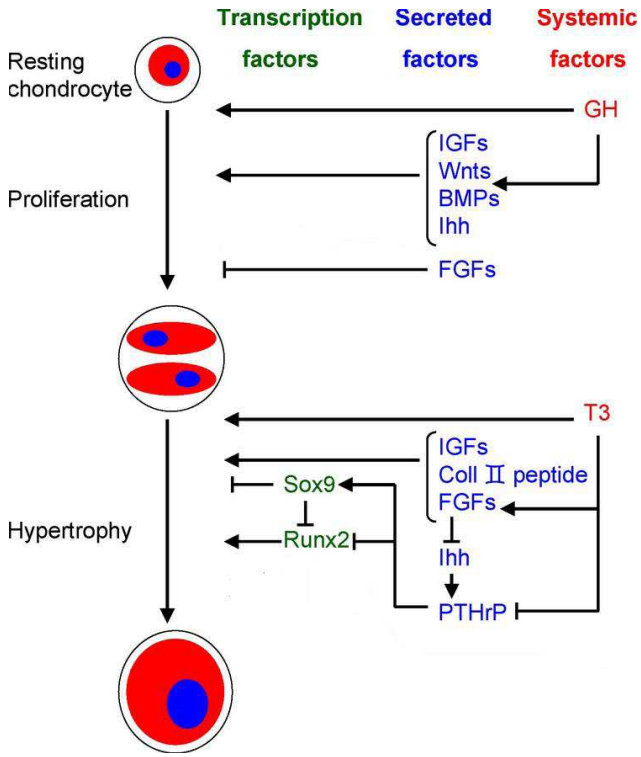

Figure 9: Schematic representation of the roles of systemic, secreted and transcriptional factors in the regulation of chondrocytes proliferation and hypertrophy during endochondral ossification. Arrows and crossed lines indicate stimulatory and inhibitory pathways, respectively. Adapted from Mackie et al., 2008.

3.3 Genetic skeletal disorders

Congenital alterations of bone homeostasis can cause several skeletal pathologies: namely, dysplasias are generalized disorders of cartilage and bone, whereas dysostoses are defects of an individual bone or group of bones. These disorders are mostly rare and can have different levels of severity. Even if the bone compartment is primarily affected, a variety of neurologic, visual, cardiac, renal and psychological complications can be present, too.

The total number of different skeletal disorders is higher than 400 and the total number of affected genes higher than 350. Hence the need to provide a classification, such as the one periodically provided and revised/updated by the *Nosology and classification of genetic skeletal disorders* [98], aimed at facilitating clinical and genetic diagnosis of patients and correct management of their disease, when specific therapies are available; at delineating genotype-phenotype correlations and helping interpretation of results from next generation sequencing technologies. To this end, the *Nosology* divides skeletal disorders into 42 groups defined either by a single gene or a group of related genes, by a particular phenotypic feature or by specific radiological findings [98].
In this context, group 23 comprises the large family of osteopetroses and related disorders, while group 34 comprises dysostoses with predominant craniofacial involvement.

3.4 Osteopetrosis

The term osteopetrosis derives from the Greek “osteo” that means bone and “petros”, stone; indeed, osteopetrosis describes a group of rare, heritable disorders that share the hallmark of increased bone density on radiographs due to a failure in bone resorption [9, 99, 100]. The osteopetroses can be divided in two main groups based on the mode of inheritance: autosomal dominant osteopetrosis (ADO, also called Albers-Schönberg disease, after the name of the German radiologist who described the pathology for the first time in 1904) and autosomal recessive osteopetrosis (ARO). An X-linked form also exists, which is extremely rare (only 4 unrelated patients have been reported thus far in literature) and specifically associated with mutations in the *NEMO* gene [101-103].
ADO has an incidence of 1 in 20,000 births and is generally considered benign, since clinical manifestation most often occurs in adolescence or adulthood and life expectancy is usually normal. However, this form displays a wide range of severity, from asymptomatic cases to severely affected individuals, where the disease is evident already in childhood.
ARO has an incidence of 1 in 250,000 births in the general population, but in specific geographic regions (such as Costa Rica, the Middle East, the Chuvash Republic of Russia) is more frequent due to a founder effect, geographic isolation or high parental

consanguinity [104, 105]. ARO is also called malignant infantile osteopetrosis, because it presents soon after birth and is associated with diminished life expectancy; in fact, untreated patients often die in the first decade of life due to bone marrow suppression and consequent infections.

3.4.1 Clinical presentation

ADO can be recognized based on the typical radiographic sign of "sandwich vertebrae" determined by endplate thickening. Increased bone density is particularly evident at the spine, pelvis and skull base in the so called ADO type II, while in ADO type I, which would be more properly classified as a form of high bone mass, generalized osteosclerosis is more pronounced in the cranial vault.

Complications are mainly confined to the skeleton; they include frequent fragility fractures (ADO I differs also for this aspect: in fact, it's the only form of osteopetrosis not associated with increased fracture rate), bone pain, scoliosis and osteomyelitis, affecting in particular the mandible with dental abscess or caries [106]. The outcome of orthopedic surgery interventions often is limited by nonunion events (i.e. permanent healing failure), infections, prosthesis loosening and intraoperative fractures. Cranial nerve compression leading to hearing and/or visual loss and/or facial palsy affects only a minority of patients. Similarly, secondary hematological defects are not common.

ARO is clinically heterogeneous. It presents at birth or during the neonatal period. The defect in bone resorption causes extremely high bone mineral density and a typical *facies*, with macrocephaly despite general growth retardation, frontal bossing, exophthalmos (eye protrusion), micrognathia (abnormally small jaw) and hypertelorism (increased distance between the eyes) (Figure 10A).

Typical findings at radiological investigation are "bone-in-bone" appearance, "sign du masque" of the skull and Erlenmeyer flask deformity of the distal femoral and humeral metaphyses (Figure 10B). Pathological fragility fractures after minor trauma may occur and the healing process may be delayed.

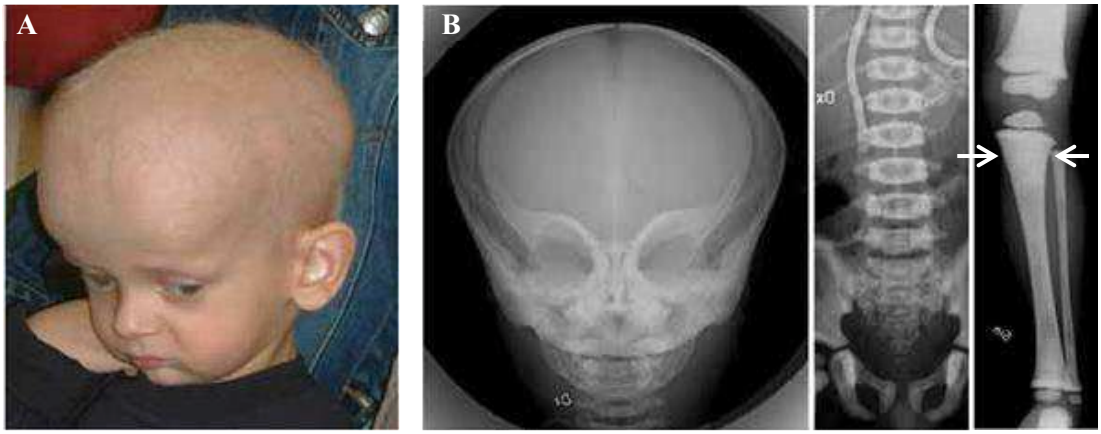

Figure 10: (A) Clinical picture showing the typical facies of an osteopetrotic patient with macrocephaly, frontal bossing and exophthalmos. (B) Representative radiographies showing diffuse increase in bone density, "sign du masque" of the skull, bone-in-bone appearance, absence of bone marrow cavity in the long bones and Erlenmeyer flask deformity (arrows). Adapted from Pangrazio et al., 2013.

Skull abnormalities, such as calvarial thickening and stenosis of the cranial foramina that are crossed by nerves, lead to increased intracranial pressure and neurological defects, such as progressive blindness and/or deafness, cerebellar tonsillar herniation and hydrocephalus [107]. Choanal stenosis can result in respiratory difficulties. In some cases, craniosynostosis (i.e. premature fusion of cranial sutures) is present and is responsible for abnormal skull shape and intracranial hypertension.

The reduction of bone marrow space causes bone marrow failure, anemia, thrombocytopenia, variable leucocyte counts, compensatory extramedullary hematopoiesis, hepatosplenomegaly and recurrent infections. Hypogammaglobulinemia has been reported in some patients [108-110].

Dental defects include absence of teeth, delayed tooth eruption, higher risk of severe caries; moreover, osteomyelitis of the jaw is a common complication after tooth extraction.

Patients frequently show low serum Ca^{2+} levels causing secondary hyperparathyroidism and occasionally hypocalcaemic seizures; on the other hand, serum levels of alkaline phosphatase, $1,25(OH)_2D_3$ and lactate dehydrogenase vary from patient to patient, so they are not reliable biomarkers for ARO [109].

Other clinical features are found in specific ARO subtypes (Table 1): in the neuropathic form (displayed by all patients bearing mutations in the *OSTM1*, and in some patients with mutations in the *CLCN7* gene), primary progressive neurodegeneration with severe developmental delay, hypotonia and primary retinal atrophy, is present. In these patients

pathological changes can be detected by electroencephalography even before the onset of clinical signs [111, 112]. Patients with mutations in the *TCIRG1* or *SNX10* gene can present rickets together with osteopetrosis (hence, the term osteopetrorickets) because of defective Ca^{2+} uptake in the gut and consequent inability to fully mineralize newly formed osteoid [113, 114].

Other clinical features reported in sporadic cases are structural brain malformations, in particular agenesis of the corpus callosum, possibly due to a defect during early embryonic development; coagulation defects, such as Glanzmann thrombasthaenia and severe bleeding, and haemophilia A; glucose-6-phosphate dehydrogenase deficiency; congenital hypothyroidism [9].

Table 1: Classification, genetics and clinical manifestations in ARO patients. Adapted from Sobacchi et al., 2013.

Gene*	Age at presentation (years)	Growth retardation	Hypocalcaemia	Impairment		CNS symptom severity and type	Osteoclasts	Life expectancy‡ (years)	Incidence§
				Haematological	Visual				
TCIRG1	<1	Mild to severe	Severe	Severe	Mild to severe	None to moderate (hydrocephalus)	Present, non-functional	0–10	51–53%
CLCN7	<1	Mild to severe	Severe	Mild to severe	Mild to severe	None to severe (hydrocephalus, neurodegeneration)	Present, non-functional	0–3	13–16%
OSTM1	<1	Mild to severe	Moderate	Mild to severe	Mild to severe	Severe (neurodegeneration)	Present, non-functional	0–2	2–6%
SNX10	<1	Mild	Mild	Severe	Severe	None to moderate (hydrocephalus)	Present, non-functional	0–22	4%
PLEKHM1	1–10	None to moderate	None	None	None	None	Present, non-functional	14	2 cases
TNFRSF11A	<1	Moderate	Mild	Mild	Mild to severe	None to moderate (hydrocephalus)	Absent	1–10	<1–4%
TNFSF11	<1	Severe	Mild	Mild	Mild to severe	None	Absent	1–16	<1–3%

**TCIRG1, CLCN7, OSTM1, SNX10, TNFSFR11A* and *TNFSF11* are associated with classic ARO, whereas *PLEKHM1* causes ARO of an intermediate phenotype, with functional abnormalities similar to those caused by the first four genes mentioned. ‡The upper limit of the range is the oldest age reached by nontransplanted patients described in the literature or in our cohorts.[58, 150] Two patients have survived beyond this age, but this occurrence is highly exceptional. §The percentage of all patients in the osteopetrosis registry of the European Society for Immunodeficiences and the Inborn Errors Working Party of the European Group for Blood and Marrow Transplantation.[150] Where a range is given, the upper limit refers to the percentage in a cohort of 310 patients.[58] Abbreviations: ARO, autosomal recessive osteopetrosis; CNS, central nervous system.

3.4.2 The genetic bases of ARO

The first gene identified in the pathogenesis of osteopetrosis was the *CA2*. Actually, CA2 deficiency presents as an autosomal recessive syndrome in which osteopetrosis is accompanied by renal tubular acidosis, cerebral calcification and mental retardation. The defect responsible for the disease was firstly identified through biochemical studies; then, some years later, the first mutation was identified by direct sequencing of the gene [115, 116]. However, CA2 deficiency is frequently not considered a classic form of osteopetrosis, because the renal defect is preponderant as compared to the mild skeletal pathology.

The first gene found to be responsible for "pure" human ARO was the *TCIRG1* gene [117]. After that, six additional genes have been involved in ARO pathogenesis, thus providing a genetic classification for about 90% of ARO cases.

Five of these disease-genes (*TCIRG1*, *CLCN7*, *OSTM1*, *SNX10* and *PLEKHM1*) encode proteins involved in the acidification of the resorption lacunae and/or in vesicular transport. Loss-of-function mutations in these genes lead to osteoclast-rich osteopetrosis, in which osteoclasts are abundant but not functional.

Mutations in two other genes are associated with osteoclast-poor ARO, in which osteoclastogenesis is blocked: *TNFSF11* (also called *RANKL*) and *TNFRSF11A* (its receptor *RANK*).

3.4.2.1 Genes mutated in osteoclast-rich osteopetrosis

TCIRG1

The T cell immune regulator 1 (*TCIRG1*) gene is located on human chromosome 11q13 and comprises 20 exons. By alternative splicing, a shorter isoform can be produced (*TIRC7*); this transcript lacks the first 4 exons and codes for a transmembrane molecule expressed on activated T cells as an inhibitory receptor, regulating the immune response.

The longer isoform is a component of the vacuolar proton pump V-ATPase, a multimeric protein complex involved in the acidification of extra- and intra-cellular compartments including lysosomes, endosomes, the Golgi apparatus and clathrin-coated vesicles. Its function is essential for several cellular functions, such as pH and ion homeostasis, and protein and vesicle trafficking. In the osteoclasts, the V-ATPase localizes on the membrane of the ruffled border, lysosomes and also on the basolateral membrane.

The V-ATPase is composed of two reversibly assembled domains: the membrane-embedded V0 and V1. V0 is formed by subunits *a*, *c*, *c''*, *d* and *e*, and is responsible for proton translocation across the lipid bilayer; the cytosolic V1, formed by subunits A to H, is responsible for ATP hydrolysis. In addition, two accessory subunits (Ac45 and M8_9) are associated with the V0 domain. Both V1 and V0 domain work through a rotary mechanism [118].

The *TCIRG1* gene encodes the a3 subunit of the V0 domain, the largest among the V0 subunits (molecular weight: 116 kDa, hence the name "oc116"). Four different "a" subunits can be present in the V0 domain, however the a3 is more specifically expressed in osteoclasts and in gastric parietal cells. In bone, the activity of the V-ATPase is required to achieve the low pH needed for the dissolution of the inorganic matrix and the degradation of the organic matrix by acid proteases; in the stomach, it determines the low pH, which allows dietary Ca^{2+} absorption. Overall, this explains the peculiar phenotype (i.e. osteopetrorickets) deriving from *TCIRG1* mutations.

In addition to its proton-pump activity, the V0 complex is involved in vesicle trafficking; in fact, it interacts with microtubules and actin cytoskeleton, probably by means of the a3 subunit itself, and this is crucial for ruffled border formation [113, 118] [119]. Accordingly, mutations in *TCIRG1*, which account for more than 50% of ARO cases and are distributed along the entire gene, cause defects in the proton-pumping function of the V-ATPase and in vesicle trafficking/fusion in osteoclasts.

CLCN7

The chloride voltage-gated channel 7 (*CLCN7*) gene is located on human chromosome 16p13.3 and comprises 25 exons. Its protein product belongs to a large family of CLC proteins sharing the common feature of electrical neutralization of the protons actively pumped into the lumen of intracellular vesicles. The CLCN7 protein is ubiquitously expressed and found on the membrane of late endosomes and lysosomes. It has 12 transmembrane domains, a cytosolic short amino-terminus and a long carboxy-terminus, containing two cystathionine-beta-synthase (CBS) domains, which may modulate transport activity, and a (putative) ATP binding site. It acts as a slowly voltage-gated $2Cl^-/1H^+$ antiporter channel [120]: it mediates the exchange of chloride ions against protons, thus cooperating with the V-ATPase in the acidification of the resorption lacuna and of lysosomal vesicles. CLCN7 forms a dimer and each monomer contains an ion translocation pathway, with conserved gating glutamate residues; simultaneous gating of the two pores through conformational rearrangements outside the ion pathway has been demonstrated [121].

Gene inactivation in mouse causes osteopetrosis, optic atrophy and neurodegeneration with severe lysosomal storage disease, accumulation of electron-dense material in

neurons, autofluorescent structures, microglial activation and astrogliosis; in addition, fur color changes are evident [122, 123]. In agreement with the mouse phenotype, some patients carrying biallelic mutations in the *CLCN7* gene have primary neurological defects besides osteopetrosis [111, 124, 125]. Recessive mutations in the *CLCN7* gene are responsible for about 15% of ARO cases, while dominant ones cause ADO II. Key questions about CLCN7-deficient osteopetrosis still have to be answered: for example, is there a genotype-phenotype correlation? In particular, are there mutations specifically associated with the neuropathic presentation? If this is the case, what is the underlying mechanism responsible for it? With respect to dominant osteopetrosis: why can the same mutation lead to variable disease severity in different individuals, even in the same family? The answers to these questions are relevant for genetic counseling, prognosis and treatment; moreover, by allowing understanding a peculiar aspect of bone biology, may have implications well beyond osteopetrosis.

OSTM1

The osteopetrosis-associate transmembrane protein 1 (*OSTM1*) gene is located on human chromosome 6q21 and is composed of 6 exons. Its protein product is post-translationally processed and specifically N-glycosylated.

OSTM1 encodes a type I transmembrane protein which localizes to intracellular vesicles (mainly endosomes and lysosomes) and primarily acts as the β subunit of ClC-7 (Figure 11). Its highly glycosylated N-terminus stabilizes ClC-7 and protects it from lysosomal degradation; OSTM1 aminoterminus and transmembrane domain are required for ClC-7 $2Cl^-/1H^+$ exchange, whereas the transmembrane domain is important for ClC-7-dependent trafficking to the lysosomes [120, 126]. OSTM1 has also been suggested to function as an E3 ubiquitin ligase for the heterotrimeric G-protein $G\alpha_{i3}$ and to potentiate Wnt canonical signaling by modulating β-catenin/LEF1 interaction [127, 128].

More recently, additional cytosolic OSTM1 binding partners have been identified, suggesting that OSTM1 might behave as an adaptor molecule within a cytosolic scaffolding multiprotein complex. In particular, a direct interaction of OSTM1 with the kinesin 5B heavy chains has been demonstrated, playing a role in intracellular trafficking and dispersion of cargos from the endoplasmic reticulum to late

endosomal/lysosomal subcellular compartments, which is relevant in physiopathological conditions [129].

Mutations in the *OSTM1* gene account for about 6% of ARO cases and invariably cause an extreme severe phenotype with rapidly progressing primary neurodegeneration. Almost all the identified mutations are truncating defects. In line, *in vitro* studies have recently demonstrated that a secreted form of truncated OSTM1 inhibits osteoclast formation through down-regulation of the BLIMP1-NFATc1 axis, thus providing a putative additional pathogenetic mechanism for OSTM1-deficient ARO [64].

PLEKHM1

The pleckstrin homology domain-containing family M (with RUN domain) member 1 (*PLEKHM1*) gene is located on human chromosome 17q21.31 and is composed of 11 exons [9].

It encodes a cytosolic protein implicated in endosomal trafficking pathways and containing a RUN domain, two pleckstrin homology (PH) domains separated from one another by an LC3-interacting region (LIR), a rubicon homology (RH) domain and a C1 zinc finger.

PLEKHM1 interacts with the small GTPases Ras-related protein Rab 7 (RAB7) and the ADP-ribosylation factor-like protein 8 (ARL8) and essentially acts as an effector, establishing multiple protein-protein interactions which ultimately permit trafficking, positioning and fusion of endosomes and lysosomes (Figure 11) [130]. [131]. In addition, PLEKHM1 participates in the fusion of autophagosomes and lysosomes, required for clearance of diverse protein aggregates. Disruption of the RUN or the PH domains, or loss of PLEKHM1 abrogates proper vesicle distribution and impairs secretion and ruffled border formation, leading to a detrimental effect on bone resorption in osteoclasts [132-135].

Recessive mutations in this gene have been identified only in two affected siblings, while in two unrelated patients two different putatively dominant mutations have been reported [9, 136].

SNX10

The sorting nexin 10 (*SNX10*) gene is located on human chromosome 7p15.2 and is composed of 7 exons.

The SNX family comprises a number of cytoplasmic and membrane-bound proteins sharing as common feature the presence of a phosphoinositide-binding domain, called PX domain. In general, SNX proteins take part in protein sorting and membrane trafficking by establishing protein-protein and protein-lipid interactions. In particular, SNX10 interacts with the V1 D subunit of V-ATPase (Figure 11) and regulates its subcellular trafficking. Recent studies in human cells and mouse bone tissue have definitely established that SNX10-deficient ARO is osteoclast-rich and is caused by defective osteoclast function due to disrupted V-ATPase trafficking to the ruffled border [114, 137]. Accordingly, the osteopetrosis associated with *SNX10* mutations closely resembles *TCIRG1*-dependent ARO and, since *SNX10* is expressed in the gastric epithelium too, it presents as osteopetrorickets.

Of note, mutations in *SNX10*, which overall account for about 6% of ARO cases, are responsible for "Västerbottenian osteopetrosis", so called from the name of the Swedish Province where a higher incidence of the disease has been reported.

3.4.2.2 Genes mutated in osteoclast-poor osteopetrosis

The vast majority of ARO cases in humans are osteoclasts-rich forms, in which a normal to high number of non-functional osteoclasts is present. On the contrary, osteoclast-poor cases are only a minority [138, 139]. Thus far, loss of function mutations in two genes have been involved in the pathogenesis of osteoclast-poor ARO: the *TNFSF11* (alias *RANKL*) and *TNFRSF11A* (alias *RANK*) genes [108, 140].

We have already extensively described the RANKL/RANK signaling axis (see chapter 3.1.1.4). Here we would just underline that the key difference between these two subgroups of patients is the fact that in RANKL-deficient ARO osteoclast precursors have a non-cell autonomous defect; indeed, they are able to correctly differentiate into functional osteoclasts *in vitro* and *in vivo* (in the *Rankl* knock-out mouse), once recombinant RANKL is exogenously provided [140, 141]. On the other hand, in RANK-mutated ARO a cell autonomous defect in the osteoclast lineage is present, so

osteoclast precursors *in vitro* and *in vivo* fail to differentiate and generate osteoclasts [108, 110].

Inactivation of either gene in mouse models causes also defects of the immune system, because of the critical involvement of the RANKL/RANK signaling axis in many immunological functions [142]. In patients, as far as it was investigated, a partial defect in cytokine production from T-cell in RANKL-deficient ARO [143] and a partial defect in B-cell immunoglobulin production in RANK-mutated ARO have been described [110].

3.4.2.3 Atypical forms of osteopetrosis

Osteopetrosis is sometimes associated with other pathologies, which results in extremely rare, atypical and more complex phenotypes.

An example is represented by dysosteosclerosis (DSS), a form of osteopetrosis characterized by red-violet macular atrophy of skin, platyspondyly and metaphyseal osteosclerosis, and caused by mutations in the solute carrier family 29 (nucleoside transporter), member 3 (*SLC29A3*) gene [144]. *SLC29A3* encodes a lysosomal nucleoside transporter present in different cell types, including osteoclasts. Its involvement in the pathogenesis of a skeletal disease underlines the importance of endosomal and lysosomal function in bone physiology (Figure 11).

X-linked osteopetrosis caused by mutation in the *NEMO* gene is peculiar in that the skeletal defect is accompanied by lymphedema, hypohidrotic ectodermal dysplasia (a congenital disorder of teeth, hair and eccrine sweat glands) and immunodeficiency (OL-HED-ID) affecting both T and B cells and responsible for multiple life-threatening infections [102, 145, 146]. NEMO (also called IKKγ) is a subunit of the I*k*B kinase complex that activates NF-κB (Figure 11). In the osteoclasts, NEMO deficiency blocks the activation of the IKK complex in the osteoclast precursors, thus impeding the osteoclastogenic process [147].

Additionally, in few patients osteopetrosis is associated with severe bleeding despite normal platelet counts, hemoglobin levels, and peripheral blood cell morphology; recurrent bacterial infections are present, too. These patients carry mutations in the fermitin family member 3 (*FERMT3*) gene, which encodes for kindlin-3, one of the three members of kindlin family. Kindlin-3 is an intracellular protein linked to the actin

cytoskeleton and expressed in hematopoietic cells (Figure 11). Mutations in the *FERMT3* gene are responsible for the rare autosomal recessive disease called leukocyte adhesion deficiency (LAD-III); interestingly, some LAD-III patients also suffer from severe osteopetrosis [148, 149]. Kindlin-3 interacts with multiple integrin classes and mediates their adhesive function and inside-out signaling, which in bone is essential for osteoclast resorptive activity. Indeed, kindlin-3 deficiency causes a severe morphological alteration of osteoclasts and impairs their ability to adhere to bone surfaces [150].

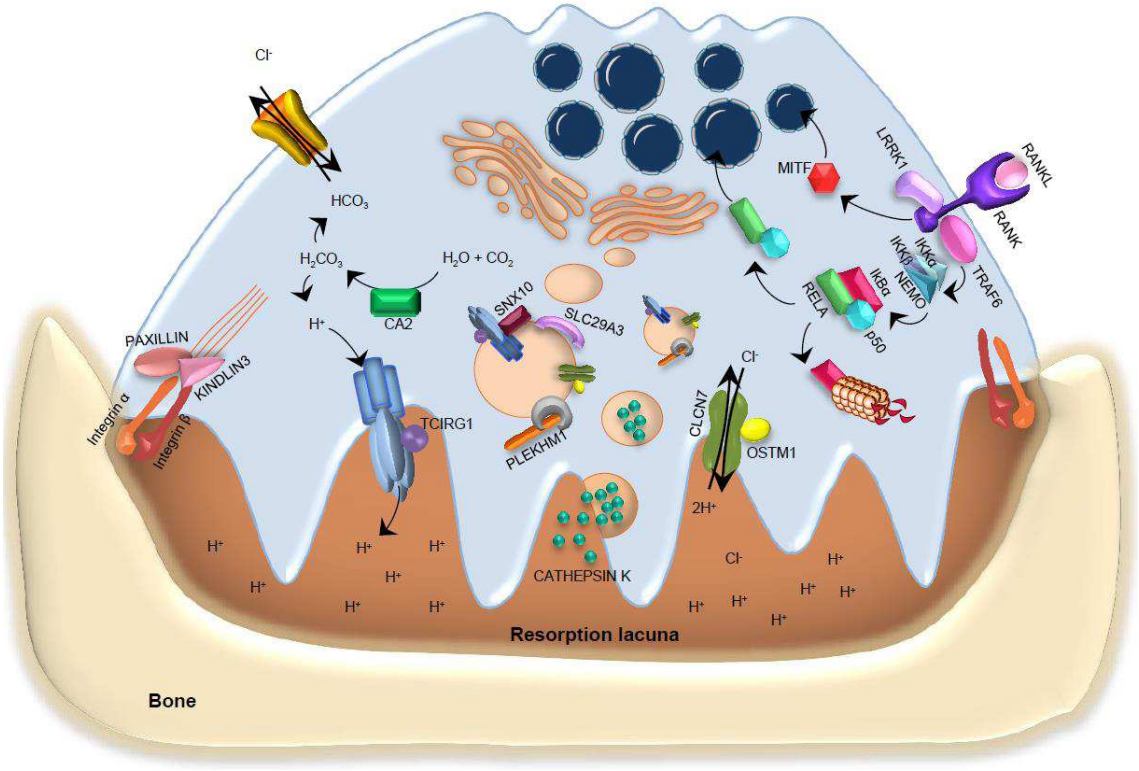

Figure 11: Schematic representation of genes important for osteoclast resorption that cause osteopetrosis when mutated.

Furthermore, a complex syndrome has been recently described in two unrelated patients and named COMMAD, because of the coexistence of coloboma, osteopetrosis, microphtalmia, macrocephaly, albinism and deafness. All these defects are explained by the presence of compound heterozygous mutations in the *MITF* gene in the two probands, altering nuclear migration and DNA binding properties of the encoded transcription factor [145].

Finally, two affected siblings have been very recently reported to display osteopetrosis and severe combined immunodeficiency (SCID) due to a homozygous genomic deletion encompassing the 5' region of *TRAF6*, recombination activating gene 1 and 2 (*RAG1*, *RAG2*) genes (the RAG proteins are essential for recombination of B and T cell receptors, and for the survival and differentiation of these cells) [146].

3.4.3 Diagnosis of osteopetrosis

Osteopetrosis can be recognized due to the presence of the typical clinical manifestations and radiographic appearance of the skeleton above described.

For the benign form of osteopetrosis, creatine kinase BB isoenzyme and TRAP can be informative [151]. For the recessive form, the presence of peculiar features like neurodegeneration, mental retardation, skin and immune system involvement or renal tubular acidosis, can point to a particular subtype of osteopetrosis. Bone biopsy can distinguish between osteoclast-poor and osteoclast-rich subtypes of ARO, but it is rarely performed because it is invasive and risky in these severely affected children.

Genetic testing confirms the clinical diagnosis and allows classifying each case in a specific ARO subtype, to provide additional information on prognosis and response to treatment, and for genetic counseling of family members and prenatal diagnosis.

3.4.4 Therapeutic treatment

In the majority of ARO patients, the functional defect is intrinsic to osteoclasts, cells of hematopoietic origin. Therefore, repopulation of the bone marrow with “healthy” donor cells via hematopoietic stem cell transplantation (HSCT) can cure the disease. The exception is TNFSF11-dependent ARO in which the osteoclast differentiation defect caused by absence of RANKL is non-cell autonomous, therefore cannot be corrected by HSCT.

The first bone marrow transplantation with a favorable outcome in an osteopetrotic patient was reported in 1980 [152]; so far, HSCT is the only curative treatment for ARO. According to the registry of the european society for immunodeficiences (ESID) and the inborn errors working party of the EBMT (IEWP-EBMT), nowadays ARO patients receiving an human leukocyte antigen (HLA)-identical HSCT have 88% of 5-

year disease-free survival, 80% in the case of HLA-matched unrelated donor and about 66% in the case of HLA-haplotype-mismatched related donor. Actually, percentages may vary (actually, may be lower) in different cohorts of patients [153].

In order to achieve the higher benefit for the patient, HSCT should be performed as soon as possible after diagnosis in order to prevent the establishment of irreversible secondary deficits. On the other hand, HSCT cannot cure neurological symptoms in patients, such as the OSTM1-defective subgroup, with early development of primary progressive neurodegeneration, which invariably leads them to death. Therefore, careful neurological assessment and monitoring of these patients is essential to define the treatment strategy.

Supportive care based on gamma-interferon, vitamin D/calcium supplementation or PTH is offered when HSCT is not performed because of a variety of hindrances, such as poor clinical condition of the patient. For the dominant form of osteopetrosis a standardized treatment protocol is not available: supportive care is usually offered and life-style strategies are suggested in order to reduce the risk of fracture. In very few, early onset ADO patients HSCT has been performed, but this is not a standard care, of course.

3.5 Acrofrontofacionasal dysostosis 1

The dysostoses are caused by defects in embryonic development. They may have high heterogeneity of clinical presentation; different skeletal compartments like cranium, face, axial or appendicular skeleton can be affected and symptoms at other organ can be present. In many cases, the molecular defect that causes the pathology is known, but some forms lack a molecular classification.

One of these cases is acrofrontofacionasal dysostosis 1 (AFFND1, OMIM: 201180) in which the mutated gene that leads to the disease is unknown.

AFFDN1 is a very rare syndrome (estimated prevalence less than 1:1,000,000 individuals) with predominant craniofacial and limb involvement. Principal features of the patients are short stature, facial and skeletal abnormalities such as cleft lip/palate, campo-brachy-poly-syndactyly and marked anomalies of foot structures, and intellectual disability (Figure 12).

AFFND1 is distinct from the form 2 (AFFND2), in which genitourinary anomalies are also present [154-157].

Until now, only four families, three of Brazilian and one of Indian origin, have been described as affected by AFFND1 [158-161]. The segregation of the disease in the families suggested an autosomal recessive pattern of inheritance, but the underlying genetic defect has not been identified, yet.

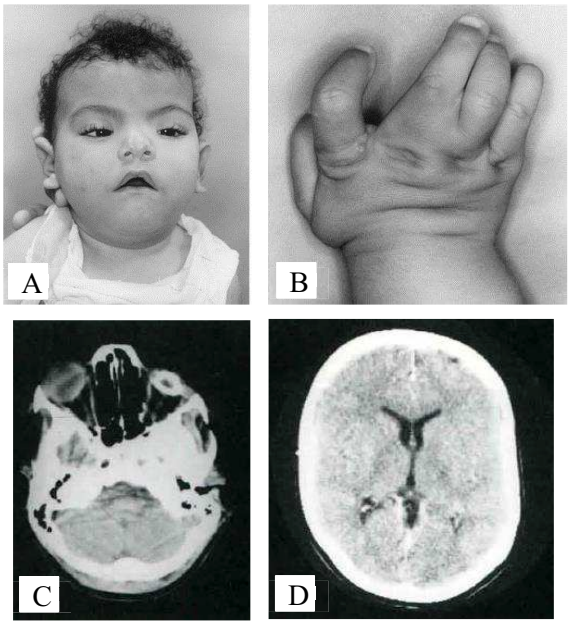

Figure 12: Representative pictures of the hallmarks of AFFND1. (A-B) A Brazilian patient showing wide forehead, broad-notched nasal tip, bilateral cleft lip and palate, camptodactyly. (C-D) Computed tomography (CT scan of one Brazilian patient showing normal cerebral parenchyma, microphthalmia with dense calcification of eye structures at left. Adapted from Richieri-Costa et al., 1992 and Guion-Almeida et al., 2003.

3.6 Next Generation Sequencing technology

The first human genome sequence was published in parallel in Science and Nature in 2001 and it took 15 years to sequence it [162, 163]. Since 2003, when the human genome project ended, the importance of genomics (the study of genomes) in biomedical research has become evident [164]. Therefore, more powerful tools have been designed, in order to achieve automation, dramatic shortening of the time required for the analysis (e.g. nowadays, a complete human genome can be read in a single day),

adaptation to different needs, substantial reduction of costs and wide exploitation. This modern high-throughput sequencing, also known as next generation sequencing (NGS), is based on capillary electrophoresis (CE) sequencing: it exploits fluorescently labeled deoxyribonucleotide triphosphates (dNTPs) that are identified by fluorophore excitation after the incorporation into a DNA template strand during each cycle. The essential step forward of NGS is the possibility to perform the same procedure as CE sequencing across millions of fragments at the same time (the so called massive parallel sequencing). Briefly, NGS workflow can be divided in 4 steps (Figure 13):

1. *Library preparation*. The DNA or complementary DNA (cDNA) sample is randomly fragmented by mechanical or enzymatic breakage, then adapters are added at the 5' and 3' ends.
2. *Cluster generation*. The library is loaded onto a flow cell where surface-bound oligonucleotides bind the complementary adapters linked to the DNA fragments. Each fragment is amplified into distinct clonal clusters through bridge amplification.
3. *Sequencing*. Fluorescent dNTPs are added; each time a base is incorporated, the corresponding emission of each cluster is recorded. The emission wavelength and its intensity identify the inserted base; this cycle is repeated "n" times to create an "n"-bases-long read.
4. *Data Analysis*. The reads are aligned to a reference genome and possible variations are identified [165].

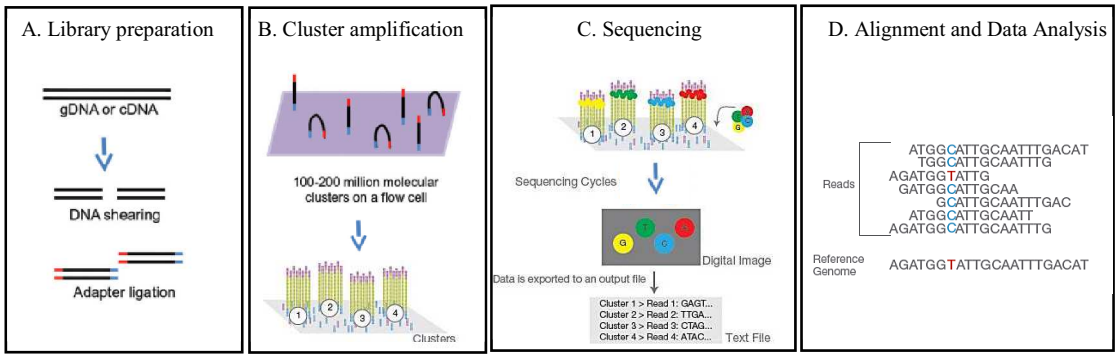

Figure 13: Next Generation Sequencing workflow. Adapted from Bahassi et al., 2014.

3.6.1 NGS applications

The study of the human genome using NGS technology is extremely useful for the understanding of the pathogenesis of human diseases and the improvement of clinical practice in terms of time to precise diagnosis and therapy. NGS clinical applications are divided according to the targeted sequences [166].

Briefly, whole genome sequencing (WGS) covers the entire genome of an individual. It is mainly exploited in genome-wide association studies, in which a high number of patients are sequenced to gain information about the connection between a certain disease or trait and genetic variants, including also those located in non-coding regions. This increases the knowledge of the pathophysiological mechanisms and can have implications for patient treatment, when the genetic component of a disease is searched.

Whole exome sequencing (WES) or sequencing of a panel of genes related to a specific disease or a category of disorders may find novel mutations in patients and is a useful tool in clinical diagnostics. The need to use targeted sequencing is due to the complexity of human diseases: on one hand, mutations in genes involved in the same pathway sometimes lead to similar clinical phenotypes; on the other, different mutations in the same gene can cause different disease manifestations.

NGS can be applied also to the study of the epigenome; in this case, platforms such as CHIP (chromatin immunoprecipitation)-seq-protein-DNA binding and histone modification allowing the mapping of the methylome of a genome, are used. Results achieved through these strategies are uncovering the importance of epigenetic alterations in physiopathology.

RNA-sequencing (RNA-seq) is a combination of hybridization capture of cDNA and NGS to analyze the full transcriptome of a cell and identify mutations, structural alterations and alternative splicing variants, and to quantify expression levels.

Finally, NGS can be applied to the analysis of microbial populations, which generated the new and rapidly expanding research field called metagenomics [167, 168].

3.6.2 Whole exome sequencing to diagnose Mendelian diseases

The human genome contains 3 billion base pairs comprising coding and noncoding sequences; only about 1-2% of the entire genome is translated into proteins, however it is estimated that almost 85% of the mutations causing Mendelian diseases are in gene coding and functional regions [169]. Hence, the rationale for applying WES to the diagnosis of Mendelian disorders stems.

The sequencing of an exome produces a list of hundreds of thousands of variants, which can be filtered using several parameters and prioritized on the basis of different strategies [170] such as:

1. Overlap-based strategy: in the absence of genetic heterogeneity for a given disease, sequencing unrelated patients with the same phenotype allows substantially decreasing the number of putative causative variants to further investigate.
2. Linkage-based strategy: in large families with known mode of inheritance, by sequencing individuals from different (preferably distant) generations presenting the phenotype and non-affected individuals, the causative variant(s) may be easily found in the small fraction of the genome shared by the affected subjects.
3. *De novo*-based strategy. For sporadic patients with a rare Mendelian disease, after sequencing of a *trio* (unaffected parents and affected child) a variant that is not present in the parents and appears for the first time in the patient is searched.
4. Allele frequency. More than 95% of the identified variants in exomes are polymorphisms present in the general population. Extremely large databases are available; the most comprehensive is the GnomAD browser, which collects genetic data from many large sequencing projects. Dealing with rare diseases, it is reasonable to exclude variants with allele frequencies > 0.01.
5. Predicted effect. Many *in silico* tools are available to predict the effect of a genetic change; some examples are SIFT, PolyPhen, Provean. The best strategy is to use more than one, since they are based on different algorithms. Loss-of-function variants such as insertions/deletions, stop codon gain or loss, and splicing defects are usually considered strong candidates, based on their obvious impact on the protein product. However, genome-sequencing studies have recently indicated the presence of a non-negligible number of loss-of-function

changes in the general population, suggesting a really unexpected tolerance for gene inactivation [171].

6. Presence in genes or molecular pathways already associated or with plausible association with the disease, based on data from literature.

At the end, the remaining variants have to be validated by Sanger sequencing and functionally tested in order to draw a definitive conclusion regarding their pathogenicity [171].

Whole Exome Sequencing limitation

Some limitations inherent in WES may hamper its final result in terms of disease-gene identification: first, also variants outside coding exons (i.e. in introns, untranslated regions, microRNAs, promoters, regulatory regions) can be responsible for the disease, but for their location are very likely missed by WES. Moreover, the databases used for variant filtering, in which a high number of exomes is reported, cannot effectively exclude non-pathogenic variants; this happen if these variants are specific of a populations not sufficiently represented in those sequencing projects leading to misinterpretation of results. On the same line, synonymous variants are most often filtered out in the early steps of a standard analysis workflow, based on the assumption that they are silent; actually, this may be an error: in fact, several recent reports in literature show that some of them can cause diseases through different mechanisms. In addition, the presence of GC-rich sequences can lead to uneven coverage and incomplete capture, while variable base quality and errors introduced during library preparation may affect variant calling [170].

4. **AIMS OF THE WORK**

The general objective of my project was to contribute to the understanding of bone pathophysiology by identifying new molecules involved in skeletal homeostasis. To this end, I initially focused on human osteopetrosis, in whom a precise molecular diagnosis has already been demonstrated to be relevant with respect to the prognosis of the disease and the response to therapy.

In detail, the specific aims of my project were:

1. To characterize the molecular defect in human osteopetrosis through:

1A. Molecular analysis of the known osteopetrotic genes by Sanger sequencing.

1B. Identification of a group of patients with atypical phenotype and unknown genetic defect; for this group I performed exome sequencing to obtain a list of variants possibly associated with the disease.

2. To evaluate the possible pathogenetic consequences of the putative mutations by *in silico*, *in vitro* and *in vivo* studies.

3. To apply the same technology and experimental approach to a different skeletal disorder. In particular, we collected patients from 3 different families affected by Acrofrontofacionasal dysostosis type 1 that is a neglected pathology in which the causative genetic defect is unknown.

5. **RESULTS**

5.1 Osteopetrosis project

During my PhD, in order to characterize the molecular defect in ARO patients I performed the analysis of the known osteopetrotic genes in 41 unrelated patients through PCR amplification and direct Sanger sequencing, according to protocols well established in our lab. Patients with atypical phenotype and unknown genetic defect were further investigated by exome sequencing to obtain a list of variants possibly associated with the disease (Figure 14).

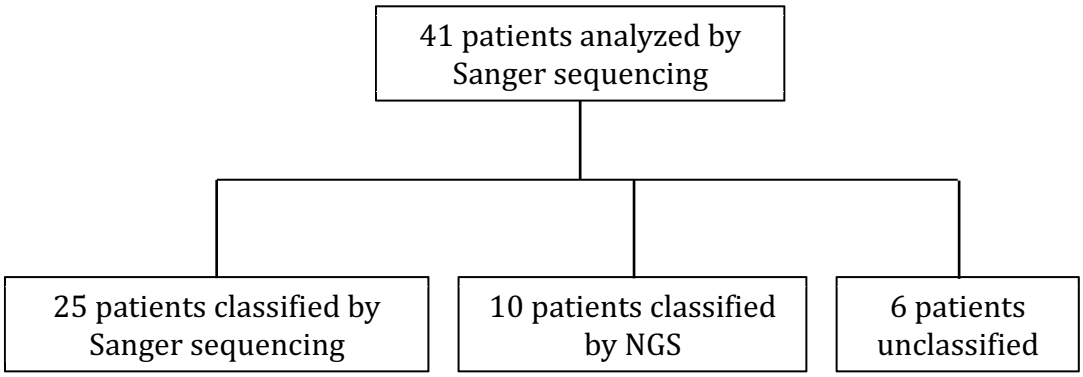

Figure 14: Scheme of the group of ARO patients classified by Sanger sequencing, NGS or without identification of causative mutations.

In detail, for 25 of these patients we identified the causative mutation (Table 2), whereas 6 patients remained unclassified.

The clinical diagnosis was ARO in most of the analyzed patients , ADO II in 2 patients and also ADO I in two patients. S23 was reclassified as Raine syndrome and will be specifically addressed below. Most of the analyzed patients were of Turkish (about 30%) and Caucasian origin (about 15%), the others included Iranians, Brazilians, Caribbeans, Ecuadorians and Kurdish. In this relatively small cohort of patients we confirmed that in ARO patients the most frequently mutated gene was *TCIRG1* (more than 40%); other mutations were located *CLCN7*, *SNX10*, *RANK*, *OSTM1*, *CA2*. The mutations that we found were missense mutations (51%), insertion/deletion (InDel) and nonsense mutations (32%) and mutations that impact in the splicing process (around 17%). Most of them were known mutations; in addition, we found 12 novel mutations that have been verified with *in silico* prediction. For 2 of them we confirmed the

negative effect of the splice site mutations analyzing the cDNA obtained from Peripheral blood mononuclear cells (PBMCs) of the patients.

Table 2: Mutations found in subjects with clinical diagnosis of osteopetrosis

Subject	Origin of subject	Diagnosis	Mutated gene	State	Specific mutation[§]
S1	Caribbean	ARO	*TCIRG1*	Homozygous	c.793C>T
S2	Turkish	ARO	*TCIRG1*	Homozygous	c.1384_86delAAC
S3	Brazilian	ARO	*TCIRG1*	Homozygous	c.346C>T
S4	Ecuadorian	ARO	*TCIRG1*	Homozygous	c.979C>T
S5	Turkish	ARO	*TCIRG1*	Homozygous	c.862delCinsAA
S6	Caucasian	ARO	*TCIRG1*	Homozygous	c.1559G>A
S7	Turkish	ARO	*TCIRG1*	Homozygous	c.196+5G>A
S8	Turkish	ARO	*TCIRG1*	Homozygous	c.1384_86delAAC
S9	Turkish	ARO	*TCIRG1*	Homozygous	c.1384_86delAAC
S10	Turkish	ARO	*TCIRG1*	Homozygous	del ex11_13
S11	Turkish	ARO	*TCIRG1*	Homozygous	c.702delG
S12	Turkish	ARO	*TCIRG1*	Homozygous	c.1165+5G>A
S13	Caucasian	ARO	*TCIRG1*	Homozygous	c.2236+1G>A
S14	Iranian	ARO	*CLCN7*	Homozygous	c.1727A>T
S15	Turkish	ARO	*SNX10*	Homozygous	c.152G>C
S16	Kurdish	ARO	*RANK*	Homozygous	c.443A>T
S17	Turkish	ARO	*RANK*	Homozygous	c.385C>T
S18	Turkish	ARO	*RANK*	Homozygous	c.443A>T
S19	Turkish	ARO	*FAM20C*	Homozygous	c.708C>A
S20	Iranian	ARO	*OSTM1*	Homozygous	c.811C>T
S21	Pakistan	ARO	*CA2*	Homozygous	c.291G>A
S22	Indian	ADO I	*LRP5*	Heterozygous	c.713C>T
S23	Caucasian	ADO I	*LRP5*	Heterozygous	c.200C>A
S24	Caucasian	ADO II	*CLCN7*	Heterozygous	c.2071A>G
S25	Caucasian	ADO II	*CLCN7*	Heterozygous	c.643G>A

[§]Accession number of the TCIRG1 variant cDNA: NM_006019; CLCN7: NM_001114331; LRP5: NM_001291902; SNX10: NM_013322; RANK: NM_003839; FAM20C: NM_020223; OSTM1: NM_014028; CA2: NM_000067. The numbering used starts with nucleotide +1 for the A of the ATG-translation initiation codon.

We also analyzed a patient born from consanguineous parents of Turkish origin and presenting at birth with respiratory distress, general osteosclerosis, craniosynostosis and visual problems, overall raising the suspect of ARO. However, the *facies* of the patient was reminiscent of a different pathology called Raine syndrome, which is included in the differential diagnosis of osteopetrosis; in fact, it presents as a neonatal osteosclerotic bone dysplasia, but periosteal bone formation differentiates it from osteopetrosis. Accordingly, we found a novel mutation (c.708C>A; p.Tyr236X) that causes the formation a stop codon in the *FAM20C* gene, which is known to cause Raine syndrome. *FAM20C* encodes a Golgi serine/threonine protein kinase that phosphorylates serine residues of proteins involved in bone mineralization including FGF23 and OPN.
Furthermore, we analyzed 2 ADO I patients of Indian and Caucasian origin that, as expected, demonstrated mutations in the *LRP5* gene and 2 ADO II patients both of Caucasian origin that showed the typical clinical features of a mild/benign osteopetrosis. Both patients presented visual impairment and were not diagnosed in infancy with a general clinical picture of benign osteopetrosis, only one of them reported several fractures. The molecular analysis, as expected, demonstrated mutations in the *CLCN7* gene.

In addition to patients analyzed by direct Sanger sequencing, I also performed exome sequencing analysis on 10 patients from 7 unrelated families (Table 3). Results are reported in the next paragraph.

Table 3: List of the families analyzed by exome sequencing and corresponding mutations

Family ID	# samples	Gene	State	Mutation[§]
1	2	*CLCN7*	Compound heterozygous	c.269T>C c.982-1G>T
2	3	*CLCN7*	Heterozygous	c.746C>T
3	1	*OSTM1*	Homozygous	c.25C>T
4	3	*FERMT3*	Homozygous	c.1802delA
5	4	*TCIRG1*	Homozygous	c. 1884+146G>A
6	3	*TCIRG1*	Homozygous	c.1371C>A
7	4	*C16orf57*	Homozygous	c.683del-AGGAACTACAGG

[§]Accession number of the CLCN7 cDNA variant: NM_001114331; OSTM1: NM_014028; FERMT3: NM_178443; C16orf57: NM_024598; TCIRG1: NM_006019. The numbering used starts with nucleotide +1 for the A of the ATG-translation initiation codon.

5.1.1 WES results: mutations in known ARO genes

Family 1 comprised the patient and his mother. The patient was diagnosed at 3 months of age as affected by severe ARO presenting also macrocephaly, frontal bossing and hepatosplenomegaly. The analysis of the exome showed that the patient was a compound heterozygous for two mutations in the *CLCN7* gene. A missense mutation, found also in his mother, in the exon 3 (c.269T>C) causes an amino acid change (p.Leu90Pro); a nucleotide change in the canonical acceptor splice site (c.982-1G>T), absent in his mother so presumably of paternal origin (the paternal DNA was not available), causes an alteration in the splicing process.

Family 2 was composed of 3 affected siblings with a typical ADO II presentation (Figure 15). The analysis revealed the presence of the known mutation c.746C>T in the exon 9 of the *CLCN7* gene that causes a change at the protein level (p.Pro249Leu), in all of them in the heterozygous state.

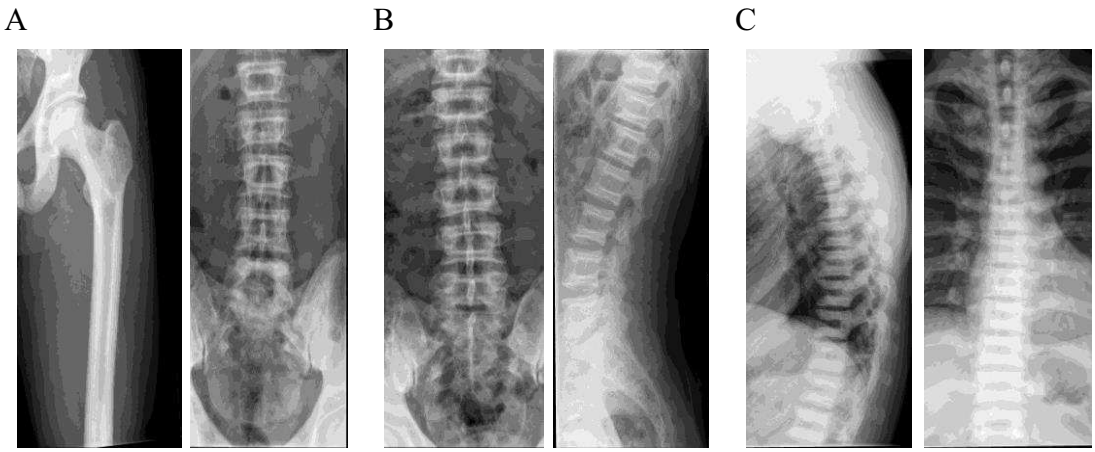

Figure 15: X-ray images of the patients of Family 2 showing the classical sandwich vertebrae and bone-in-bone appearance. (A), (B) and (C) show pictures of the three distinct patients, respectively.

In Family 3 WES was performed on the patient only. She was born from consanguineous parents, diagnosed at 15 days of age due to severe osteopetrosis, anemia, hepatosplenomeglay and thrombocytopenia. WES revealed the presence of a known mutation in the *OSTM1* gene (c.25C>T), causing a premature stop codon

(p.Gln9X), in the homozygous state, confirmed in the heterozygous state in the parents by Sanger sequencing.

Family 4 was composed of the proband and her parents. The patient was a female born from Pakistani consanguineous parents (first degree consanguinity) that presented at birth with widespread purpuric/petechial rash, hepatomegaly, limited bleeding of the scalp and severe anemia. The clinical picture included also very dense bones noted in radiographic analysis, and abnormal bone architecture, increased osteoclast number with limited signs of remodeling, and reduced residual hematopoiesis shown by bone biopsy examination (Figure 16A and 16B). Overall this suggested a diagnosis of osteoclast-rich ARO. At 2 months of age the patient underwent allogeneic HSCT from a match unrelated umbilical cord donor, which corrected the bone pathology (Figure 16C).

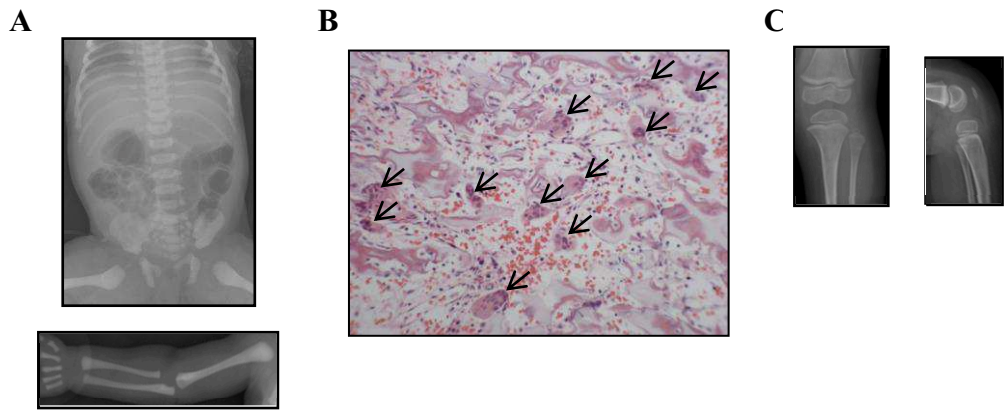

Figure 16: Clinical presentation of the patient from Family 4. (A) X-ray before HSCT, demonstrating the osteopetrotic phenotype. (B) Hematoxylin-eosin staining of iliac crest bone marrow trephine biopsy shows abnormal bone architecture (light blue) with cartilage remnants (bright pink), numerous multinucleated osteoclasts (arrows), and limited residual hematopoiesis. Magnification 10X. (C) X-ray performed 2.5 years after HSCT clearly showing restoration of normal bone density.

At the last follow-up, at 5.5 years of age, she was well, without visual, hearing or developmental problems, and attended school full time. The major complain was secondary dentition formation problems, that is common among osteopetrotic patients even after successful HSCT [9]. We performed the trio-based exome sequencing and

found a novel single nucleotide deletion (c.1802delA) in the *FERMT3* gene. This mutation was confirmed by Sanger sequencing in the homozygous state in the patient and in the heterozygous state in her parents. At the protein level, this mutation was predicted to cause a frameshift (p.Asn603Thrfs*) affecting the F3 domain which is involved in integrin binding [172]. Unfortunately, in the absence of an adequate sample from the patient, the presence of a mutated protein or absence of the wild type could not be evaluated by Western Blot; however, based on its position, the mutation was predicted to severely impact on the protein function and considered responsible for the disease in the patient.

5.1.2 Patients with particular mutations in known ARO genes

Deep intronic mutation in the TCIRG1 gene

Here we describe the study carried out on Family 5 (Table 3). Since this work has already been published, hereafter we will refer to these subjects and to all the patients reported in the manuscript according to the numbering adopted in the paper [173].

Family 1 was composed of two affected siblings (Pt 1A, female, and Pt 1B, male) born from Italian consanguineous parents (third-degree consanguinity). Pt 1A was evaluated for the first time when she was 6 years old, because of visual problems; she displayed a generalized increase in bone density (Figure 17A) and mild hepatosplenomegaly, thus a diagnosis of mild osteopetrosis was made. So, her younger brother (Pt 1B) was investigated too, and received a similar diagnosis at 2 years of age (Figure 17B).

Figure 17: Radiographic analysis of the patients showing the typical signs of the disease. (A) Pt 1A at 6 years of age. (B) Pt 1B at 2 years of age. (C) Pt 2 at 22 years of age.

During the follow up, both patients suffered from recurrent fractures (8 in Pt 1A and 11 in Pt 1B), dental problems, and progressive deterioration of the visual acuity in Pt 1A; laboratory investigations did not show significant alterations of the evaluated parameters. The histological analysis on a bone specimen from Pt 1A showed an incomplete osteopetrosis with some areas containing mineralized cartilage, normal lamellar bone in well-formed trabecular bone and osteoclasts (Figure 18).

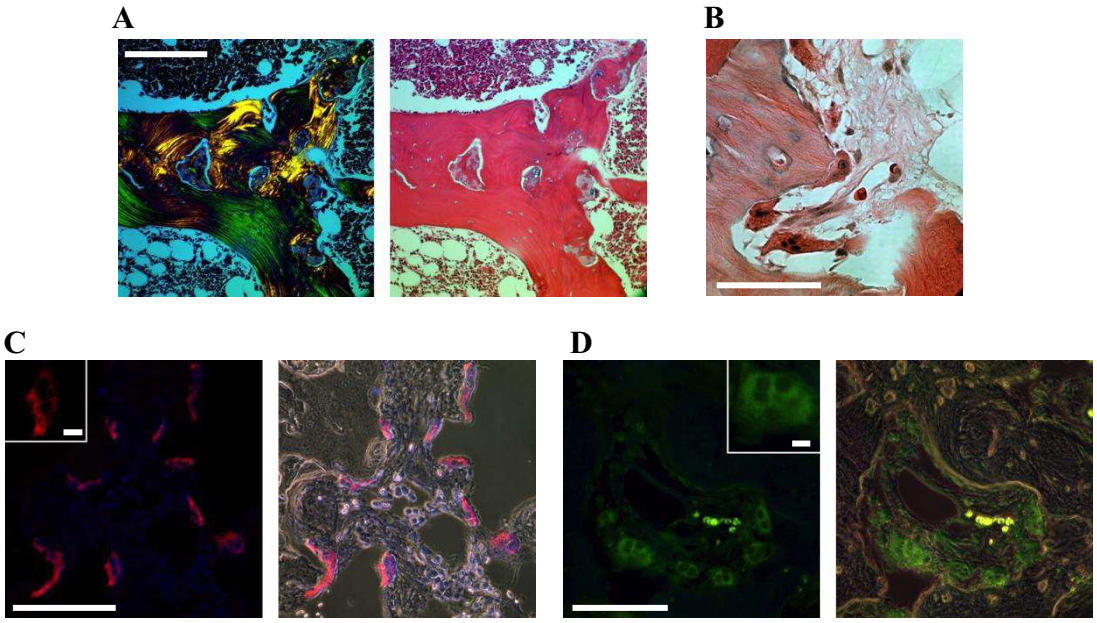

Figure 18: Representative histological sections of a formalin-fixed paraffin-embedded decalcified bone specimen of Pt 1A at 35 years of age. (A) Visualization in polarized light (left) and hematoxilin-eosin (right) staining: the mature cortical bone shows lamellae in polarized light; islands of retained mineralized cartilage are present. Scale bar: 200 µm. (B) Hematoxilin-eosin staining showing several multinucleated osteoclasts. Scale bar: 100 µm. (C) TRAP fluorescent antibody labeling (red) and phase contrast with the fluorescence image overlaid; nuclei are stained with Hoechst (blue). Scale bar: 100 µm. The inset shows a single osteoclast at twice the magnification. Scale bar: 10 µm. (D) TCIRG1 fluorescent antibody labeling (green) and phase contrast with the fluorescence overlaid (right). Scale bar: 100 µm; inset: 10 µm.

When we performed this work, both patients (Pt 1A 37 years old, Pt 1B 33 years old) were not receiving any specific therapy and overall their clinical picture could be considered benign. The molecular analysis of the genes known to cause recessive osteopetrosis did not identify any mutation. Therefore, we performed WES on both patients and their parents and found 32 homozygous variants in coding regions not including obvious candidate genes, so we focused our attention on variants in 3'

untranslated regions (UTR) based on the assumption that they could influence gene expression [174]. In particular, we noted a variant in the 3'UTR of the choline kinase alpha (*CHKA*) gene, which maps to chromosome 11q13.2 on the reverse strand as compared to the *TCIRG1* gene. Because of the close proximity of the two genes, we asked if the variant in the *CHKA* could influence the expression of the *TCIRG1* gene. Investigation at the cDNA level in the patients through reverse transcriptase-polymerase chain reaction (RT-PCR) spanning exons 14 to 17 did not show a reduction in the expression of TCIRG1, but the unexpected formation of at least two different transcripts in both affected siblings (Figure 19A), suggesting a splicing aberration. So we sequenced the entire genomic region between exons 14 and 17, including the intronic parts, and identified a single nucleotide change in the middle of intron 15 (c.1884+146G>A) which was present in the homozygous state in both patients and in the heterozygous state in their parents (Figure 19B). Moreover, this variant was absent in dbSNP and in 100 control chromosomes from a matched population. *In silico* analysis suggested a potential alteration of the splicing process even though this change was far from both the canonical donor and acceptor splice site. In order to confirm this prediction, we cloned the cDNA PCR product spanning exons 14 to 17, sequenced 73 independent clones, and found that the large majority carried aberrant transcripts (namely, we identified at least 8 different transcripts), while only 4 clones displayed the wild type sequence. The two most abundant molecular species showed either retention of 144 nucleotides of intron 15 (22/73 clones) or skipping of the first 183 nucleotides of exon 15 and retention of 144 of intron 15 (30/73 clones) (Figure 19C). Overall, these data supported the hypothesis of a pathogenic role of this intronic variant.

This unexpected result prompted us to sequence *TCIRG1* intron 15 in 26 osteopetrotic patients without molecular diagnosis and in 7 ARO patients in which we had previously identified a single mutated *TCIRG1* allele [104, 109]. We did not find any mutation in the 26 unclassified patients, but in 3 out of 7 patients carrying a single mutated *TCIRG1* allele we found additional heterozygous single nucleotide changes in intron 15.

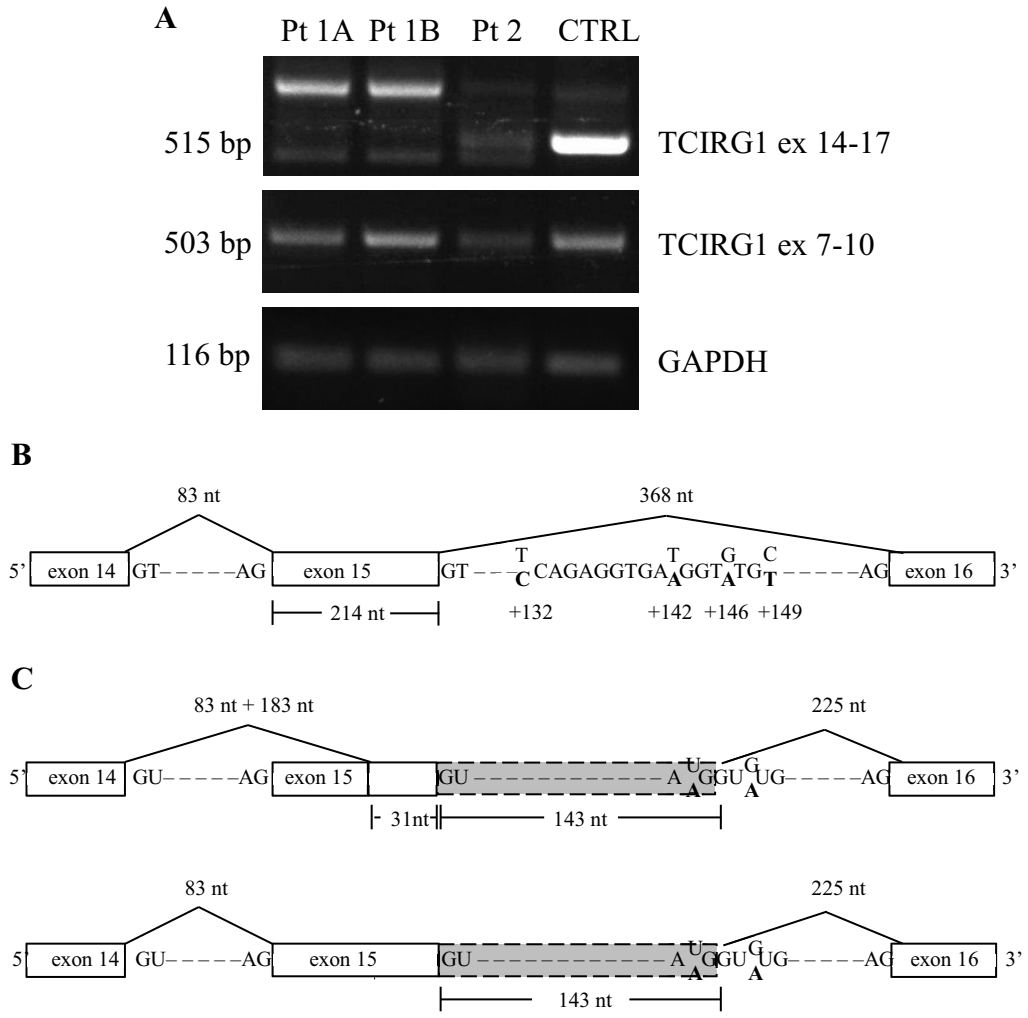

Figure 19: (A) Semi-quantitative RT-PCR spanning either exons 14 to 17 (upper panel), showing the presence of at least two abnormal bands in the patients (the normal band visible in Pt 2 is from the other mutated allele), or exons 7 to 10 (middle panel), showing only the presence of the expected band in all the samples. The amplification of the GAPDH gene is used as housekeeping (lower panel). (B) Schematic representation of the region of the TCIRG1 gene from exon 14 to 16, highlighting the position of the mutations identified in intron 15; the nucleotide change found in each patient is in bold in the lower line. (C) Structure of the most frequent aberrant transcripts found in Pt 1A, Pt 1B and Pt 2: clones in which only the last 31 nucleotides of exon 15 are retained, followed by 143 nucleotides of intron 15 (upper panel), and clones retaining 143 nucleotides of intron 15 (lower panel). The nucleotide change found in each patient is in bold in the lower line, as in (B).

Among these 3 patients, Patient 2 (Pt 2) was the third child of unrelated Italian parents and was diagnosed at 4 years of age with a generalized increase in bone density (Figure 17C). He reported 7 non-traumatic fractures; he did not display neurological or sensorial deficits, and was alive and reasonably well at 24 years of age.

Patient 3 (Pt 3) was already described as Pt 6 in Mazzolari et al., 2009 [109]; she was diagnosed at 6.5 months of age as classical ARO with bone defect and secondary hematological and neurological deficits. She received HSCT from a matched unrelated donor at 20.5 months with a favorable outcome: she was alive and well 7.5 years after transplantation.

Patient 4 (Pt 4) was born from unrelated parents from Southeastern Asia, presented with bone defects, blindness and hepatosplenomegaly in neonatal life. He received HSCT but unfortunately died 4 years after the treatment without engraftment.

All the mutations found in these patients were in close proximity to that present in Pt 1A and Pt 1B: c.1884+142T>A in Pt 2 (mutation confirmed in the heterozygous state in Pt 2's healthy mother and in one unaffected brother), c.1884+132T>C in Pt 3 and c.1884+149C>T in Pt 4 (Figure 19B, Table 4).

Table 4: Deep intronic mutations in intron 15 of the TCIRG1 gene

Patient	Genomic change[#]	Location	cDNA change[§]	Effect
1A and 1B	g.10466G>A	Intron 15	c.1887+146G>A	Putative aberrant splicing
	g.10466G>A	Intron 15	c.1887+146G>A	Putative aberrant splicing
2	g.9909G>A	Exon 14	c.1559G>A	p.Trp520X
	g.10462T>A	Intron 15	c.1887+142T>A	Putative aberrant splicing
3	g.11622T>C	Exon 19	c.2345T>C	p.Met782Thr
	g.10452T>C	Intron 15	c.1887+132T>C	Putative aberrant splicing
4	g.8600T>C	Intron 11	c.1305+2T>C	Putative aberrant splicing
	g.10469C>T	Intron 15	c.1887+149C>T	Putative aberrant splicing

[#] *_Accession number genomic sequence of the TCIRG1 gene: AF033033.*
[§] *_Accession number of the TCIRG1variant1 cDNA: NM_006019; the numbering used starts with nucleotide +1 for the A of the ATG-translation initiation codon.*

Also for these novel variants, *in silico* analysis predicted a potential disruptive effect on splicing process. The confirmation was performed in Pt 2, because his cell sample was the only available, by RT-PCR, cloning and sequencing of the PCR product. We found the same pattern of aberrant transcripts already described for Pt 1A and Pt 1B; in detail, 12/75 clones retained 143 nucleotides of intron 15, 20/75 clones skipped the first 183 nucleotides of exon 15 and retained 143 nucleotides of intron 15, 20/75 clones skipped the first 183 nucleotides of exon 15 and retained 141 nucleotides of intron 15. In

addition, other less frequent species and a residual amount of wild type transcript (5/75 clones) were also present.

Based on sequence analysis of the aberrant transcripts, we hypothesized that the molecular pathogenetic mechanism elicited by all these mutations in intron 15 could be the usage of an internal, cryptic acceptor site in exon 15 and of an intronic, cryptic donor site in intron 15, causing loss of part of exon 15 and retention of 143 nucleotides of intron 15, respectively (Figure 20).

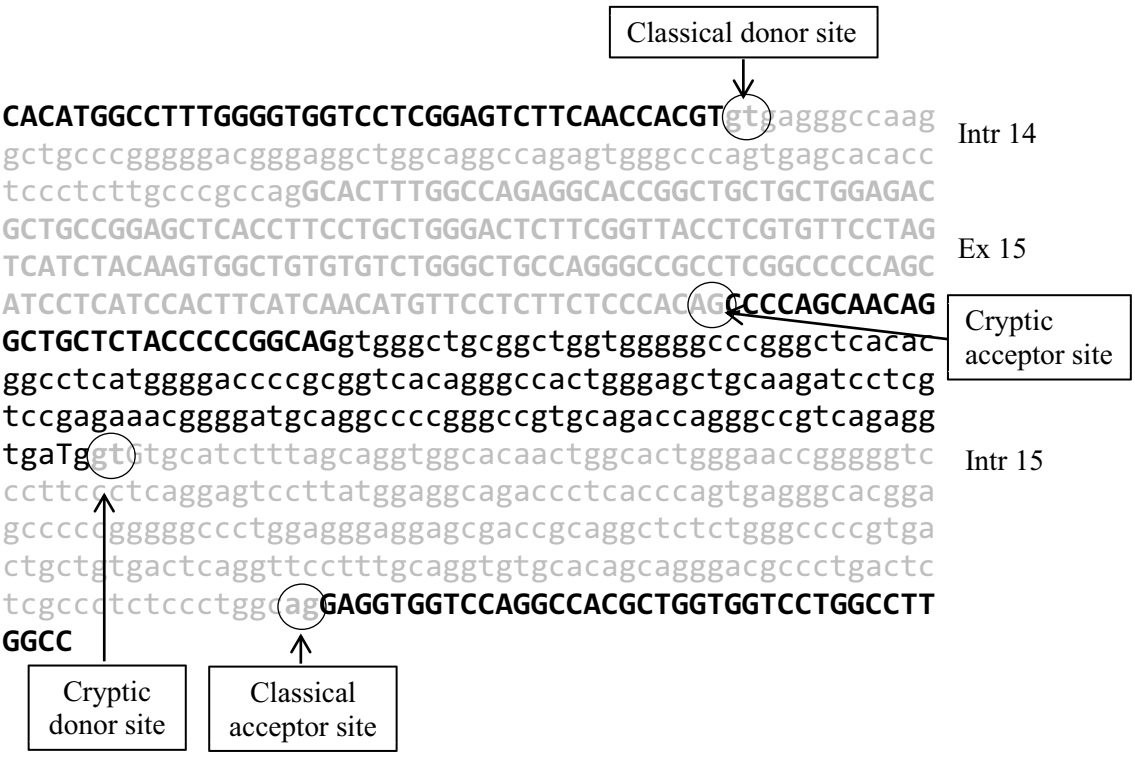

Figure 20: Proposed mechanism of aberrant splicing; upper case indicates exonic regions, lower case intronic ones. In grey was reported the intronic and exonic part lost after the aberrant splicing and in black the part maintained in the aberrant transcript.

Synonymous but not silent mutations

Family 6 analyzed in my thesis (Table 3) has been described in our work Palagano et al., J Bone Miner Res 2017, therefore the subjects therein described will be hereafter numbered as in the paper [175]. Patient 1 was diagnosed at 2 months of age as severe osteopetrosis; in the absence of a matched donor, HSCT was not performed and she died at 18 months of age because of septic shock (patient described in Mazzolari et al., 2009, as Pt 14) [109]. Since Sanger sequencing of the patient had not identified obvious mutations in the known ARO genes, the entire family (i.e. the proband and her parents)

was analyzed by WES. Also WES did not detect variants possibly responsible for the disease, after application of common filters to exclude low quality, common and synonymous variants. However, a synonymous variant attracted our attention: it was located in exon 12 of the *TCIRG1* gene (c.1371C>A, p.Thr457Thr), segregated as expected based on parental consanguinity (it was present in the homozygous state in the patient and in the heterozygous state in his parents) and was absent both in single-nucleotide polymorphisms (SNPs) databases and in our in-house database. This specific threonine residue is highly conserved during evolution and in particular the adenosine nucleotide in the third position of the corresponding codon was never present (Figure 21A). Moreover *in silico* studies with different software confirmed the possible formation of a new acceptor site that could alter the splicing process (Human Splicing Finder prediction of +49.30% of variation, Fruitfly software score of 0.85).

Unfortunately we did not have an RNA sample from the patient or his parents, so we tested these predictions by means of the well-known minigene technology. The minigene vector is an hybrid construct that allows performing a functional splicing assay reproducing the splicing pattern of a specific genomic sequence inserted therein after transfection in eukaryotic cell lines [176]. In detail, we cloned the wild type or the mutated *TCIRG1* genomic region spanning exons 11 to 13 into the pTB minigene vector (Figure 21B), transfected the constructs in HeLa cells and 48 hour later analyzed the pattern of transcripts obtained. We confirmed that the variant c.1371C>A caused aberrant splicing, with loss of 67 nucleotides (Δ67nt) of exons 12, due to the usage of the internal acceptor site created by the mutation (Figure 21C e 21D). The minigene vector is an artificial system, so it is expected that a variety of transcripts are also produced in HeLa cells transfected with the wild type construct. However, the key point is the complete absence of the splicing aberration Δ67nt in clones carrying the wild type TCIRG1 sequence (Figure 21C). At the protein level the Δ67nt transcript was predicted to result in frameshift and premature termination (p.Ile436AlafsX70).

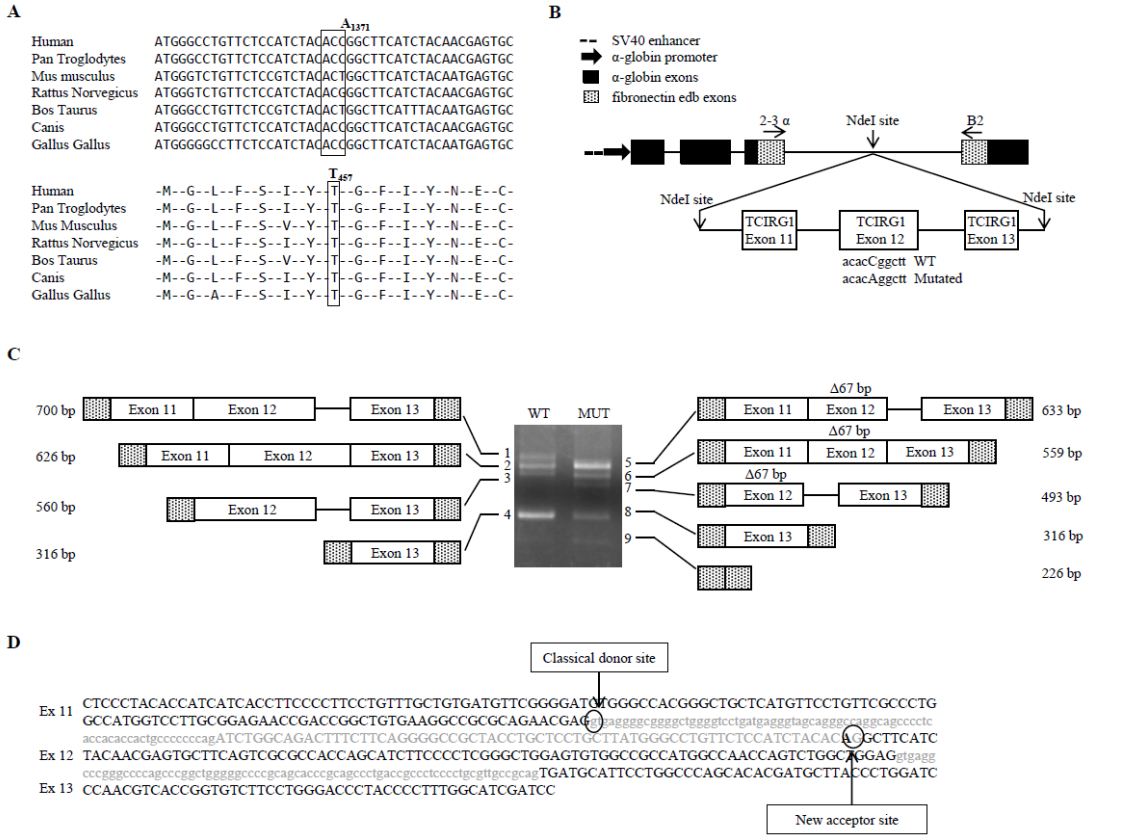

Figure 21: (A) Sequence alignment of the TCIRG1 gene and protein in the region of interest in different species. The alignments show absence of the adenosine residue (A1371) in the last position of codon 457 (referring to number of the human sequence) in the gene, and evolutionary conservation of the Threonine residue in the protein. (B) Schematic representation of the insertion of TCIRG1 sequence in the minigene vector. (C) Analysis of the amplicons obtained from minigene constructs carrying the normal or the mutant TCIRG1 sequence; schematic representation of the sequence of the different transcripts. (D) Sequence of the most abundant aberrant transcript of TCIRG1 gene; upper case illustrates exonic regions, lower case intronic ones. The creation of a new acceptor site in exon 12 (circled), possibly used instead of the canonical one, causes the loss of part of the exon 12.

Prompted by this finding, we checked other osteopetrotic patients in our series lacking a molecular diagnosis and we obtained a similar finding in another patient (Pt 2). He was born from an Italian mother and a Moroccan father. At 2 months of age he showed splenomegaly, thrombocytopenia and anemia. Total body radiography revealed a generalized increase in bone density (Figure 22A); all these findings led to the diagnosis of ARO. At 7 months of age he received HSCT from a fully matched unrelated donor, 3 months later hemoglobin and platelet levels were in the normal range and 1 year after transplantation the bone defect was completely corrected (Figure 22B). At last follow up at 5.6 years, the patient was alive and well, despite impaired vision.

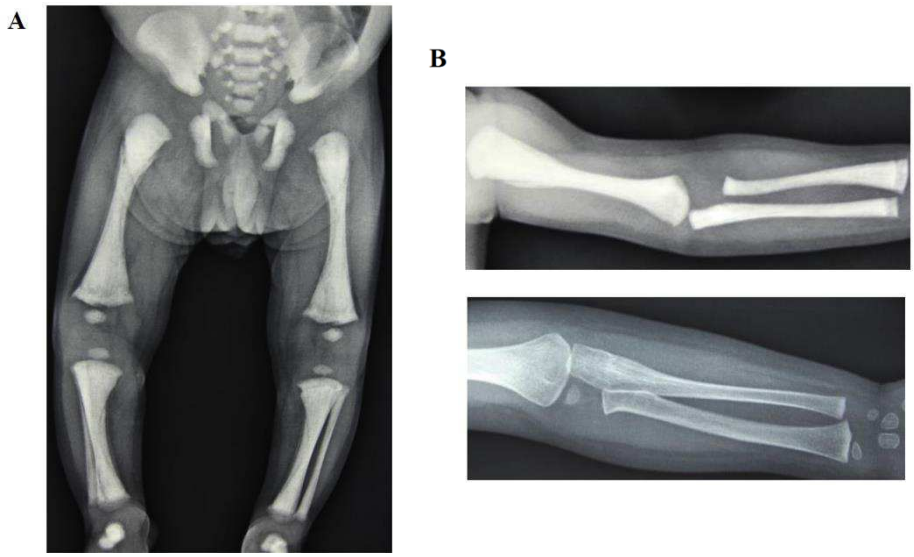

Figure 22: Representative radiographs of Pt 2 showing (A and B, upper panel) diffuse increase in bone density compatible with osteopetrosis diagnosis; (B, lower panel) complete restoration of bone phenotype and marrow cavity after transplantation.

In this patient a synonymous mutation was found in the *CLCN7* gene in a compound heterozygous state: the mutation, located on the paternally-inherited allele, was a single nucleotide change (c.1098G>A) in the last base of exon 12, that caused an amino acid synonymous substitution (p.Glu366Glu) never reported in any database to the best of our knowledge. On the maternally-inherited allele, a deletion of two nucleotides in intron 17 (c.1617+6_1617+7delTG), close to the canonical acceptor splice site, was detected.

Both mutations were predicted to cause splicing aberration. To confirm this prediction, we analyzed the cDNA of the patient by amplifying separately the two relevant regions spanning exons 11 to 16 and exons 16 to 20, respectively, cloning the RT-PCR products and sequencing about 50 independent clones (Figure 23A). Sequence analysis revealed that the synonymous mutation c.1098G>A caused in-frame skipping of exon 12 thus demonstrating a non-neutral effect (Figure 23B, left panel); on the other hand, the c.1617+6_1617+7delTG mutation gave rise to at least 3 aberrant transcripts showing either retention of 230 nucleotides of intron 17 or complete skipping of exon 17, both predicted to cause frameshift, or deletion of 93 nucleotides of exon 17 that could cause in frame loss of 31 amino acids (Figure 23B, right panel). To understand if normal transcripts were present too, we amplified a larger *CLCN7* cDNA region spanning

exons 11 to 18 containing both mutations. We cloned the RT-PCR product and sequenced independent clones, but we could never find the wild type transcript (Figure 23C); even the band that migrated similarly to the normal transcript, once sequenced, turned out to lack 13 nucleotides as compared to the wild type.

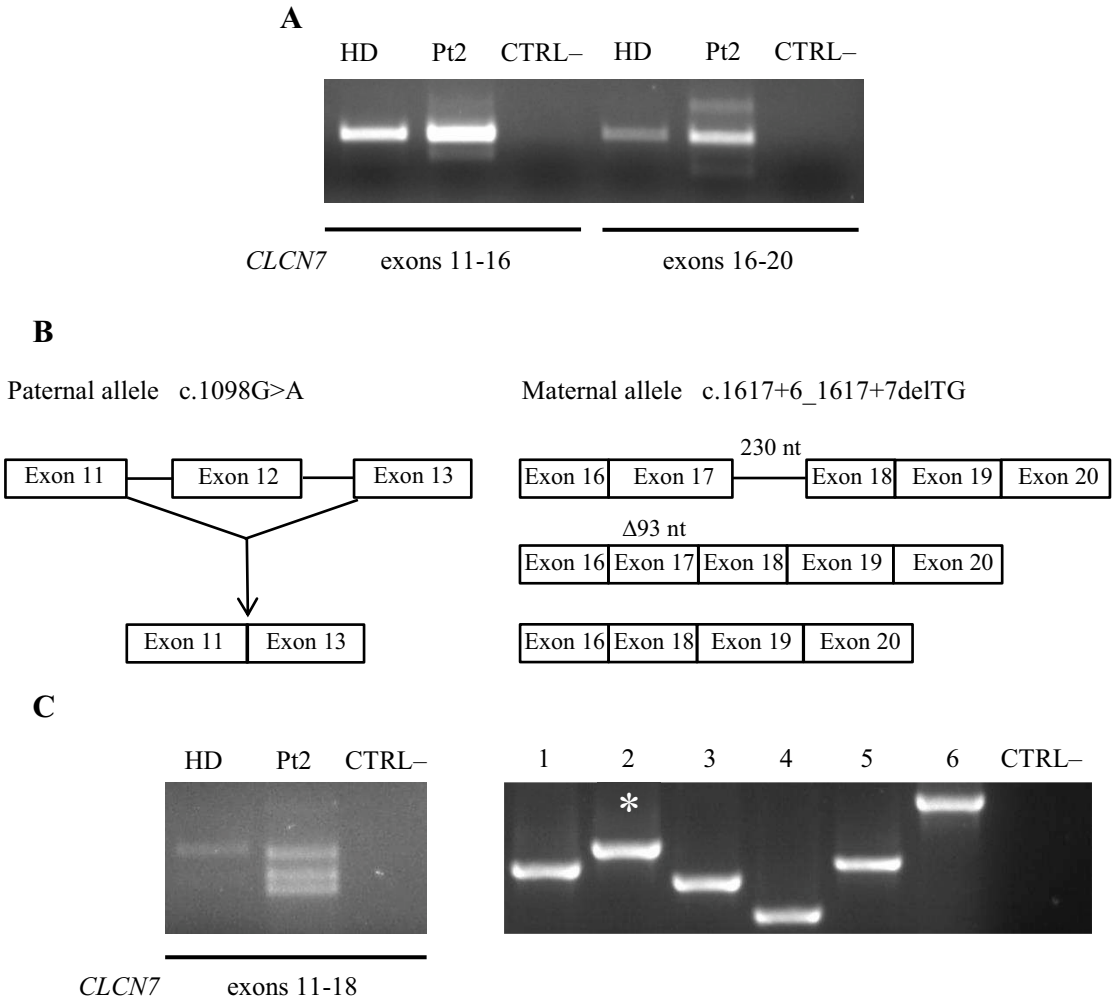

Figure 23: (A) RT-PCR of the CLCN7 gene in Pt 2 separately amplifying the two mutations. (B) Schematic representation of the principal aberrant transcripts: the mutation of paternal origin caused skipping of exon 12 (on the left), whereas the maternal one led to at least three different transcripts (on the right). (C) RT-PCR spanning exons 11 to 18 of the CLCN7 gene in Pt 2 cDNA (left panel) and PCR amplification of 6 independent clones (right panel). The asterisk indicates the apparently normal transcript lacking 13 bases respect the wild type. HD= healthy donor; CTRL–: negative control.

Overall, these results confirmed that both mutations affected the splicing process and did not allow any residual normal transcript.

5.1.2 Atypical genes involved in the pathogenesis of osteopetrosis

The patient of Family 7 was born from Italian consanguineous parents (second degree consanguinity). Osteopetrosis was diagnosed at 2 months of age; at presentation, he displayed anemia, thrombocytopenia, neutropenia, hepatosplenomegaly, hyperferritinemia and hyperbilirubinemia. The bone biopsy showed the presence of many osteoclasts with scarce signs of resorption, suggesting a diagnosis of osteoclast-rich osteopetrosis, confirmed by radiological investigation (Figure 24). At 7 months of age growth and development were normal, neurological defects absent, hemoglobin levels normalized, spleen and liver were palpable, but in normal range of size. In this patient we performed Sanger sequencing of the known ARO genes but we didn't find mutations. So, WES of the entire family, comprising the proband, his healthy sister and parents, was performed. While the analysis was ongoing, at 9 months of age the patient started displaying translucent papular skin lesions, which worsened over time and were classified as poikiloderma after histological examination. Moreover, neutropenia became more pronounced and was treated with G-CSF; on this basis, the diagnosis of poikiloderma with neutropenia (PN) was made. Interestingly, a single patient affected by PN and osteopetrosis (OP) has been described in literature [177].

In 2010, two different groups, analyzing unrelated patients, found *C16orf57* (also known as *USB1*) as the gene responsible for PN [178, 179].

Accordingly, in our patient, WES revealed a 12-nucleotide deletion in the *USB1* gene (c.683_693+1del) in the homozygous state in the proband and heterozygous in the other family members (confirmed by Sanger sequencing). The same mutation had been already reported in a PN patient at the heterozygous state and caused skipping of exon 6 at the cDNA level [178].

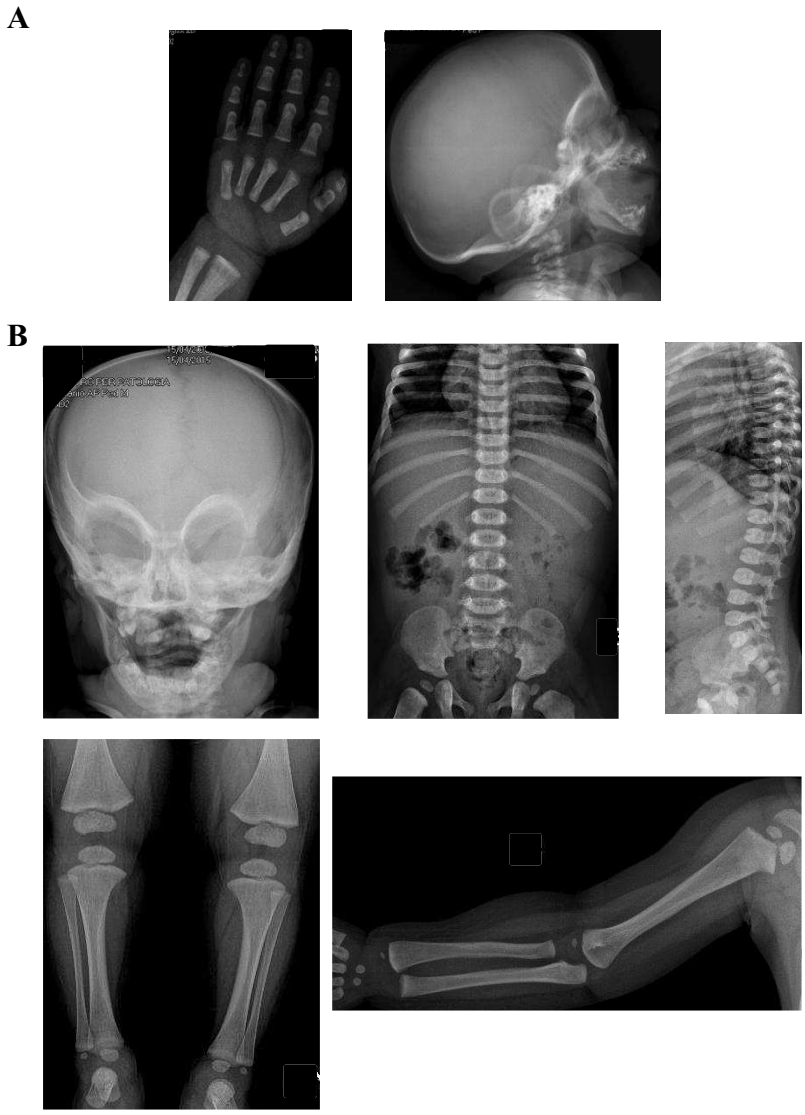

Figure 24: Representative radiological images of the patient of Family 7 at diagnosis (2 months of age; panel A) and at 1 year of age (panel B). Typical signs of osteopetrosis, such as thickening of the skull base, sign du masque, sandwich vertebrae, diaphiseal thickening of long bones and clubbing of metaphyses, were clearly visible.

5.2 Acrofrontofacionasal dysostosis 1 project

Acrofrontofacionasal dysostosis type 1 is a very rare syndrome: only four families, three of Brazilian and one of Indian origin, have been described so far and an autosomal recessive pattern of inheritance has been suggested.

In order to define the molecular basis of AFFND1, we collected DNA samples from the Indian family (Family 8) and from two Brazilian families (Family 9 and 10) (Table 5).

Table 5: list of AFFND1 families analyzed by exome sequencing

Family ID	# samples	gene	mutation
8	4	*NBAS*	c.6237-3C>G
9	2	ongoing	
10	3	ongoing	

[$] *Accession number of the NBAS cDNA variant: NM_015909. The numbering used starts with nucleotide +1 for the A of the ATG-translation initiation codon.*

Family 8 was composed of two affected siblings (the elder one had already been described in Prontera et al.) and their parents [161]; the two Brazilian families included a single patient already reported in Richieri-Costa et al., and in Guion-Almeida and Richieri-Costa; in Family 9 only one parent was available for the analysis [159, 160]. Parental consanguinity is reported in two out of these three patients (the Indian and Brazilian families) and suspected in the other one.

5.2.1 Clinical presentation of patients

All the patients (Figure 25) shared a common presentation of the disease, with craniofacial abnormalities including brachycephaly, wide forehead and nasal bridge, hypertelorism, abnormal hairline, cleft lip and palate, ear anomalies, malar hypoplasia; limb defects, including campto-brachy-poly-syndactyly, broad thumbs, mesomelic shortness of the legs, hypoplastic nails and phalanges of toes; and severe intellectual disability. The Indian patient also showed oligodontia, hypoplastic gums, wide and protruding upper central incisors.

Her younger sibling presented at birth with several dysmorphic features, including hypertelorism, epicanthus, long and dystrophic eyelashes, palatoschisis, brevity of arms with cutaneous folds, clinodactyly, flexed and adducted thumbs, sacral dimple with abundant fuzz and microcephaly with diastasis of anterior and posterior cranial suture.

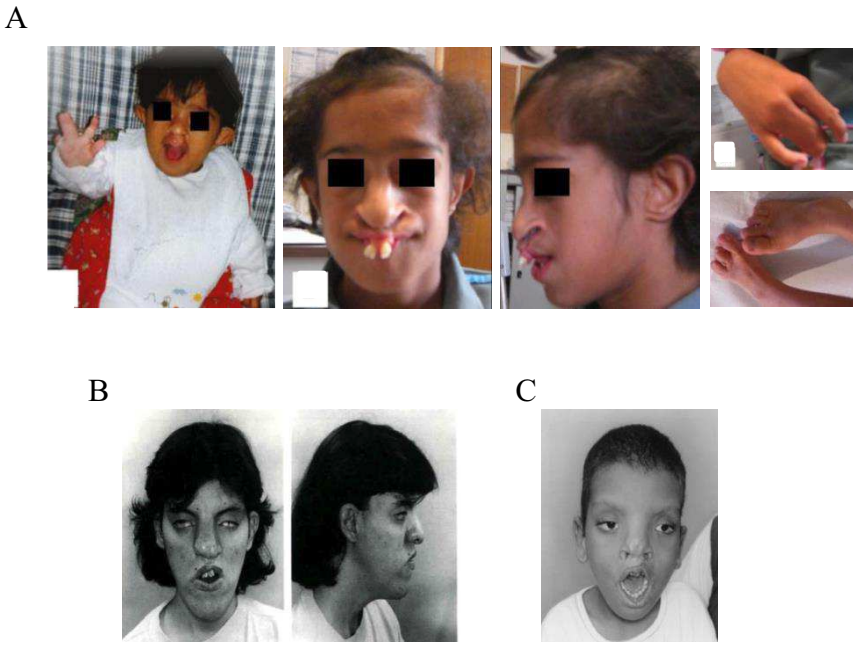

Figure 25: Clinical aspects of AFFND1 patients. (A) Clinical pictures of the elder patient of Family 8 at 3 months of age (first panel on the left) and at 12 years, showing wide nasal bridge, wide and protruding upper central incisors, downturned ears with wide conchae, thin helices and absent lobules and camptodactyly and clinodactyly of the 5th digit. (B) Clinical pictures of the patient of Family 9 at 26 years of age. (C) Clinical picture of the patient of Family 10 showing macrobrachycephaly, a wide forehead, a widow's peak, macrostomia with open mouth, mild S-shaped palpebral fissures, palpebral ptosis and convergent strabismus.

At 8 months of age, microcephaly (orbitofrontal cortex, OFC 38.8 cm) with open anterior and posterior fontanel, dysmorphisms (hypertelorism, exotropia, posterior palatoschisis and short lingual frenulum) and marked growth defects with diffuse muscular hypotrophy were observed. Neurological examination clearly documented severe neuropsychomotor delay: the patient displayed drastic truncal hypotonia with very limited control of the head, and distal hypertonus with increased tendon reflexes. Eye examination confirmed bilateral optic atrophy and brain Magnetic Resonance Imaging (MRI) showed slightly thinned corpus callosum (Figure 26).

The karyotype was normal (46, XX) and search for subtelomeric deletions (22q11 microdeletions) possibly responsible for the severe neurological impairment was negative, as also previously observed in her older daughter. A subsequent examination was performed at 2 years and 7 months of age; progressive neuropsychomotor delay was evident: she achieved trunk control, but showed pyramidal signs, stereotyped and a-finalistic movements, poor social interaction, absence of verbal language.

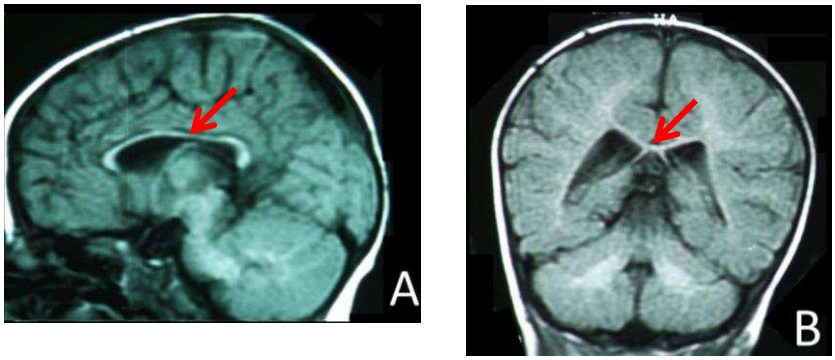

Figure 26: Brain MRI of the younger sibling of Family 8 at 8 months of age. The images show slight thinning of the corpus callosum in sagittal (A) and coronal (B) view (red arrow).

Microcephaly, growth retardation and diffuse muscular hypotrophy were still present. Her intelligence quotient (IQ) measured with the Griffiths Scales of Mental Development was 20, indicating severe intellectual disability.

At present, at 19 and 18 years of age respectively, the two siblings are alive, in very similar serious clinical conditions.

5.2.2 Exome sequencing analysis

WES identified a list of 17, 8 and 7 putative candidate variants in Family 8, 9 and 10, respectively. No candidates were shared by all 3 families, which could be partly expected based on the heterogeneous geographic and ethnic origin of the patients. We addressed more in detail the analysis of the results obtained in the Indian family. Among the 17 variants identified, 2 were located in coding regions, 1 was located in an intronic region and predicted to impact on the splicing process, while the remaining ones were in 3' or 5' UTR regions. We selected 5 variants located respectively in the *SOX11*, neuroblastoma-amplified sequence (*NBAS*), TWIST neighbor (*TWISTNB*), suppressor of cytokine signaling 1 (*SOCS1*) and solute carrier family 19 (folate transporter) member 1 (*SLC19A1*) genes, on the basis of data in literature on the function of these candidates. For example, *SOX11* was involved in the regulation of embryonic development and in the determination of the cell fate [180]; *NBAS* was suggested to play a role in embryogenesis from studies in zebrafish [181]; *TWISTNB* was located in the microdeletion syndrome 7p21 region, associated with a syndrome called Saethre-Chotzen, presenting with craniosynostosis, mild abnormalities of the hands and feet and in some cases developmental delay and learning disability [182];

SOCS1 was involved in regulation of cytokine receptor signaling and knock-out mice displayed impaired osteoblast differentiation [183]; *SLC19A1* had a pattern of expression in mouse embryos (in particular, the developing neural tube, craniofacial region, limb buds and heart displayed positivity at embryonic day (E) 9-11.5) that could support a role for the corresponding protein product in AFFND1 pathogenesis [184].

First of all, we confirmed the variants identified in these genes by Sanger sequencing in the patients and their parents; however, we found 4 out of 5 investigated variants in the homozygous state also in a control population of the same geographic origin, consequently we considered them neutral polymorphisms common to the Indian population, and discarded them. The remaining one was a single nucleotide substitution in the *NBAS* gene (c.6237-3C>G) close to the acceptor splice site. *In silico* analysis with the Human Splicing Finder software predicted a splicing aberration that we verified on a cDNA sample produced from PBMCs of the patient. RT-PCR analysis showed aberrant splicing; accordingly, by cloning the amplified band we confirmed skipping of exon 48 and premature termination of transcription, but also a residual amount of wild type messenger RNA (mRNA) (Figure 27).

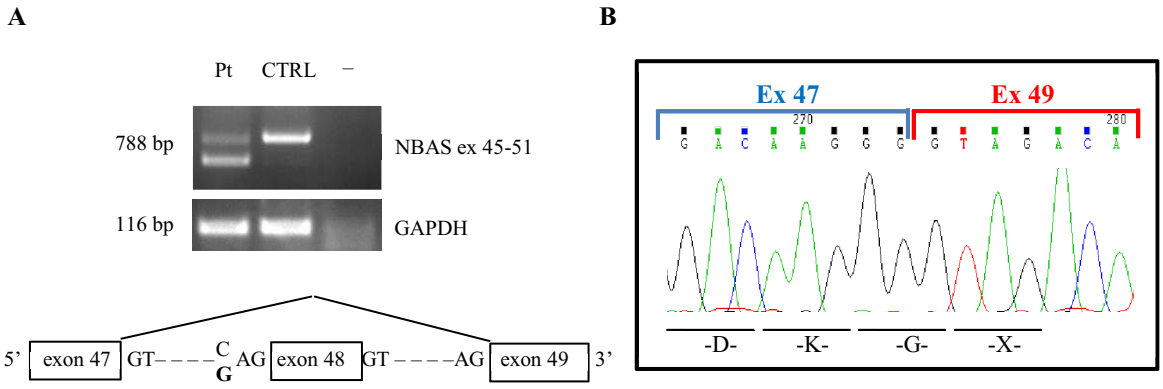

Figure 27: (A) RT-PCR spanning exon 45 and 51 showing aberrant transcripts in the patient as compared to the control; GAPDH was used as housekeeping (upper panel). Schematic representation of the most abundant aberrant mRNA of NBAS in the proband (lower panel); the nucleotide change found in the patient is in bold in the lower line. (B) Chromatogram of sequence of the most abundant aberrant transcript found cloning the PCR product spanning ex 45-51 of the patient's cDNA. The picture shows skipping of exon 48 and formation of a premature stop codon (down in the figure).

5.2.3 Functional valuation of mutated NBAS

We tried to evaluate the effect of this new *NBAS* mutation (c.6237-3C>G) at the protein level using total lysate of the patient's frozen PBMCs, which was the only cell sample available, as well as from frozen PBMCs of a normal donor, as a control. In particular, we aimed to assess whether a truncated protein was produced from the mutated cDNA of the patient or whether itself underwent nonsense-mediated decay. Unfortunately, Western Blot analysis with two different anti-NBAS antibodies failed to detect a protein band in both the PBMC samples, while a strong signal was visualized in the lane of SH-SY5Y cells (which was loaded on the gel as positive control, as indicated by the manufacturers' instructions for the anti-NBAS antibodies, in agreement with data in literature). This made us suspect that in PBMCs the NBAS protein was not expressed at sufficient levels to be detectable by Western Blot, so this technique was not suitable for my purpose. To circumvent this problem, we took advantage of the pcDNA3xFLAGhNBAS vector carrying the human full-length NBAS cDNA to introduce a modification reproducing the effect of c.6237-3C>G on cDNA. We performed site directed mutagenesis to form a stop codon immediately at the end of exon 47 and overexpressed the mutant construct in HEK293T cells. Western Blot analysis on transfected and non-transfected HEK293T cells using anti-FLAG antibodies allowed us to verify that the mutation caused the formation of a truncated NBAS protein (Figure 28A).

Next, we tried to understand if the truncated protein was functional or not. The NBAS protein is involved in essential cellular functions, namely the nonsense-mediated decay (NMD) pathway, which recognizes and degrades mRNAs containing premature termination codons in order to prevent the synthesis of truncated protein products [185]; and the retrograde transport from the Golgi to the endoplasmic reticulum for the recycling of vesicular components [186].

Longman and colleagues previously proposed the hypothesis of a negative loop between NBAS and the major components of NMD (in particular the regulator of nonsense transcripts 2, UPF2). Another role of NMD is the posttranscriptional regulation of selected transcripts. This dual role for NMD raises the possibility that this pathway is regulated to prevent the potentially catastrophic alterations in gene expression that would contrarily occur if NMD were altered in response to external signals, such as

stress, or to genetic insults. In addition, a negative regulatory loop directly acts on NMD factors in order to regulate its response after perturbations. In particular, they demonstrated that the new NMD components DHX34 and NBAS carry out a control of the NMD homeostasis [187]. Thus, we checked the quantity of UPF2 protein after overexpression of NBAS in HEK293T cells. We found a marked reduction of UPF2 in the total lysate of HEK293T cells overexpressing wild type NBAS as compared to the controls (i.e., HEK293T cells transfected with 3xFLAG empty or treated with Lipofectamine only), in agreement with the suggested feedback loop; on the other hand, in HEK293T overexpressing mutated NBAS the amount of UPF2 was similar to both controls, suggesting partial loss of the regulatory loop (Figure 28B).

During the secretory pathway, some of the vesicular components are recycled back through the retrograde pathway. In mammalian cells, at least 36 soluble N-ethylmaleimide-sensitive factor attachment protein (SNAP) receptors (SNAREs) are localized in membrane compartments and play a role in transport vesicles. Syntaxins are a members of this family of proteins and in particular syntaxin 18 is implicated in retrograde transport from Golgi to ER. This complex is composed of three SNAREs (p31 well-known as USE1, BNIP1 and Sec22) and three peripheral membrane proteins (Sly1, ZW10, and RINT-1). Aoki and colleagues demonstrated that NBAS is the protein that mediates the interaction between USE1 and ZW10/RINT-1. In particular, NBAS was identified as a new component of syntaxin 18 interacting directly with the extreme N-terminal region of USE1 [186].

Thus, we performed a coimmunoprecipitation for USE1 to check the possible alteration of the retrograde transport function. The total lysate of HEK293T cells not transfected, or transfected with the empty vector, or with the vector expressing either wild type NBAS or mutated NBAS was immunoprecipitated with USE1 antibody and assayed by Western blot. We found that the mutated NBAS interacted less with USE1 as compared to wild type NBAS (Figure 28C).

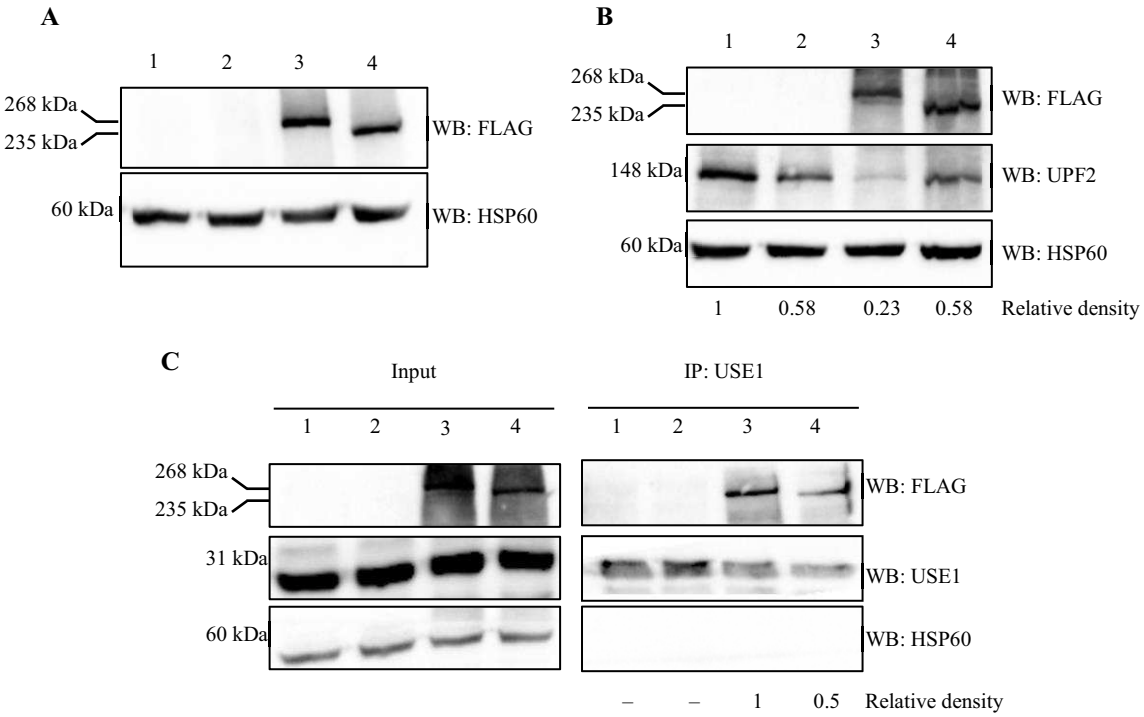

Figure 28: (A) Western blot analyzed with anti-FLAG antibody and anti-HSP60 as housekeeping of proteins extract from HEK293T cells not transfected (lane 1), transfected with empty vector (lane 2) and vector carrying wild type (lane 3) or mutated (lane 4) hNBAS. The picture shows the production of a truncated NBAS protein at the expected molecular weight. (B) Western blot analysis for anti-FLAG, anti-USE1 and anti-HSP60; the loading is as reported in A. The expression of UPF2 protein is higher in lane 4 than in lane 3, suggesting reduced negative loop in the presence of mutated NBAS. (C) Western blot for anti-FLAG, anti-USE1 and anti-HSP60 after co-immunoprecipitation for USE1; the lanes are loaded as in A. The left panel represents the total extract before immunoprecipitation showing a comparable starting amount of USE1. On the right, the Western blot after immunoprecipitation demonstrate a lower interaction of mutated NBAS with USE1 compared to wild type NBAS. Numbers indicate relative density determined using the ImageJ software.

5.2.4 Analysis in mouse and zebrafish model

To assessed the possible involvement of NBAS in development, we used two different animal models: mouse and zebrafish model.

NBAS expression during mouse development

To support the hypothesis of a possible role of NBAS in the bone tissue and in skeletal morphogenesis, we evaluated NBAS expression during murine fetal life starting at embryonic day 11.5, since at this stage skeletal elements start to form. We performed immunohistochemical analysis for NBAS on fixed embryos from C57BL/6 wild type mice.

Analyzing the body at E13.5 and E16.5 we found that NBAS expression was widely distributed, with higher levels in specific tissues such as liver, spleen, stomach, lung, glandular structures and hypertrophic cartilage (Figure 29A).

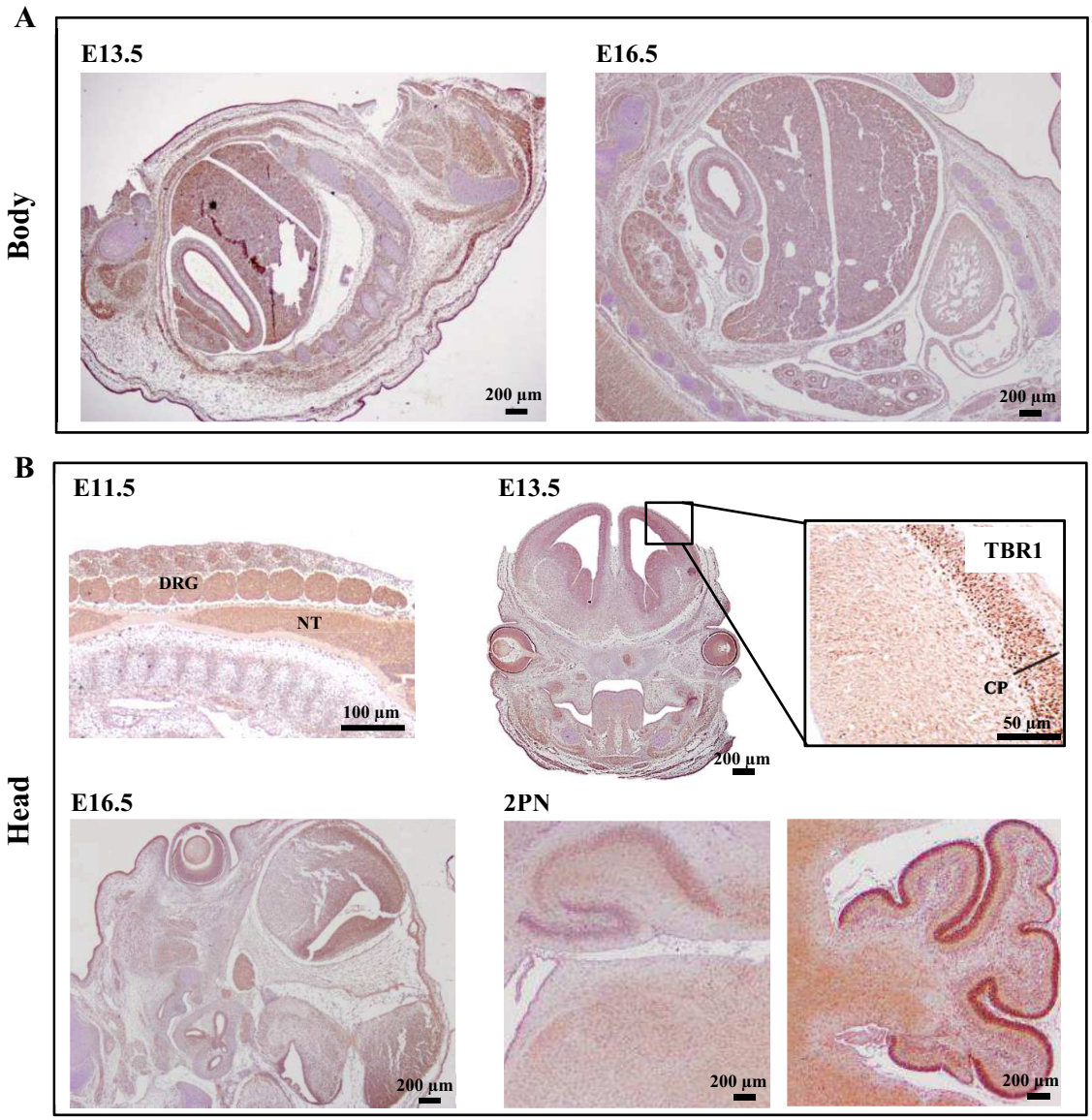

Figure 29: NBAS expression during murine embryonic development. (A) Representative images of longitudinal section of the body at E13.5 and E16.5 show widely distribution of NBAS expression, specifically in liver, spleen, stomach, lung, glandular structures and hypertrophic cartilage. (B) Representative parasagittal section of the total body at E11.5 shows NBAS expression in the NT and DRG. NT: neural tube; DRG: dorsal root ganglia. Representative images of coronal section of the skull at E13.5 and E16.5 show positive signal in specific elements of the head including eyes, dental buds and brain. The inset demonstrates the positivity of NBAS in cortical plate (CP), stained with the cortical plate marker Tbr1. Lower panels show a representative parasagittal section at PN2 in which NBAS expression is evident in the hippocampus and cerebellum.

Regarding the central nervous system, at E11.5 stage, high expression of NBAS was detected in the neural tube (brain and spinal cord) and neural ganglia. Staining at E13.5 confirmed high expression in the forebrain: for example the cortical plate, also stained on serial sections for TBR1 (a transcriptional regulator involved in brain development and considered a marker of cortical plate). The section of the head at E16.5 showed positive NBAS staining in the brain and in different elements of the head and face including eye and dental buds; furthermore, in the brain at post-natal day 2 (PN2) NBAS expression was present in the hippocampus and cerebellum (Figure 29B).

For what specifically pertains to the limbs, the staining for NBAS was quite diffuse at E11.5; at a subsequent stage (E13.5) cartilaginous condensations displayed low expression, while higher expression was found in the ectoderm and perichondral mesoderm. For the E16.5 stage we performed immunostaining on limb serial sections with different antibodies specific for COL II, RUNX2, SOX9 and Tenomodulin (TNMD) and we confirmed the presence of NBAS in the hypertrophic cartilage, periosteum and tendons (Figure 30).

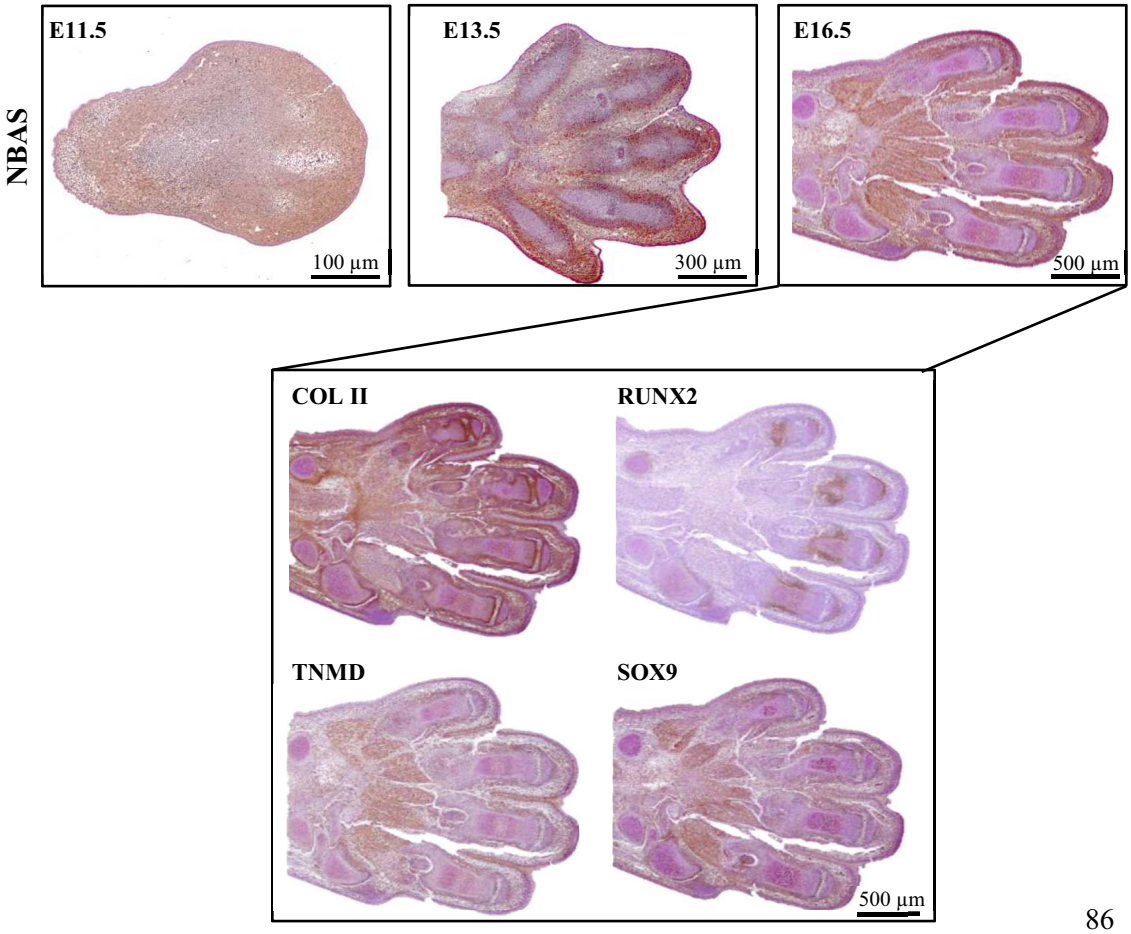

Figure 30: NBAS expression during mouse limb embryonic development. Representative image of longitudinal section of the limb at E11.5 showing widely diffuse NBAS expression at this early stage, while at E13.5 and 16.5 NBAS expression is displayed mainly in the ectoderm and perichondral mesoderm. The inset shows longitudinal serial sections of the limb at E16.5 stained for COLII, RUNX2, TNMD and SOX9 showing that NBAS is specifically expressed in hypertrophic cartilage, periosteum and tendons.

Zebrafish experiments

We took advantage from previous studies in zebrafish, in which, using morpholino oligonucleotides (MOs) specifically designed to block z-nbas mRNA translation or to alter z-nbas pre-mRNA splicing, showed that the depletion of NBAS protein resulted in very severe developmental defects, developmental delay/arrest and reduced embryonic viability [181]. These data were consistent with the essential role of core nonsense mediated decay factors during zebrafish embryogenesis [188], but the role of zebrafish NBAS (z-nbas) during development could not be clearly established due to the severe disruption of the morphants' phenotype.

In collaboration with Giorgio Merlo's lab in Turin, we decided to repeat the experiment injecting lower doses (1/3 of the original dose) of the same MOs (the translation block (TB), the splice site (SS) and the scrambled (scr) oligonucleotides, this latter as control containing a 5-bp mismatch) in order to prevent embryo lethality or severe developmental anomalies, and to allow embryo development to proceed. Injection of a reduced dose of MO was able to deplete the level of endogenous z-nbas mRNA approximately by 80%, as detected by RT-PCR on whole injected fish embryos (Figure 31).

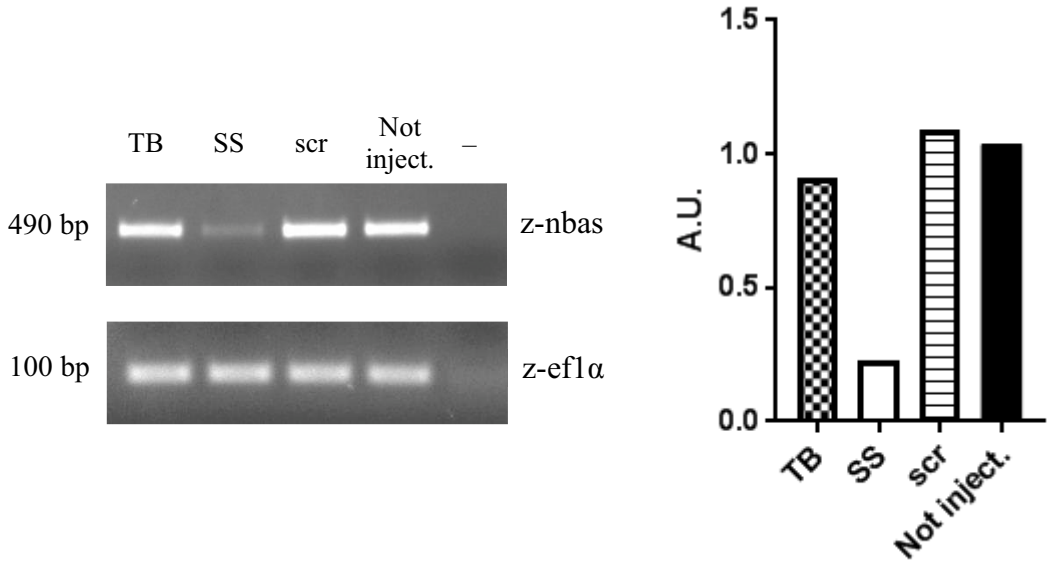

Figure 31: Z-nbas expression after MO injection in zebrafish. RT-PCR analysis for z-nbas and the housekeeping gene (ef1α) on zebrafish embryos injected with either the translation block (TB), or the splice site (SS) or the scrambled (scr) MO and in not-injected control embryos shows reduction of z-nbas expression in embryo injected with SS (left panel). The right panel shows the quantification of the z-nbas reduction in SS as compared to the controls.

After injections, morphants were allowed to develop for 5 days post fertilization (dpf) in a quarantine incubator, a time appropriate for chondrocranium development and compatible with the half-life of the MO. This modified protocol did allow staining and evaluating the cartilage head skeleton. At 5 dpf, embryos were fixed, and we analyzed the chondrocranium, in particular the "splanchno" cranium e.g. that derived from Neural Crest Cells (NCC) of the branchial arches. We observed an alteration of the angle between the Meckel's cartilage (Mck) and the palatoquadrate (pq)/ceratohyale (ch) cartilages and an alteration of the angle between the right and left ceratohyale cartilages (second branchial arch). Based on the examination of the WT (not injected embryos) we defined the threshold for the alterated phenotype as an angle > 14 degrees between pq and ch and as an angle > 60 degrees between the second branchial arch. Using these criteria, we quantified the frequency of injected and not injected embryos in terms of increased angle (vs. absence of phenotype) over the total number of surviving embryos in each condition. The injection with both SS and TB anti z-nbas MOs brought to a significantly higher number of embryos showing the alterated phenotype compare to the controls, in agreement with a putative role of z-nbas in morphogenetic processes (Figure 32).

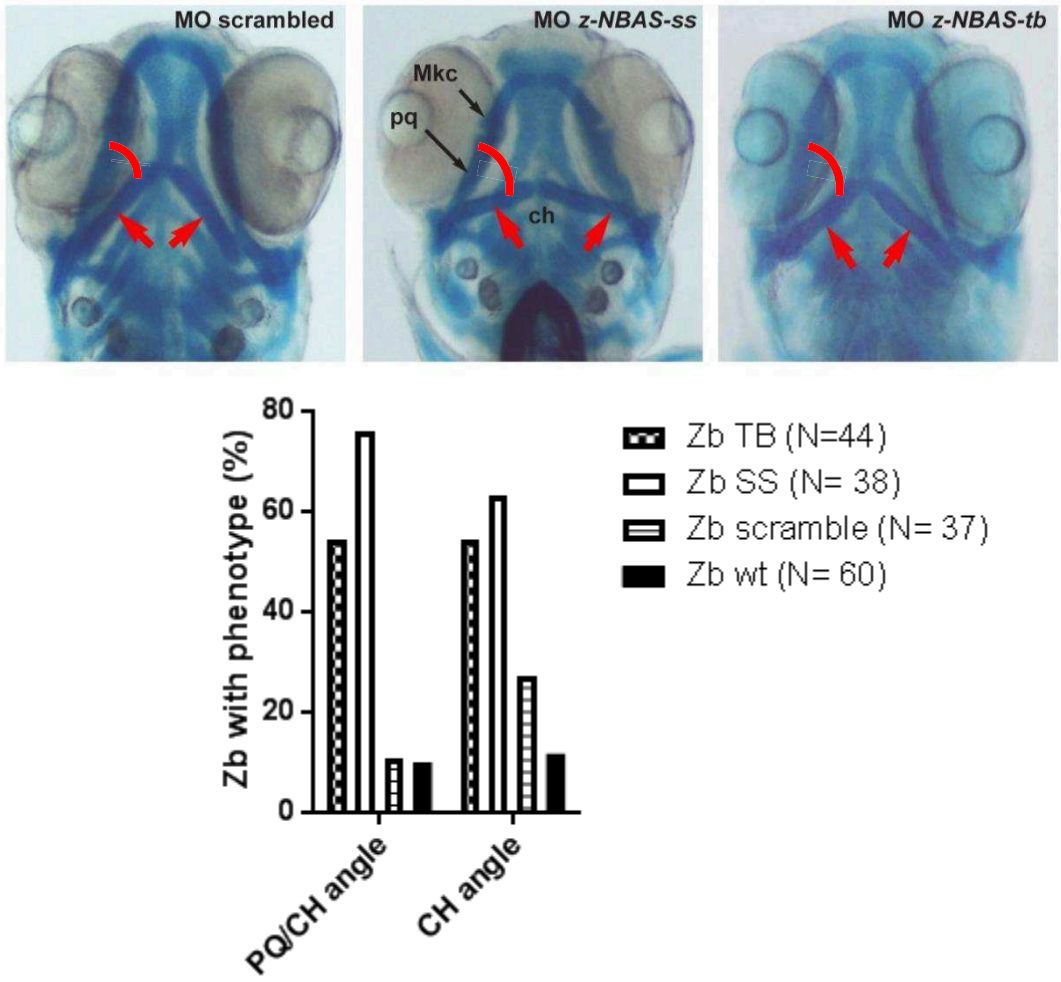

Figure 32: Representative images of splanchnocranium of embryos fixed in formalin and stained with Alcian blue. Fish injected with z-nbas-SS and z-nbas-TB, compared to the control scramble, presented a significant enlargement of the angle formed by the left and right ceratohyal (ch) cartilages (red arrows in the picture) and a significant widening of the distance (red arch in the picture) between the palatoquadrate (pq) and the second branchial arch. Mkc: Meckel's cartilage (upper panel). Quantization of the number of zebrafish showing an altered phenotype of the mentioned structural elements. Structural abnormalities were found in a very small fraction of wild type (wt) and scramble-injected zebrafish (lower panel).

6. DISCUSSION

Next generation sequencing was introduced in 2005 as a powerful technology to detect genetic variations ranging from single nucleotides to large rearrangements. In particular, whole exome sequencing is mainly targeted to exonic regions, since it is known that in the 85% of cases of Mendelian disorders the mutation is located in protein coding regions. WES is particularly useful in the identification of the causative genes in rare genetic disorders, which typically affect a very small number of people (less than 1:2000).

The identification of the gene causative for the pathology is essential to define a molecular diagnosis for the patients and the carrier status for their relatives, and to provide genetic counseling. In addition, it can constitute the starting point to develop targeted therapeutic interventions and to better understand the pathophysiological role of the protein product [189]. Choosing the correct strategy to filter and prioritize the variants identified by WES is crucial; commonly adopted criteria include the mode of inheritance, the frequency of the disease and of the variant in the general population, the clinical features of the patients, and the severity of the pathology.

During my PhD project I applied WES to two different rare skeletal diseases: osteopetrosis and acrofrontofacionasal dysostosis type 1.

The molecular and clinical heterogeneity of human osteopetrosis is confirmed by the results I achieved during my PhD, which describe “classical” ARO and ADO II patients, with mutations in already known genes, but also peculiar cases.

We analyzed by Sanger sequencing 25 osteopetrotic patients and we found the causative mutations. These analysis confirmed *TCIRG1* as the most frequently mutated gene and mutations were found also in the known genes *CLCN7*, *LRP5*, *SNX10*, *RANK*, *OSTM1*, and *CA2*.

In some patients lacking a molecular classification, we performed WES.

The spectrum of clinical features of osteopetrotic patients with mutations in *CLCN7* gene includes infantile malignant recessive and autosomal dominant osteopetrosis. These different phenotypes were evident in Families 1 and 2: in fact, in the former the patient showed classical ARO with no primary neurological involvement and was a heterozygous compound for two different mutations in the *CLCN7* gene, whereas in the

latter the patients displayed a typical ADO II phenotype and carried a heterozygous *CLCN7* mutation rather common in this subgroup of patients. So far, no precise correlation between the clinical manifestation and the type of *CLCN7* mutations has been defined.

The patient of Family 3 carried a homozygous mutation in the *OSTM1* gene; accordingly, she displayed a severe form of ARO with primary CNS involvement.

The patient of Family 4 carried a homozygous mutation in the *FERMT3* gene, which codes for kindlin-3 protein, prevalently expressed in hematopoietic cells and involved in integrin inside-out activation. This mechanism is crucial for platelet aggregation, leukocyte extravasation and also for osteoclast adhesion and spreading [150]. *FERMT3* mutations cause the LAD-III, a rare pathology characterized by severe bleeding and recurrent infections due to alteration in integrin function. In literature, 22 LAD-III patients have described and 9 of them also showed osteopetrosis; the disease was cured by HSCT in 7 out of 13 transplanted patients [148, 149, 190-193]. At least 10 different mutations in the *FERMT3* gene have been described, including mainly truncating mutations, but also missense mutations, single nucleotide substitutions and deletions. The majority affected the C-terminus of the protein, specifically in F3 domain, important to bind integrin, with likely loss of interaction and consequent detrimental effect. The limited number of reported patients did not allow defining specific genotype-phenotype correlations. Interestingly, our patient displayed early-onset bone marrow failure and osteoclast-rich osteopetrosis with absence of visual and neurological impairment, but did not show recurrent bleeding and infection, which are typically present in Kindlin3 mutated patients. This was probably due to the fact that our patient was transplanted at a very young age, so possibly before these features could become apparent. The curative potential of HSCT for the severe phenotype of kindlin3 deficiency was confirmed in our patient.

Families 5 and 6 shared the presence of very peculiar mutations, not yet reported in osteopetrosis cases: deep intronic mutations in the *TCIRG1* gene and synonymous but not silent mutations in genes associated with ARO.

As already mentioned, intermediated and atypical forms of osteopetrosis are more difficult to solve and manage.

In 2014, a young girl with benign, recessive osteopetrosis carrying an incomplete splicing defect in the *TCIRG1* gene was reported. At that time it was reasoned that the *TCIRG1* mutations leading to a mild phenotype were extremely rare because no other similar finding was present in literature. Nevertheless, our recent data suggest that this is not the case. We identified 4 different mutations in intron 15 of the *TCIRG1* gene that were predicted to impact on the splicing process. For 2 out of 4 variants, the cDNA analysis of the patients carrying these mutations, confirmed aberrant splicing and also the production of a small amount of wild-type mRNA. Interestingly, all these mutations were located in close proximity in intron 15, probably identifying a hot spot region that impact in the splicing process. In particular, mutations were in the middle of *TCIRG1* intron 15, which is composed of 368 nucleotides, so quite far from the canonical splice sites, thus explaining why their identification through our standard molecular analysis, based on amplification and direct sequencing of exons and exons-introns boundaries, as well as by WES failed. Analyzing the sequence of the aberrant transcript we could highlight the usage of a cryptic acceptor site in *TCIRG1* exon 15 and a cryptic donor site in intron 15. In accordance with our results, deep intronic mutations, leading to the formation of alternative transcripts through the activation of alternative splice sites, have been recently reported in several diseases, such as Lowe Syndrome, Fukuyama congenital muscular dystrophy, hypertrophic cardiomyopathy and also in patients with bone dysplasias [194-197]. In general, these data clearly highlighted the possible impact of noncoding mutations on the onset of human diseases and suggested the need to verify the pathogenicity of intronic variants in known disease genes, when obvious mutations are not immediately identified.

In our cohort, the patients carrying these particular mutations displayed a different level of disease severity: 2 of them were diagnosed in early life and were treated with HSCT, whereas the other 2 presented bone defect at school age and the pathology progression was slow and overall benign, examples of typical intermediate cases. The range of severity was particularly evident in the two siblings of Family 5: the elder showed secondary neurological defects, whereas her younger brother seemed to be less affected. Actually, this is common in ADO II, in which a role for SNPs in modifier genes has

been suggested but not formally demonstrated. Of note, we found that the siblings of Family 5 carried a different set of SNPs in the *CLCN7* gene and in particular the brother, with the milder phenotype, presented 2 heterozygote SNPs in exon 15 (rs12926089 and rs12926669) which had already been associated with low bone mineral density in different populations [198, 199]. Likewise, it was possible that additional variants in other genes could have influenced bone metabolism and modulated clinical manifestations. Furthermore, in adolescence and adult life, sexual hormones could have impacted on the phenotype.

The analysis of Family 6 identified a synonymous mutation in the homozygous state as causative for the disease. Actually, during the workflow of exome sequencing, a challenging step is the filtering of the called variants, since the list of variants produced for further investigation may change based on the adopted criteria. In particular, synonymous variants are usually filtered out because of the common assumption that synonymous mutations, which by definition do not cause an amino acid change, do not have an impact on the protein structure and function. So, the involvement of synonymous mutations in pathogenetic mechanisms has likely been underestimated.
Our results add to the limited number of reports in literature demonstrating that some synonymous changes cause different pathologies [200, 201], including skeletal defects [202, 203]. In our work, we found 2 patients that carried synonymous variants in *TCIRG1* and *CLCN7*, respectively, leading to an alteration of the splicing process due to the creation and activation of a cryptic splice site. This would cause a frameshift with consequent no protein production, if the formation of a premature stop codon targets the aberrant mRNA to nonsense-mediated RNA decay, and/or lower amount of normal protein, if the mutation is hypomorphic.
Because of the high number of variants obtained by WES, it is clearly not possible to perform functional evaluations for all synonymous changes, but it might be considered to further investigate those located in genes already associated with the pathology when obvious mutations are not found at a first analysis.
Moreover, the synonymous mutation found in *CLCN7* in the second patient, might raise the hypothesis that this type of changes contributes to the spectrum of severity of CLCN7-dependent osteopetrosis.

The patient of Family 7 was affected by osteopetrosis and poikiloderma with neutropenia, and carried a homozygous mutation in the *C16orf57* (*USB1)* gene.

PN is a rare autosomal recessive syndrome, first described by Clericuzio and colleagues in 1991 [204], characterized by a skin manifestation and an immunological defect. For the skin, a papular erythematous rash typically starts in early infancy on the limbs, then spreads towards the trunk and face and becomes a frank poikiloderma with generalized hyperkeratosis. In the bone marrow, myelodysplasia with neutrophil maturation defects and chronic neutropenia responsive to growth factors, is responsible for recurrent infections, particularly affecting the airway tract [205-207]. Thickening of the toenails, growth retardation, facial dysmorphism, mild splenomegaly with transient anemia, and photosensitivity are present in some patients. The association between OP and PN seems to be extremely rare: in literature only one patient has been described so far [177], while in the other reported individuals only minor skeletal defects were present. The reason for this phenotypic variability is not known.

PN is caused by mutations in *USB1* that encodes a 265-amino acid protein highly conserved among vertebrates and broadly expressed, with high levels in myeloid lineage cells and moderate in the skin, adipose tissue, kidney, intestine, cerebral cortex, smooth muscle, adrenal and thyroid glands. USB1 is involved in the processing of U6 small nuclear RNA (snRNA), an essential component of the RNA splicing machinery [208]. Lymphoblasts from a PN patient bore elongated non-templated oligo(U) tracts and oligo(A) tails at the U6 snRNA 3' end, targeting it to nuclear RNA surveillance and degradation, pointing to USB1 role in a quality control pathway [209].

In 2015, a zebrafish model of PN was developed by morpholinos (MOs) injection into one-cell-stage embryos, for usb1 gene knock-down [210]. A 60% reduction in Usb1 transcription was achieved as maximum; usb1-deficient zebrafish displayed severe developmental defects: bent tail, reduced body length and a thin yolk extension at 25 hours post fertilization (hpf), smaller head and eyes and pericardial edema at 50 hpf, leading all the morphants to death within a week. MOs injection in zebrafish embryos, in which neutrophils expressed GFP, highlighted impaired neutrophil development likely due to aberrant transcription of neutrophil-specific genes in the morphants [210, 211].

Moreover, other possible disease mechanisms could be explored; for example, USB1 directly interacts with SMAD4 [178], so the possibility that PN development depends on the direct or indirect regulation of SMAD4 as well as other as yet unknown partners could be considered. For the bone compartment, a defect in the osteoclast lineage could be expected, since mature osteoclasts derive from myeloid progenitors and the USB1 gene is highly expressed in myeloid cells. In addition, SMAD4 is involved in bone homeostasis and its conditional deletion in osteoclast precursors reduces osteoclast differentiation and activity [212]. Moreover, SMAD4 plays a well-known role in the skin as demonstrated by hair follicle collapse and progressive hair loss, and by epidermal hyperplasia, increased proliferation of keratinocytes and spontaneous development of skin tumors after conditional deletion in mouse keratinocytes [213, 214].
Overall, unraveling the pathogenetic mechanism will be relevant for a better understanding of the physiopathology of all the systems involved.

With respect to AFFND1, we did WES in 3 families and completed the analysis in Family 8, where we identified a novel homozygous truncating mutation in the *NBAS* gene in the two affected siblings.
The neuroblastoma amplified sequence/neuroblastoma amplified gene (*NBAS/NAG*) was originally found co-amplified with MYCN in neuroblastoma cell lines and primary tumors [215]. The gene is located in chromosome 2, it's very large and gives rise to two different transcripts (4.5 kb and 7.3 kb); the latter is more abundant and encodes for 2371 amino acid protein. It's highly expressed in connective tissues, eye, brain and spinal cord. The protein product contains two functional domains evolutionarily conserved: a quinoprotein aminedehydrogenase β chain like, β propeller domain in the N-terminal region and a Sec 39 domain in the central region, which is typical of proteins of the secretory pathway [216]. Indeed, NBAS was identified as a member of the syntaxin 18 complex, which comprises also p31 (USE1), ZW10 and RINT1 and acts in the retrograde transport from the Golgi to the endoplasmic reticulum for the recycling of vesicular components [186]. In particular, the N-terminal region of NBAS was shown to interact with and stabilize USE1 on the endoplasmic reticulum membrane, while the C-terminal with ZW10-RINT1.

Another important function assigned to NBAS is a role in the nonsense-mediated decay pathway, the complex mechanism by which mRNAs containing premature termination codons are recognized and degraded in order to prevent the synthesis of truncated protein products [185]. Morpholino-induced depletion of nbas in zebrafish caused severe developmental defects and reduced embryonic viability, as is also observed after depletion of other NMD core factors, thus suggesting that an active NMD pathway is crucial in zebrafish embryogenesis [181]. Moreover, in *caenorhabditis elegans*, in zebrafish and in human HeLa cells NBAS was suggested to be involved in an autoregulatory circuit and to contribute to the regulation of a large number of endogenous RNA targets, comprising also many genes relevant for the bone tissue, being the matrix Gla protein (*MGP*) and *BMP2* genes those with the strongest upregulation upon NBAS depletion [187]. NMD factors are required for correct embryogenesis in several animal models [217]. In humans, mutations of *UPF3B*, an important component of the NMD surveillance machinery, cause facial dysmorphism and intellectual disability [218]. The similarity with the phenotype of AFFND1 patients supports the hypothesis that the mutation in the *NBAS* gene could affect development in humans. Unfortunately, we did not have an adequate cell sample available from the patients, so we could not directly demonstrated if the mutant NBAS protein was present or not. However, our experiments in HEK293T cells demonstrated that the mutation caused the formation of a truncated protein that, if produced in the patients, might affect the NMD negative loop through partial loss of down regulation of another NMD core factor (UPF2). Moreover, the mutated NBAS displayed a reduced interaction with USE1 in the syntaxin 18 complex. Overall, these results strongly suggested that the NBAS mutation found in these AFFND1 patients altered both functions of this protein.

The importance of NBAS in skeletal morphogenesis was supported by our experiments in two different species, mouse and zebrafish, which are widely exploited as models of skeletal development [219, 220].

In the wild type mouse we focused particularly on limbs and on the craniofacial region characterizing the pattern of NBAS expression during embryo development. We found NBAS expression in cartilage cells and early tendons of the skeletal system and in progenitor cells of the embryonic cortex and cerebellum, supporting a possible role of

the NBAS protein in skeletal and brain development, and in general in morphogenetic processes.

In the zebrafish model we found a phenotype specifically associated with *z-nbas* down regulation in early phases of life. In more detail, we injected the z-nbas morpholino oligonucleotides (splice site, translation block or scrambled) at the 1-to-4 cell stage and performed the analysis at 5 dpf. We found alterations of different structures in the chondrocranium upon z-nbas depletion, strengthening the hypothesis that NBAS defects could determine phenotypic abnormalities such as those present in our AFFND1 patients.

For what pertains human pathologies, mutations in the *NBAS* gene have been recently associated to different diseases: SOPH syndrome, presenting with short stature, facial dysmorphisms, optic nerve atrophy and Pelger-Huet anomaly of the neutrophils [221]; recurrent acute liver failure (RALF) with onset in infancy [222-224]; a multisystem disorder reported in two patients and involving bone, connective tissue, liver, immune system and retina [225] and atypical osteogenesis imperfecta (OI) [226].

The mutations reported in literature are distributed along the *NBAS* gene with particular frequency in the first half part and no clear association between genotype and phenotype. Indeed, the most common missense mutation (p.Arg1914His) was reported in different disease as SOPH, RALF and OI.

Very few studies tried to define the exact pathogenetic mechanism underlying these diseases; in detail, functional studies were performed in 2016 in fibroblasts of RALF patients. This study showed reduced intracellular protein levels of NBAS and USE1, thermal instability of mutant NBAS and impaired tethering of vesicles associated with endoplasmic reticulum/Golgi [224].

Very recently, Balasubramanian and colleagues measured circulating MGP in a OI patient with mutated *NBAS* gene and any alteration was found, in contrast with previously reported up-regulation of this gene in HeLa cells after its depletion [226]. So the influence of NBAS deficiency on MGP in the skeletal phenotype is under debate.

Interestingly, the presence of short stature and bone alterations, including delayed bone age, low bone mineral density and fractures, and various dysmorphic traits, such as facial dysmorphism and hypo/hypertelorism, is shared by the majority of patients bearing mutations in the NBAS gene, independently from the specific clinical diagnosis

(including also AFFND1) suggesting a link between *NBAS* gene and skeletal formation and homeostasis. On the other hand, some clinical features are specific for AFFND1 patients.

Different hypothesis could explain this phenotypic heterogeneity: each specific mutation might otherwise affect either or both molecular function of the transcript, and this might have a different effect depending on the specific cell type; moreover, modifier genes might modulate the phenotypic manifestation [227].

7. CONCLUSIONS AND FUTURE PROSPECTIVES

We exploited WES analysis in two different rare skeletal diseases (osteopetrosis and acrofrontofacionasal dysostosis 1). In particular, we confirmed the utility of WES in the molecular diagnosis of a genetically heterogeneous disorder and in patients with atypical phenotype. Beyond genes already associated with osteopetrosis we also identified single patient with mutation in gene rarely (or, even, just once) linked with ARO (*FERMT3* and *USB1,* respectively). On the other hand, we demonstrated some limitations of the WES approach, specifically for what pertains the identification of two classes of mutations, deep intronic and synonymous variants, because of the criteria adopted by standard workflow for variants selection. Instead, we validated the pathogenetic effect of the deep intronic single-nucleotide changes found in the *TCIRG1* gene and of two synonymous mutations found in *TCIRG1* and *CLCN7*.

Therefore, we underlined the need to implement strategies to integrate the technological power of WES with a better capacity to interpret mutations, identifying the clinically relevant ones. Even when data in literature sufficiently support the suspect of a detrimental effect of the identified variant, it is important to investigate the pathogenetic mechanism. In this respect, based on the results achieved by WES on AFFND1, the conservation of intronic nucleotide in mouse species and the confirmation of the alteration of splicing by *in vitro* prediction, we're in the process to generate a knock-in (ki) mouse model bearing the *NBAS* mutation (c.6237-3 C>G) identified in the Indian patients above described. We will characterize the new mouse model: first of all we will determine if homozygous ki mice are embryonic lethal, performing timed mating to determine the stage of death and genotype litters at different stages of development, from E8.5 to E17.5. On the other hand, if homozygous mice are viable, we will look whether any dysmorphic sign (including for example abnormal skull shape, micro- or macrocephaly, proportionate or disproportionate dwarfism, supernumerary digits or absence of any finger or toe) is present in the mutant mice. In addition, we will perform Alcian Blue/Alizarin Red preparations for skeleton analysis in order to visualize cartilage and bone and to perform measurements of the different skeletal elements. Moreover, we will try to define the molecular signature deriving from the mutant NBAS by performing a transcriptomic profiling as compared to wild type littermates. In this way we will be able to detect differences in the levels of transcripts, but also different levels of alternative splicing isoforms with specific functions and the presence of

aberrant products resulting from splicing impairment. We will group differentially expressed genes into functional classes, thus refining the exact cellular function of NBAS protein for further investigations.

8. MATERIALS AND METHODS

8.1 Samples

Samples, including blood and DNA, were collected from patients and their relatives after informed consent. This research complies with the World Medical Association Declaration of Helsinki–Ethical Principles for Medical Research Involving Human Subjects, and with the standards established by the Independent Ethical Committee of the Humanitas Clinical and Research Centre, Rozzano (Milan), Italy.

Peripheral blood mononuclear cells (PBMC) were isolated from blood of patients, parents or healthy donor. The blood was diluted with sodium chloride 0.9% (Baxter) (ratio 1:1) and subjected to density gradient separation on Lympholyte® Cell Separation Media (Cedarlane) and centrifuged for 20 minutes 800 G. After centrifugation the PBMC layer was collected and washed twice time with Dulbecco's phosphate buffer saline (PBS) 1X.

8.2 PCR analysis and Sanger Sequencing

The molecular analysis of genes was performed by polymerase chain reaction (PCR) amplification and sequencing of the exons and intron-exon boundaries. The technique was well established in our lab. Briefly, the thermocycling conditions were: initial denaturation step at 94°C for 3 minutes, followed by 34 cycles of denaturation at 94°C for 30 seconds, annealing at temperature between 55°C and 62°C for 40 seconds (depending on specific primers), and amplification at 72°C for 50 seconds. The PCR products were purified with Wizard® SV Gel and PCR Clean-Up System kit (Promega) following manufacturers' instruction and sequenced by BioFab Research laboratory. The chromatogram files were visualized by chromas software (version 2.4.4) and aligned with the reference genomic sequence by basic local alignment search tool (BLAST https://blast.ncbi.nlm.nih.gov/Blast.cgi).

8.3 Exome sequencing

For the exome sequencing we used 1.5 µg of high-quality genomic DNA from patients and their parents, and the exome capture was performed with the TruSeq Expandend Exome Enrichment Kit (Illumina Inc., San Diego, CA, USA). The Agilent DNA 1000 Kit (Agilent Technologies Inc., Santa Clara, CA, USA) was used to validate the

enriched library and the clonal clusters was created on the cBot Station (Illumina Inc.) loading the library on the flow cell. Sequencing was performed on the Hiseq2000 Instrument. Reads obtained after sequencing were aligned to the reference genome hg19 by using BWA-MEM [228] and stored in compressed binary files (BAM). All the variants, single nucleotide variations, insertions, and deletions were found calling with the Genome Analysis Toolkit (GATK) [229]. The entire analysis was performed using the Orione platform [230]. The variants identified were merged in a VariantCallingFormat (VCF) file, annotated by KGGSeq [231], prioritized, and filtered considering the paternal consanguinity and the incidence of the disease.

8.4 RNA isolation and RT-PCR

RNA was extracted from PBMCs and from HeLa cells using Trizol reagent (Thermo Fisher Scientific, Waltham, MA, USA) and retrotranscribed with the High-capacity cDNA Reverse Transcription Kit (Applied Biosystems, Waltham, MA, USA), according to the manufacturers' instructions. The RT-PCR analysis was performed on 2 µl of the cDNA with the primers reported in table 6.

Table 6: primers used for RT-PCR analysis

Gene	Exons	Primers
TCIRG1	14-17	F: GCCTGGCTGCCAACCACTTG R: CATCGGAGCTCCAGCCATT
TCIRG1	7-10	F: GGGGTGAGCAGATCGGACAG R: TGTAGGGAGCGGGTTGACC
CLCN7	11-16	F: TCCTGTTCAGCTTGGAGGAG R: TCACCACGCTCTTCTCCG
CLCN7	16-20	F: GTACAACTCCATGGCTGCG R: TGAGTGAGTGTGAGGTGACC
CLCN7	11-18	F: TCCTGTTCAGCTTGGAGGAG R: CAGTGTCATCCGCACAATCC
NBAS	45-51	F: AGTGAGCAGGAAACACTGCA R: TCCTTCACACCCTCTGCAGG
GAPDH	8-9	F: GGTCTCCTCTGACTTCAACA R: AGCCAAATTCGTTGTCATAC

8.5 Cloning and vectors

TA cloning: the PCR product obtained from each experiment was cloned in the TA cloning vector (Life Technologies) following the manufacturer's instructions; about 70 independent clones were sequenced using the M13F primer.

Minigene vector: the hybrid pTB minigene vector contains the alpha globin promoter region with the SV40 enhancer. This promoter is followed by a genomic containing exon 1, 2 and 3 of the human alpha globin gene; in particular exon 3 carries a portion of the fibronectin gene and presents an unique intronic NdeI restriction site used to clone the genomic region of interest. This hybrid vector has been previously demonstrated to reproduce the splicing pattern of several gene systems [176, 232]. In this case we inserted the *TCIRG1* genomic region spanning exon 11 to 13 amplifying with forward primer 5'-TTTTCATATGctgtgcctggctgctaagtg-3' in intron 10 and reverse primer 5'-CCCCTCGACCATATGcccactcccagctgccttca-3' in intron 13. Upper case identifies the nucleotides added to reproduce the NdeI enzyme restriction site to clone it into minigene vector.

pcDNA3xFLAGhNBAS vector: this vector carrying the human full-length NBAS cDNA was kindly provided by Prof. Caceres. It contains the FLAG-tag sequence (5'-GACTACAAAGACCATGACGGTGATTATAAAGATCATGATATCGATTACAAG GATGACGATGACAA-3') immediately after the ATG start site and in frame with the NBAS cDNA sequence, thus it drives the production of a fusion protein in which the FLAG oligopeptide, that is repeated three times (DYKDHDGDYKDHDIDYKDDDDK) in front of NBAS protein sequence, allows the detection of the whole product by means of the anti-FLAG antibody. The pcDNA3xFLAG empty vector, without *NBAS* gene insert, was obtained using NheI restriction enzyme.

Each plasmid was transformed in One Shot™ TOP10 Chemically Competent E. coli (Thermo Fisher Scientific Inc.) following manufacturer's instruction and then DNA was obtained with PureYield™ Plasmid Miniprep System (Promega) kit.

8.6 Site-directed mutagenesis

Site-directed mutagenesis was performed in the pcDNA3xFLAGhNBAS vector at *NBAS* level using the QuickChange Site-Directed Mutagenesis Kit (Stratagene) following the manufacturer's instructions. Briefly: the PCR was performed using the modified primers forward 5′-GGTGAAACCAGCTCCTACCCCTTGTCCACACTGG-3′ and reverse 5′-CCAGTGTGGACAAGGGGTAGGAGCTGGTTTCACC-3′ to synthesize the mutant strand. The PCR product was digested with DpnI enzyme and then the transformation in Supercompetent cells was performed. The mutated inserted sequence was verified by DNA sequencing.

8.7 Cell culture

HeLa (epitheloid cervix carcinoma), HEK293T (human embryonic kidney) and SH-SY5Y (neuroblastoma from neural tissue) cell lines were purchased from ATCC®.

HeLa cells and HEK293T cells were cultured in DMEM (Lonza) supplemented with 10% fetal bovine serum (FBS), 1% penicillin/streptomycin (P/S) (Invitrogen) and 2 mM L-glutamine.

SH-SY5Y cells were expanded in MEM (minimum essential medium eagle, Lonza) supplemented with 10% FBS, 1% P/S, 2 mM L-glutamine, 1% non-essential amino acids (NEAA) and 1% Sodium Pyruvate.

Cells were kept in a humidified 5% CO2 incubator at 37°C.

8.8 Cell transfection

All the transfections were performed using Lipofectamine 2000 (Life Technologies) following the manufacturer's instruction.

In particular, the HeLa cells were seeded in 6 well plates and at about 80% confluence were transfected with 4 μg of minigene vector carrying the WT or mutated *TCIRG1* genomic sequence. RNA was extracted after 48 hours and cDNA obtained as described above. PCR was carried out with the forward 2-3α and reverse B2 primers specific for minigene vector [176].

HEK293T cells were seeded in T25 flask and at 80% confluence were transfected with 6 μg of the WT or mutated pcDNA3xFLAGhNBAS and empty vector was used as control. After 48 hours, cells were lysed for protein analysis.

8.9 Western blot analysis

Total protein extracts, gel electrophoresis, transfer and visualization were performed using standard techniques. Briefly, cells were lysed in homemade RIPA buffer (50mM tris-HCl pH 7.6, 150mM NaCl, 0,5% deoxycholate, 1% NP-40, 0,1% SDS, 1X protease inhibitor). DCTM protein assay kit II (Bio-Rad) was used to quantify protein concentration following the manufacturer's instructions, on a SynergyTM H4 instrument (BioTek Instruments, Inc.). Thirty micrograms of protein extracts were separated on an 8% or 10% sodium dodecyl sulfate polyacrylamide gel electrophoresis (SDS-PAGE), according to the experimental condictions, transferred to a nitrocellulose membrane (Biorad) and blocked overnight at 4°C with milk 5% in TBST (tris-buffered saline, 0.1% Tween 20). The membrane was then incubated for 4 hours at room temperature with different primary antibodies: anti-NBAS antibodies, 1:500 (Proteintech Group, Inc) and 1:1000 (St John's Laboratory Ltd); anti-UPF2, 1:200 (Santa Cruz Biotechnology, Inc); anti-HSP60, 1:10,000, anti-FLAG, 1:1000, and anti-USE1, 1:200 (all from Sigma-Aldrich). After incubation, the membrane was washed three times with TBST and incubated for 1 hour at room temperature with the rabbit secondary antibody (for NBAS, USE1 and HSP60), the mouse secondary antibody for FLAG and the goat secondary antibody for UPF2 (1:2500, Thermo Fisher Scientific Inc.) conjugated with HRP. After three times washing with TBST, the membrane was developed using the ImmobilonTM Western kit (Millipore). Images were captured using the ChemiDoc™ MP Imaging System equipped with Image Lab™ Software (Bio-Rad). Quantization of bands was performed with ImageJ software (National Institutes of Health, USA, http://imagej.nih.gov/ij).

8.10 Immunoprecipitation

The total cell lysate was obtained by lysing not-transfected HEK293T cells and cells transfected with the pcDNA3xFLAG empty vector or the vector carrying either the wild

type (WT) or the mutant NBAS sequence with home-made lysis buffer (50 mM Hepes, 50 mM NaCl, 1% glycerol, 1% triton X-100, 1.5 mM MgCl2, 5 mM EGTA, 1X protease inhibitor). Two hundred-fifty µg of total protein extracts from each condition were incubated overnight at 4°C with 60 µl of slurry 50% G sepharose beads (Thermo Fisher Scientific Inc.) and 1 µg anti-USE1 antibody (Santa Cruz Biotechnology, Inc). The beads were then washed twice with lysis buffer to remove the unbound proteins; then, the purified antibody-antigen complexes were eluted with 2X sample buffer and subjected to SDS-PAGE as above described.

8.11 Histological and immunofluorescence analysis

Bone biopsy of Family 5 patient was used to perform histological analysis. The bone was fixed in 4% paraformaldehyde (PFA), decalcified for 4 hours at 20°C in 5% HCl, rinsed in water and then paraffin-embedded. It was sectioned at 6 µm thickness and deparaffinized for hematoxylin-eosin staining and for fluorescent antibody detection as described [233]. A monoclonal mouse TCIRG1 antibody (Sigma Aldrich Co., St. Louis, MO, USA) and a rabbit polyclonal TRAP antibody (Abcam) were used both at 1:100 dilution. Sections were blocked in PBS with 2% BSA for 2 hours, reacted overnight with primary antibodies in PBS 0.01% Tween 20, then labeled for fluorescent analysis using Alexa Fluor 488 Donkey Anti-Mouse IgG (H+L) Antibody (green) or Alexa Fluor 594 Donkey Anti-Rabbit IgG (H+L) Antibody (red) antibodies, at 1:1000 (Life Technologies) for 1 hour. For nuclear labeling, Hoechst 33342 blue (Invitrogen) was used. A Nikon TE2000 inverted microscope was used for imaging, via 14-bit 2048x2048 pixel monochrome CCD and RGB filters to reconstruct color (Spot, Sterling Heights, MI, USA).

8.12 *In silico* analysis

The prediction of the effect of mutations on splicing process was analyzed using two different software: Human Splicing Finder, version 3.0 (http://www.umd.be/HSF3/HSF.html) and Berkeley Drosophila Genome Project (http://www.fruitfly.org/seq_tools/splice.html).

8.13 Mouse model: immunohistochemical analysis

All the procedures involving mice were execute in accordance with ethical rules of the Institutional Animal Care and Use Committee of Humanitas Clinical and Research Institute and with international laws. Wild type C57Bl/6J mouse embryos were collected from pregnant females at embryonic day (E) 11.5, 13.5 and 16.5, considering E0.5 the day when the vaginal plug was visible. Embryos were fixed in 4% paraformaldehyde, embedded in paraffin and 3 μm thick parasagittal sections for total body, coronal sections for the head and longitudinal serial sections for the limb, were obtained and mounted on glass slides. All the sections were deparaffinized, treated for antigens retrieval in citrate-based buffer, incubated with 2% H_2O_2 for 20 min in the dark, washed with PBS 0,05% Tween 20 (PBST) (GIBCO® and Merck Millipore, respectively) and blocked with background sniper (from Biocare Medical) for 40 min at room temperature (RT). Then, they were incubated with the following primary antibodies, diluted in PBST: anti-NBAS, 1:300 (St John's Laboratory Ltd); anti-COL II, 1:200, anti-SOX9, 1:200, and anti-RUNX2, 1:2000, anti-TBR1, 1:400 (all Abcam) and anti-TNMD, 1:50 (Biorbyt). All but the anti-RUNX2 primary antibody were incubated overnight at 4°C whereas anti-RUNX2 was incubated 1 hour at room temperature (RT). Sections were then rinsed in PBST and incubated with secondary antibodies Mach 1 (from Biocare Medical) for 30 min at RT, rinsed in PBST, developed with 3,3'-diaminobenzidine (DAB) and counterstained with hematoxylin. Images were acquired on an Olympus XC50 Microscope.

8.14 Zebrafish model: gene knockdown

All procedures using zebrafish (Danio rerio) were authorized by the Ethical Committee of the University of Turin and the Italian Ministry of Health. Adult fishes (TL-AB strain) were maintained and bred according to standard procedures [234], kept under a 14/10 light/dark photoperiod at a constant temperature of approximately 28°C. Eggs were fertilized, collected and embryos were grown in the presence of 0.003% 1-phenyl-2-thiourea (PTU) to prevent formation of melanin pigment.

The antisense morpholino oligonucleotides (MO) used to knockdown z-nbas (Ensembl gene ID: ENSDARG00000008593) were designed based on a sequence previously described [181] and synthesized by GeneTools, LLC. The MOs were: translation block

(TB) (5'-ATCACCTGCCATGTTTTCAATGAAC-3'), designed to anneal on the ATG start codon; splice site (SS) (5'-GCCAGCCATGCTCCACATACCTGAC-3'), to block splicing at the exon 2-intron 2 junction; scrambled (scr, negative control) in which 5 mismatches were introduced in the TB sequence. Fertilized eggs were collected at one cell stage and injected with 4 nl of 100 μM of each MO, under a stereomicroscope, in the presence of phenol red for further selection of the injected embryos. They developed for 5 days and then processed for Alcian Blue staining. Embryos were fixed in 4% PFA at 4°C overnight, washed in PBS and stained with Alcian Blue for the visualization of chondrocyte condensations, according to published protocols [235, 236]. Finally, stained embryos were either kept floating in PBS or embedded in 4% low melting agarose, and examined with a low-magnification stereomicroscope (Leika MZ12), equipped with a digital photocamera (Leika IC80 HD). Digital images were contrast balanced and color matched using Photoshop 7 (Adobe), cropped, rotated and assembled into figures with QuarkXpress software (Pantone Inc.).

8.15 Zebrafish model: gene expression analysis

Total RNA was extracted from pools of 5-6 zebrafish embryos at the age 3 dpf using the Trizol reagent and retrotranscribed as above. RT-PCR analysis to evaluate z-nbas expression was conducted using a forward primer in exon 7 (5'-GTGCTCTGCTGGCATATGCC-3') and a reverse primer in exon 11 (5'-CTGGGCATCTTGAAGAATCC-3') of the transcript; the housekeeping elongation factor 1 α (z-ef1α) mRNA was used as a control of the total input mRNA with the forward primer 5'- CTGGAGGCCAGCTCAAACAT-3' and reverse primer 5'-ATCAAGAAGAGTAGTACCGCTAGCATTAC-3'. ImageJ software was used to perform bands quantifications.

9. BIBLIOGRAPHY

1. Robling, A.G., A.B. Castillo, and C.H. Turner, *Biomechanical and molecular regulation of bone remodeling.* Annu Rev Biomed Eng, 2006. **8**: p. 455-98.
2. Florencio-Silva, R., et al., *Biology of Bone Tissue: Structure, Function, and Factors That Influence Bone Cells.* Biomed Res Int, 2015. **2015**: p. 421746.
3. Datta, H.K., et al., *The cell biology of bone metabolism.* J Clin Pathol, 2008. **61**(5): p. 577-87.
4. Sims, N.A. and J.H. Gooi, *Bone remodeling: Multiple cellular interactions required for coupling of bone formation and resorption.* Semin Cell Dev Biol, 2008. **19**(5): p. 444-51.
5. Langdahl, B., S. Ferrari, and D.W. Dempster, *Bone modeling and remodeling: potential as therapeutic targets for the treatment of osteoporosis.* Ther Adv Musculoskelet Dis, 2016. **8**(6): p. 225-235.
6. Eriksen, E.F., *Normal and pathological remodeling of human trabecular bone: three dimensional reconstruction of the remodeling sequence in normals and in metabolic bone disease.* Endocr Rev, 1986. **7**(4): p. 379-408.
7. Matsuo, K. and N. Irie, *Osteoclast-osteoblast communication.* Arch Biochem Biophys, 2008. **473**(2): p. 201-9.
8. Khosla, S., M.J. Oursler, and D.G. Monroe, *Estrogen and the skeleton.* Trends Endocrinol Metab, 2012. **23**(11): p. 576-81.
9. Sobacchi, C., et al., *Osteopetrosis: genetics, treatment and new insights into osteoclast function.* Nat Rev Endocrinol, 2013. **9**(9): p. 522-36.
10. Sobacchi, C., et al., *Soluble Factors on Stage to Direct Mesenchymal Stem Cells Fate.* Front Bioeng Biotechnol, 2017. **5**: p. 32.
11. Bianco, P., et al., *The meaning, the sense and the significance: translating the science of mesenchymal stem cells into medicine.* Nat Med, 2013. **19**(1): p. 35-42.
12. Mackie, E.J., *Osteoblasts: novel roles in orchestration of skeletal architecture.* Int J Biochem Cell Biol, 2003. **35**(9): p. 1301-5.
13. Capulli, M., R. Paone, and N. Rucci, *Osteoblast and osteocyte: games without frontiers.* Arch Biochem Biophys, 2014. **561**: p. 3-12.
14. Shiozawa, Y. and R.S. Taichman, *Getting blood from bone: an emerging understanding of the role that osteoblasts play in regulating hematopoietic stem cells within their niche.* Exp Hematol, 2012. **40**(9): p. 685-94.
15. Komori, T., et al., *Targeted disruption of Cbfa1 results in a complete lack of bone formation owing to maturational arrest of osteoblasts.* Cell, 1997. **89**(5): p. 755-64.
16. Nakashima, K., et al., *The novel zinc finger-containing transcription factor osterix is required for osteoblast differentiation and bone formation.* Cell, 2002. **108**(1): p. 17-29.
17. van de Peppel, J., et al., *Identification of Three Early Phases of Cell-Fate Determination during Osteogenic and Adipogenic Differentiation by Transcription Factor Dynamics.* Stem Cell Reports, 2017. **8**(4): p. 947-960.
18. Bialek, P., et al., *A twist code determines the onset of osteoblast differentiation.* Dev Cell, 2004. **6**(3): p. 423-35.
19. Samee, N., M.C. de Vernejoul, and G. Levi, *Role of DLX regulatory proteins in osteogenesis and chondrogenesis.* Crit Rev Eukaryot Gene Expr, 2007. **17**(3): p. 173-86.
20. Yang, X., et al., *ATF4 is a substrate of RSK2 and an essential regulator of osteoblast biology; implication for Coffin-Lowry Syndrome.* Cell, 2004. **117**(3): p. 387-98.
21. Ducy, P., et al., *Osf2/Cbfa1: a transcriptional activator of osteoblast differentiation.* Cell, 1997. **89**(5): p. 747-54.
22. Grigoriadis, A.E., J.N. Heersche, and J.E. Aubin, *Differentiation of muscle, fat, cartilage, and bone from progenitor cells present in a bone-derived clonal cell population: effect of dexamethasone.* J Cell Biol, 1988. **106**(6): p. 2139-51.

23. Schena, F., et al., *Murine Rankl-/- Mesenchymal Stromal Cells Display an Osteogenic Differentiation Defect Improved by a RANKL-Expressing Lentiviral Vector.* Stem Cells, 2017.
24. Baron, R. and G. Rawadi, *Targeting the Wnt/beta-catenin pathway to regulate bone formation in the adult skeleton.* Endocrinology, 2007. **148**(6): p. 2635-43.
25. Soltanoff, C.S., et al., *Signaling networks that control the lineage commitment and differentiation of bone cells.* Crit Rev Eukaryot Gene Expr, 2009. **19**(1): p. 1-46.
26. Kang, S., et al., *Wnt signaling stimulates osteoblastogenesis of mesenchymal precursors by suppressing CCAAT/enhancer-binding protein alpha and peroxisome proliferator-activated receptor gamma.* J Biol Chem, 2007. **282**(19): p. 14515-24.
27. Evenepoel, P., P. D'Haese, and V. Brandenburg, *Sclerostin and DKK1: new players in renal bone and vascular disease.* Kidney Int, 2015. **88**(2): p. 235-40.
28. Mazon, M., D. Masi, and M. Carreau, *Modulating Dickkopf-1: A Strategy to Monitor or Treat Cancer?* Cancers (Basel), 2016. **8**(7).
29. Pangrazio, A., et al., *Identification of the first deletion in the LRP5 gene in a patient with autosomal dominant osteopetrosis type I.* Bone, 2011. **49**(3): p. 568-71.
30. Kawano, Y. and R. Kypta, *Secreted antagonists of the Wnt signalling pathway.* J Cell Sci, 2003. **116**(Pt 13): p. 2627-34.
31. Shi, G.X., et al., *The role of R-spondins and their receptors in bone metabolism.* Prog Biophys Mol Biol, 2016. **122**(2): p. 93-100.
32. Luo, J., et al., *Regulation of bone formation and remodeling by G-protein-coupled receptor 48.* Development, 2009. **136**(16): p. 2747-56.
33. Wu, M., G. Chen, and Y.P. Li, *TGF-beta and BMP signaling in osteoblast, skeletal development, and bone formation, homeostasis and disease.* Bone Res, 2016. **4**: p. 16009.
34. Salazar, V.S., L.W. Gamer, and V. Rosen, *BMP signalling in skeletal development, disease and repair.* Nat Rev Endocrinol, 2016. **12**(4): p. 203-21.
35. Anderson, H.C., *Matrix vesicles and calcification.* Curr Rheumatol Rep, 2003. **5**(3): p. 222-6.
36. Lacey, D.L., et al., *Osteoprotegerin ligand is a cytokine that regulates osteoclast differentiation and activation.* Cell, 1998. **93**(2): p. 165-76.
37. Baud'huin, M., et al., *Factor VIII-von Willebrand factor complex inhibits osteoclastogenesis and controls cell survival.* J Biol Chem, 2009. **284**(46): p. 31704-13.
38. Emery, J.G., et al., *Osteoprotegerin is a receptor for the cytotoxic ligand TRAIL.* J Biol Chem, 1998. **273**(23): p. 14363-7.
39. Lamoureux, F., et al., *Glycosaminoglycans as potential regulators of osteoprotegerin therapeutic activity in osteosarcoma.* Cancer Res, 2009. **69**(2): p. 526-36.
40. Negishi-Koga, T. and H. Takayanagi, *Bone cell communication factors and Semaphorins.* Bonekey Rep, 2012. **1**: p. 183.
41. Schaffler, M.B., et al., *Osteocytes: master orchestrators of bone.* Calcif Tissue Int, 2014. **94**(1): p. 5-24.
42. O'Brien, C.A., T. Nakashima, and H. Takayanagi, *Osteocyte control of osteoclastogenesis.* Bone, 2013. **54**(2): p. 258-63.
43. Xiong, J., et al., *Osteocytes, not Osteoblasts or Lining Cells, are the Main Source of the RANKL Required for Osteoclast Formation in Remodeling Bone.* PLoS One, 2015. **10**(9): p. e0138189.
44. Plotkin, L.I., *Apoptotic osteocytes and the control of targeted bone resorption.* Curr Osteoporos Rep, 2014. **12**(1): p. 121-6.
45. Bonewald, L.F. and M.J. Wacker, *FGF23 production by osteocytes.* Pediatr Nephrol, 2013. **28**(4): p. 563-8.
46. Bonewald, L.F., *The amazing osteocyte.* J Bone Miner Res, 2011. **26**(2): p. 229-38.
47. Everts, V., et al., *The bone lining cell: its role in cleaning Howship's lacunae and initiating bone formation.* J Bone Miner Res, 2002. **17**(1): p. 77-90.

48. Kim, S.W., et al., *Sclerostin Antibody Administration Converts Bone Lining Cells Into Active Osteoblasts.* J Bone Miner Res, 2017. **32**(5): p. 892-901.
49. Andersen, T.L., et al., *A physical mechanism for coupling bone resorption and formation in adult human bone.* Am J Pathol, 2009. **174**(1): p. 239-47.
50. Donahue, H.J., et al., *Cell-to-cell communication in osteoblastic networks: cell line-dependent hormonal regulation of gap junction function.* J Bone Miner Res, 1995. **10**(6): p. 881-9.
51. Cappariello, A., et al., *The Great Beauty of the osteoclast.* Arch Biochem Biophys, 2014. **558**: p. 70-8.
52. Crockett, J.C., et al., *New knowledge on critical osteoclast formation and activation pathways from study of rare genetic diseases of osteoclasts: focus on the RANK/RANKL axis.* Osteoporos Int, 2011. **22**(1): p. 1-20.
53. Miyamoto, K., et al., *Osteoclasts are dispensable for hematopoietic stem cell maintenance and mobilization.* J Exp Med, 2011. **208**(11): p. 2175-81.
54. Blin-Wakkach, C., M. Rouleau, and A. Wakkach, *Roles of osteoclasts in the control of medullary hematopoietic niches.* Arch Biochem Biophys, 2014. **561**: p. 29-37.
55. Boyce, B.F., *Advances in the regulation of osteoclasts and osteoclast functions.* J Dent Res, 2013. **92**(10): p. 860-7.
56. Ibanez, L., et al., *Inflammatory Osteoclasts Prime TNFalpha-Producing CD4+ T Cells and Express CX3 CR1.* J Bone Miner Res, 2016. **31**(10): p. 1899-1908.
57. Li, H., et al., *Cross talk between the bone and immune systems: osteoclasts function as antigen-presenting cells and activate CD4+ and CD8+ T cells.* Blood, 2010. **116**(2): p. 210-7.
58. Tondravi, M.M., et al., *Osteopetrosis in mice lacking haematopoietic transcription factor PU.1.* Nature, 1997. **386**(6620): p. 81-4.
59. Grigoriadis, A.E., et al., *c-Fos: a key regulator of osteoclast-macrophage lineage determination and bone remodeling.* Science, 1994. **266**(5184): p. 443-8.
60. Soysa, N.S., et al., *Osteoclast formation and differentiation: an overview.* J Med Dent Sci, 2012. **59**(3): p. 65-74.
61. Boyce, B.F., et al., *NF-kappaB-Mediated Regulation of Osteoclastogenesis.* Endocrinol Metab (Seoul), 2015. **30**(1): p. 35-44.
62. Kim, K., et al., *NFATc1 induces osteoclast fusion via up-regulation of Atp6v0d2 and the dendritic cell-specific transmembrane protein (DC-STAMP).* Mol Endocrinol, 2008. **22**(1): p. 176-85.
63. Bae, S., et al., *MYC-dependent oxidative metabolism regulates osteoclastogenesis via nuclear receptor ERRalpha.* J Clin Invest, 2017. **127**(7): p. 2555-2568.
64. Shin, B., et al., *Secretion of a truncated osteopetrosis-associated transmembrane protein 1 (OSTM1) mutant inhibits osteoclastogenesis through down-regulation of the B lymphocyte-induced maturation protein 1 (BLIMP1)-nuclear factor of activated T cells c1 (NFATc1) axis.* J Biol Chem, 2014. **289**(52): p. 35868-81.
65. Luo, J., et al., *LGR4 is a receptor for RANKL and negatively regulates osteoclast differentiation and bone resorption.* Nat Med, 2016. **22**(5): p. 539-46.
66. Teitelbaum, S.L., *Bone resorption by osteoclasts.* Science, 2000. **289**(5484): p. 1504-8.
67. Gay, C.V. and J.A. Weber, *Regulation of differentiated osteoclasts.* Crit Rev Eukaryot Gene Expr, 2000. **10**(3-4): p. 213-30.
68. Zaidi, M., et al., *Cathepsin K, osteoclastic resorption, and osteoporosis therapy.* J Bone Miner Res, 2001. **16**(10): p. 1747-9.
69. Picollo, A. and M. Pusch, *Chloride/proton antiporter activity of mammalian CLC proteins ClC-4 and ClC-5.* Nature, 2005. **436**(7049): p. 420-3.
70. Gimble, J.M. and M.E. Nuttall, *The relationship between adipose tissue and bone metabolism.* Clin Biochem, 2012. **45**(12): p. 874-9.
71. Muruganandan, S. and C.J. Sinal, *The impact of bone marrow adipocytes on osteoblast and osteoclast differentiation.* IUBMB Life, 2014.

72. Lo Celso, C. and D.T. Scadden, *The haematopoietic stem cell niche at a glance.* J Cell Sci, 2011. **124**(Pt 21): p. 3529-35.
73. Zhou, B.O., L. Ding, and S.J. Morrison, *Hematopoietic stem and progenitor cells regulate the regeneration of their niche by secreting Angiopoietin-1.* Elife, 2015. **4**: p. e05521.
74. Weidner, H., et al., *Myelodysplastic syndromes and bone loss in mice and men.* Leukemia, 2017. **31**(4): p. 1003-1007.
75. Weitzmann, M.N. and I. Ofotokun, *Physiological and pathophysiological bone turnover - role of the immune system.* Nat Rev Endocrinol, 2016. **12**(9): p. 518-32.
76. Mori, G., et al., *Bone-immune cell crosstalk: bone diseases.* J Immunol Res, 2015. **2015**: p. 108451.
77. Boskey, A.L., *Bone composition: relationship to bone fragility and antiosteoporotic drug effects.* Bonekey Rep, 2013. **2**: p. 447.
78. Kuivaniemi, H., G. Tromp, and D.J. Prockop, *Mutations in fibrillar collagens (types I, II, III, and XI), fibril-associated collagen (type IX), and network-forming collagen (type X) cause a spectrum of diseases of bone, cartilage, and blood vessels.* Hum Mutat, 1997. **9**(4): p. 300-15.
79. McKleroy, W., T.H. Lee, and K. Atabai, *Always cleave up your mess: targeting collagen degradation to treat tissue fibrosis.* Am J Physiol Lung Cell Mol Physiol, 2013. **304**(11): p. L709-21.
80. Kram, V., et al., *Small leucine rich proteoglycans, a novel link to osteoclastogenesis.* Sci Rep, 2017. **7**(1): p. 12627.
81. Lamoureux, F., et al., *Proteoglycans: key partners in bone cell biology.* Bioessays, 2007. **29**(8): p. 758-71.
82. Trombetta, J.M. and A.D. Bradshaw, *SPARC/osteonectin functions to maintain homeostasis of the collagenous extracellular matrix in the periodontal ligament.* J Histochem Cytochem, 2010. **58**(10): p. 871-9.
83. Wei, J. and G. Karsenty, *An overview of the metabolic functions of osteocalcin.* Rev Endocr Metab Disord, 2015. **16**(2): p. 93-8.
84. Reinholt, F.P., et al., *Osteopontin--a possible anchor of osteoclasts to bone.* Proc Natl Acad Sci U S A, 1990. **87**(12): p. 4473-5.
85. Lund, S.A., C.M. Giachelli, and M. Scatena, *The role of osteopontin in inflammatory processes.* J Cell Commun Signal, 2009. **3**(3-4): p. 311-22.
86. Feng, X., *Chemical and Biochemical Basis of Cell-Bone Matrix Interaction in Health and Disease.* Curr Chem Biol, 2009. **3**(2): p. 189-196.
87. Bala, Y. and E. Seeman, *Bone's Material Constituents and their Contribution to Bone Strength in Health, Disease, and Treatment.* Calcif Tissue Int, 2015. **97**(3): p. 308-26.
88. Cowin, S.C. and L. Cardoso, *Blood and interstitial flow in the hierarchical pore space architecture of bone tissue.* J Biomech, 2015. **48**(5): p. 842-54.
89. Ojanen, X., et al., *Relationships between tissue composition and viscoelastic properties in human trabecular bone.* J Biomech, 2015. **48**(2): p. 269-75.
90. Berendsen, A.D. and B.R. Olsen, *Bone development.* Bone, 2015. **80**: p. 14-18.
91. Ding, M., et al., *Targeting Runx2 expression in hypertrophic chondrocytes impairs endochondral ossification during early skeletal development.* J Cell Physiol, 2012. **227**(10): p. 3446-56.
92. Lim, J., et al., *BMP-Smad4 signaling is required for precartilaginous mesenchymal condensation independent of Sox9 in the mouse.* Dev Biol, 2015. **400**(1): p. 132-8.
93. Takarada, T., et al., *An analysis of skeletal development in osteoblast-specific and chondrocyte-specific runt-related transcription factor-2 (Runx2) knockout mice.* J Bone Miner Res, 2013. **28**(10): p. 2064-9.
94. Colnot, C., et al., *Distinguishing the contributions of the perichondrium, cartilage, and vascular endothelium to skeletal development.* Dev Biol, 2004. **269**(1): p. 55-69.

95. Kronenberg, H.M., *Developmental regulation of the growth plate.* Nature, 2003. **423**(6937): p. 332-6.
96. Lui, J.C., O. Nilsson, and J. Baron, *Recent research on the growth plate: Recent insights into the regulation of the growth plate.* J Mol Endocrinol, 2014. **53**(1): p. T1-9.
97. Mackie, E.J., et al., *Endochondral ossification: how cartilage is converted into bone in the developing skeleton.* Int J Biochem Cell Biol, 2008. **40**(1): p. 46-62.
98. Bonafe, L., et al., *Nosology and classification of genetic skeletal disorders: 2015 revision.* Am J Med Genet A, 2015. **167A**(12): p. 2869-92.
99. Frattini, A., et al., *The Dissection of Human Autosomal Recessive Osteopetrosis Identifies an Osteoclast-Poor Form due to RANKL Deficiency.* Cell Cycle, 2007. **6**(24): p. 3027-3033.
100. Stark, Z. and R. Savarirayan, *Osteopetrosis.* Orphanet J Rare Dis, 2009. **4**: p. 5.
101. Doffinger, R., et al., *X-linked anhidrotic ectodermal dysplasia with immunodeficiency is caused by impaired NF-kappaB signaling.* Nat Genet, 2001. **27**(3): p. 277-85.
102. Roberts, C.M., et al., *A novel NEMO gene mutation causing osteopetrosis, lymphoedema, hypohidrotic ectodermal dysplasia and immunodeficiency (OL-HED-ID).* Eur J Pediatr, 2010. **169**(11): p. 1403-7.
103. Carlberg, V.M., et al., *Hypohidrotic ectodermal dysplasia, osteopetrosis, lymphedema, and immunodeficiency in an infant with multiple opportunistic infections.* Pediatr Dermatol, 2014. **31**(6): p. 716-21.
104. Sobacchi, C., et al., *The mutational spectrum of human malignant autosomal recessive osteopetrosis.* Hum Mol Genet, 2001. **10**(17): p. 1767-73.
105. Souraty, N., et al., *Molecular study of six families originating from the Middle-East and presenting with autosomal recessive osteopetrosis.* Eur J Med Genet, 2007. **50**(3): p. 188-99.
106. Benichou, O.D., J.D. Laredo, and M.C. de Vernejoul, *Type II autosomal dominant osteopetrosis (Albers-Schonberg disease): clinical and radiological manifestations in 42 patients.* Bone, 2000. **26**(1): p. 87-93.
107. Steward, C.G., *Neurological aspects of osteopetrosis.* Neuropathol Appl Neurobiol, 2003. **29**(2): p. 87-97.
108. Guerrini, M.M., et al., *Human osteoclast-poor osteopetrosis with hypogammaglobulinemia due to TNFRSF11A (RANK) mutations.* Am J Hum Genet, 2008. **83**(1): p. 64-76.
109. Mazzolari, E., et al., *A single-center experience in 20 patients with infantile malignant osteopetrosis.* Am J Hematol, 2009. **84**(8): p. 473-9.
110. Pangrazio, A., et al., *RANK-dependent autosomal recessive osteopetrosis: characterization of five new cases with novel mutations.* J Bone Miner Res, 2012. **27**(2): p. 342-51.
111. Frattini, A., et al., *Chloride channel ClCN7 mutations are responsible for severe recessive, dominant, and intermediate osteopetrosis.* J Bone Miner Res, 2003. **18**(10): p. 1740-7.
112. Pangrazio, A., et al., *Mutations in OSTM1 (grey lethal) define a particularly severe form of autosomal recessive osteopetrosis with neural involvement.* J Bone Miner Res, 2006. **21**(7): p. 1098-105.
113. Schinke, T., et al., *Impaired gastric acidification negatively affects calcium homeostasis and bone mass.* Nat Med, 2009. **15**(6): p. 674-81.
114. Ye, L., et al., *Osteopetrorickets due to Snx10 deficiency in mice results from both failed osteoclast activity and loss of gastric acid-dependent calcium absorption.* PLoS Genet, 2015. **11**(3): p. e1005057.
115. Sly, W.S., et al., *Carbonic anhydrase II deficiency identified as the primary defect in the autosomal recessive syndrome of osteopetrosis with renal tubular acidosis and cerebral calcification.* Proc Natl Acad Sci U S A, 1983. **80**(9): p. 2752-6.

116. Venta, P.J., et al., *Carbonic anhydrase II deficiency syndrome in a Belgian family is caused by a point mutation at an invariant histidine residue (107 His----Tyr): complete structure of the normal human CA II gene.* Am J Hum Genet, 1991. **49**(5): p. 1082-90.
117. Frattini, A., et al., *Defects in TCIRG1 subunit of the vacuolar proton pump are responsible for a subset of human autosomal recessive osteopetrosis.* Nat Genet, 2000. **25**(3): p. 343-6.
118. Qin, A., et al., *V-ATPases in osteoclasts: structure, function and potential inhibitors of bone resorption.* Int J Biochem Cell Biol, 2012. **44**(9): p. 1422-35.
119. Nakamura, I., et al., *Lack of vacuolar proton ATPase association with the cytoskeleton in osteoclasts of osteosclerotic (oc/oc) mice.* FEBS Lett, 1997. **401**(2-3): p. 207-12.
120. Leisle, L., et al., *ClC-7 is a slowly voltage-gated 2Cl(-)/1H(+)-exchanger and requires Ostm1 for transport activity.* EMBO J, 2011. **30**(11): p. 2140-52.
121. Ludwig, C.F., et al., *Common gating of both CLC transporter subunits underlies voltage-dependent activation of the 2Cl-/1H+ exchanger ClC-7/Ostm1.* J Biol Chem, 2013. **288**(40): p. 28611-9.
122. Kasper, D., et al., *Loss of the chloride channel ClC-7 leads to lysosomal storage disease and neurodegeneration.* EMBO J, 2005. **24**(5): p. 1079-91.
123. Weinert, S., et al., *Transport activity and presence of ClC-7/Ostm1 complex account for different cellular functions.* EMBO Rep, 2014. **15**(7): p. 784-91.
124. Kornak, U., et al., *Loss of the ClC-7 chloride channel leads to osteopetrosis in mice and man.* Cell, 2001. **104**(2): p. 205-15.
125. Pangrazio, A., et al., *Molecular and clinical heterogeneity in CLCN7-dependent osteopetrosis: report of 20 novel mutations.* Hum Mutat, 2010. **31**(1): p. E1071-80.
126. Lange, P.F., et al., *ClC-7 requires Ostm1 as a beta-subunit to support bone resorption and lysosomal function.* Nature, 2006. **440**(7081): p. 220-3.
127. Fischer, T., et al., *Promotion of G alpha i3 subunit down-regulation by GIPN, a putative E3 ubiquitin ligase that interacts with RGS-GAIP.* Proc Natl Acad Sci U S A, 2003. **100**(14): p. 8270-5.
128. Feigin, M.E. and C.C. Malbon, *OSTM1 regulates beta-catenin/Lef1 interaction and is required for Wnt/beta-catenin signaling.* Cell Signal, 2008. **20**(5): p. 949-57.
129. Pandruvada, S.N., et al., *Role of Ostm1 Cytosolic Complex with Kinesin 5B in Intracellular Dispersion and Trafficking.* Mol Cell Biol, 2015. **36**(3): p. 507-21.
130. Tabata, K., et al., *Rubicon and PLEKHM1 negatively regulate the endocytic/autophagic pathway via a novel Rab7-binding domain.* Mol Biol Cell, 2010. **21**(23): p. 4162-72.
131. Ng, P.Y., et al., *Disruption of the dynein-dynactin complex unveils motor-specific functions in osteoclast formation and bone resorption.* J Bone Miner Res, 2013. **28**(1): p. 119-34.
132. Marwaha, R., et al., *The Rab7 effector PLEKHM1 binds Arl8b to promote cargo traffic to lysosomes.* J Cell Biol, 2017. **216**(4): p. 1051-1070.
133. Fujiwara, T., et al., *PLEKHM1/DEF8/RAB7 complex regulates lysosome positioning and bone homeostasis.* JCI Insight, 2016. **1**(17): p. e86330.
134. Witwicka, H., et al., *TRAFD1 (FLN29) Interacts with Plekhm1 and Regulates Osteoclast Acidification and Resorption.* PLoS One, 2015. **10**(5): p. e0127537.
135. McEwan, D.G., et al., *PLEKHM1 regulates autophagosome-lysosome fusion through HOPS complex and LC3/GABARAP proteins.* Mol Cell, 2015. **57**(1): p. 39-54.
136. Bo, T., et al., *Characterization of a Relatively Malignant Form of Osteopetrosis Caused by a Novel Mutation in the PLEKHM1 Gene.* J Bone Miner Res, 2016. **31**(11): p. 1979-1987.
137. Stattin, E.L., et al., *SNX10 gene mutation leading to osteopetrosis with dysfunctional osteoclasts.* Sci Rep, 2017. **7**(1): p. 3012.
138. Flanagan, A.M., et al., *Macrophage colony-stimulating factor and receptor activator NF-kappaB ligand fail to rescue osteoclast-poor human malignant infantile osteopetrosis in vitro.* Bone, 2002. **30**(1): p. 85-90.

139. Blair, H.C., et al., *In vitro differentiation of CD14 cells from osteopetrotic subjects: contrasting phenotypes with TCIRG1, CLCN7, and attachment defects.* J Bone Miner Res, 2004. **19**(8): p. 1329-38.
140. Sobacchi, C., et al., *Osteoclast-poor human osteopetrosis due to mutations in the gene encoding RANKL.* Nat Genet, 2007. **39**(8): p. 960-2.
141. Lo Iacono, N., et al., *Osteopetrosis rescue upon RANKL administration to Rankl(-/-) mice: a new therapy for human RANKL-dependent ARO.* J Bone Miner Res, 2012. **27**(12): p. 2501-10.
142. Walsh, M.C. and Y. Choi, *Biology of the RANKL-RANK-OPG System in Immunity, Bone, and Beyond.* Front Immunol, 2014. **5**: p. 511.
143. Lo Iacono, N., et al., *RANKL cytokine: from pioneer of the osteoimmunology era to cure for a rare disease.* Clin Dev Immunol, 2013. **2013**: p. 412768.
144. Campeau, P.M., et al., *Whole-exome sequencing identifies mutations in the nucleoside transporter gene SLC29A3 in dysosteosclerosis, a form of osteopetrosis.* Hum Mol Genet, 2012. **21**(22): p. 4904-9.
145. George, A., et al., *Biallelic Mutations in MITF Cause Coloboma, Osteopetrosis, Microphthalmia, Macrocephaly, Albinism, and Deafness.* Am J Hum Genet, 2016. **99**(6): p. 1388-1394.
146. Weisz Hubshman, M., et al., *Homozygous deletion of RAG1, RAG2 and 5′ region TRAF6 causes severe immune suppression and atypical osteopetrosis.* Clin Genet, 2017. **91**(6): p. 902-907.
147. Swarnkar, G., et al., *Myeloid Deletion of Nemo Causes Osteopetrosis in Mice Owing to Upregulation of Transcriptional Repressors.* Sci Rep, 2016. **6**: p. 29896.
148. Mory, A., et al., *Kindlin-3: a new gene involved in the pathogenesis of LAD-III.* Blood, 2008. **112**(6): p. 2591.
149. Crazzolara, R., et al., *A new mutation in the KINDLIN-3 gene ablates integrin-dependent leukocyte, platelet, and osteoclast function in a patient with leukocyte adhesion deficiency-III.* Pediatr Blood Cancer, 2015. **62**(9): p. 1677-9.
150. Schmidt, S., et al., *Kindlin-3-mediated signaling from multiple integrin classes is required for osteoclast-mediated bone resorption.* J Cell Biol, 2011. **192**(5): p. 883-97.
151. Alatalo, S.L., et al., *Osteoclast-derived serum tartrate-resistant acid phosphatase 5b in Albers-Schonberg disease (type II autosomal dominant osteopetrosis).* Clin Chem, 2004. **50**(5): p. 883-90.
152. Coccia, P.F., et al., *Successful bone-marrow transplantation for infantile malignant osteopetrosis.* N Engl J Med, 1980. **302**(13): p. 701-8.
153. Orchard, P.J., et al., *Hematopoietic stem cell transplantation for infantile osteopetrosis.* Blood, 2015. **126**(2): p. 270-6.
154. Naguib, K.K., *Hypertelorism, proptosis, ptosis, polysyndactyly, hypospadias and normal height in 3 sibs: a new syndrome?* Am J Med Genet, 1988. **29**(1): p. 35-41.
155. Richieri-Costa, A., L. Montagnoli, and T.Y. Kamiya, *Autosomal recessive acro-fronto-facio-nasal dysostosis associated with genitourinary anomalies.* Am J Med Genet, 1989. **33**(1): p. 121-4.
156. Teebi, A.S., *Naguib-Richieri-Costa syndrome: hypertelorism, hypospadias, and polysyndactyly syndrome.* Am J Med Genet, 1992. **44**(1): p. 115-7.
157. Chaabouni, M., et al., *Autosomal recessive acro-fronto-facio-nasal dysostosis associated with genitourinary anomalies: a third case report.* Am J Med Genet A, 2008. **146A**(14): p. 1825-7.
158. Richieri-Costa, A., et al., *A previously undescribed autosomal recessive multiple congenital anomalies/mental retardation (MCA/MR) syndrome with fronto-nasal dysostosis, cleft lip/palate, limb hypoplasia, and postaxial poly-syndactyly: acro-fronto-facio-nasal dysostosis syndrome.* Am J Med Genet, 1985. **20**(4): p. 631-8.
159. Richieri-Costa, A., M.L. Guion-Almeida, and N.A. Pagnan, *Acro-fronto-facio-nasal dysostosis: report of a new Brazilian family.* Am J Med Genet, 1992. **44**(6): p. 800-2.

160. Guion-Almeida, M.L. and A. Richieri-Costa, *Acrofrontofacionasal dysostosis: report of the third Brazilian family.* Am J Med Genet A, 2003. **119A**(2): p. 238-41.
161. Prontera, P., et al., *Acrofrontofacionasal dysostosis 1 in two sisters of Indian origin.* Am J Med Genet A, 2011. **155A**(12): p. 3125-7.
162. Venter, J.C., et al., *The sequence of the human genome.* Science, 2001. **291**(5507): p. 1304-51.
163. Lander, E.S., et al., *Initial sequencing and analysis of the human genome.* Nature, 2001. **409**(6822): p. 860-921.
164. Green, E.D. and M.S. Guyer, *Charting a course for genomic medicine from base pairs to bedside.* Nature, 2011. **470**(7333): p. 204-13.
165. Bahassi el, M. and P.J. Stambrook, *Next-generation sequencing technologies: breaking the sound barrier of human genetics.* Mutagenesis, 2014. **29**(5): p. 303-10.
166. Hui, P., *Next generation sequencing: chemistry, technology and applications.* Top Curr Chem, 2014. **336**: p. 1-18.
167. Barzon, L., et al., *Applications of next-generation sequencing technologies to diagnostic virology.* Int J Mol Sci, 2011. **12**(11): p. 7861-84.
168. Xiao, M., et al., *Metaproteomic strategies and applications for gut microbial research.* Appl Microbiol Biotechnol, 2017. **101**(8): p. 3077-3088.
169. Rabbani, B., M. Tekin, and N. Mahdieh, *The promise of whole-exome sequencing in medical genetics.* J Hum Genet, 2014. **59**(1): p. 5-15.
170. Zhang, X., *Exome sequencing greatly expedites the progressive research of Mendelian diseases.* Front Med, 2014. **8**(1): p. 42-57.
171. Stranneheim, H. and A. Wedell, *Exome and genome sequencing: a revolution for the discovery and diagnosis of monogenic disorders.* J Intern Med, 2016. **279**(1): p. 3-15.
172. Rognoni, E., R. Ruppert, and R. Fassler, *The kindlin family: functions, signaling properties and implications for human disease.* J Cell Sci, 2016. **129**(1): p. 17-27.
173. Palagano, E., et al., *Buried in the Middle but Guilty: Intronic Mutations in the TCIRG1 Gene Cause Human Autosomal Recessive Osteopetrosis.* J Bone Miner Res, 2015. **30**(10): p. 1814-21.
174. Michalova, E., B. Vojtesek, and R. Hrstka, *Impaired pre-mRNA processing and altered architecture of 3′ untranslated regions contribute to the development of human disorders.* Int J Mol Sci, 2013. **14**(8): p. 15681-94.
175. Palagano, E., et al., *Synonymous Mutations Add a Layer of Complexity in the Diagnosis of Human Osteopetrosis.* J Bone Miner Res, 2017. **32**(1): p. 99-105.
176. Pagani, F., et al., *Splicing factors induce cystic fibrosis transmembrane regulator exon 9 skipping through a nonevolutionary conserved intronic element.* J Biol Chem, 2000. **275**(28): p. 21041-7.
177. Migliaccio, S., et al., *Association of intermediate osteopetrosis with poikiloderma.* J Bone Miner Res, 1999. **14**(5): p. 834-6.
178. Volpi, L., et al., *Targeted next-generation sequencing appoints c16orf57 as clericuzio-type poikiloderma with neutropenia gene.* Am J Hum Genet, 2010. **86**(1): p. 72-6.
179. Tanaka, A., et al., *Identification of a homozygous deletion mutation in C16orf57 in a family with Clericuzio-type poikiloderma with neutropenia.* Am J Med Genet A, 2010. **152A**(6): p. 1347-8.
180. Lin, L., et al., *Sox11 regulates survival and axonal growth of embryonic sensory neurons.* Dev Dyn, 2011. **240**(1): p. 52-64.
181. Anastasaki, C., et al., *Dhx34 and Nbas function in the NMD pathway and are required for embryonic development in zebrafish.* Nucleic Acids Res, 2011. **39**(9): p. 3686-94.
182. Kosan, C. and J. Kunz, *Identification and characterisation of the gene TWIST NEIGHBOR (TWISTNB) located in the microdeletion syndrome 7p21 region.* Cytogenet Genome Res, 2002. **97**(3-4): p. 167-70.
183. Trengove, M.C. and A.C. Ward, *SOCS proteins in development and disease.* Am J Clin Exp Immunol, 2013. **2**(1): p. 1-29.

184. Maddox, D.M., et al., *Reduced-folate carrier (RFC) is expressed in placenta and yolk sac, as well as in cells of the developing forebrain, hindbrain, neural tube, craniofacial region, eye, limb buds and heart.* BMC Dev Biol, 2003. **3**: p. 6.
185. Nicholson, P., et al., *Nonsense-mediated mRNA decay in human cells: mechanistic insights, functions beyond quality control and the double-life of NMD factors.* Cell Mol Life Sci, 2010. **67**(5): p. 677-700.
186. Aoki, T., et al., *Identification of the neuroblastoma-amplified gene product as a component of the syntaxin 18 complex implicated in Golgi-to-endoplasmic reticulum retrograde transport.* Mol Biol Cell, 2009. **20**(11): p. 2639-49.
187. Longman, D., et al., *DHX34 and NBAS form part of an autoregulatory NMD circuit that regulates endogenous RNA targets in human cells, zebrafish and Caenorhabditis elegans.* Nucleic Acids Res, 2013. **41**(17): p. 8319-31.
188. Wittkopp, N., et al., *Nonsense-mediated mRNA decay effectors are essential for zebrafish embryonic development and survival.* Mol Cell Biol, 2009. **29**(13): p. 3517-28.
189. Gilissen, C., et al., *Disease gene identification strategies for exome sequencing.* Eur J Hum Genet, 2012. **20**(5): p. 490-7.
190. Malinin, N.L., et al., *A point mutation in KINDLIN3 ablates activation of three integrin subfamilies in humans.* Nat Med, 2009. **15**(3): p. 313-8.
191. Suratannon, N., et al., *Adaptive immune defects in a patient with leukocyte adhesion deficiency type III with a novel mutation in FERMT3.* Pediatr Allergy Immunol, 2016. **27**(2): p. 214-7.
192. Jurk, K., et al., *Novel integrin-dependent platelet malfunction in siblings with leukocyte adhesion deficiency-III (LAD-III) caused by a point mutation in FERMT3.* Thromb Haemost, 2010. **103**(5): p. 1053-64.
193. McDowall, A., et al., *Two mutations in the KINDLIN3 gene of a new leukocyte adhesion deficiency III patient reveal distinct effects on leukocyte function in vitro.* Blood, 2010. **115**(23): p. 4834-42.
194. Rendu, J., et al., *Functional Characterization and Rescue of a Deep Intronic Mutation in OCRL Gene Responsible for Lowe Syndrome.* Hum Mutat, 2017. **38**(2): p. 152-159.
195. Kobayashi, K., et al., *Deep-intronic variant of fukutin is the most prevalent point mutation of Fukuyama congenital muscular dystrophy in Japan.* J Hum Genet, 2017.
196. Mendes de Almeida, R., et al., *Whole gene sequencing identifies deep-intronic variants with potential functional impact in patients with hypertrophic cardiomyopathy.* PLoS One, 2017. **12**(8): p. e0182946.
197. Zeevaert, R., et al., *Bone Dysplasia as a Key Feature in Three Patients with a Novel Congenital Disorder of Glycosylation (CDG) Type II Due to a Deep Intronic Splice Mutation in TMEM165.* JIMD Rep, 2013. **8**: p. 145-52.
198. Pettersson, U., et al., *Polymorphisms of the CLCN7 gene are associated with BMD in women.* J Bone Miner Res, 2005. **20**(11): p. 1960-7.
199. Chu, K., R. Snyder, and M.J. Econs, *Disease status in autosomal dominant osteopetrosis type 2 is determined by osteoclastic properties.* J Bone Miner Res, 2006. **21**(7): p. 1089-97.
200. Yamaguchi, T., et al., *The silent mutation MLH1 c.543C>T resulting in aberrant splicing can cause Lynch syndrome: a case report.* Jpn J Clin Oncol, 2017. **47**(6): p. 576-580.
201. Austin, F., et al., *Synonymous mutation in TP53 results in a cryptic splice site affecting its DNA-binding site in an adolescent with two primary sarcomas.* Pediatr Blood Cancer, 2017. **64**(11).
202. Cassina, M., et al., *A synonymous splicing mutation in the SF3B4 gene segregates in a family with highly variable Nager syndrome.* Eur J Hum Genet, 2017. **25**(3): p. 371-375.

203. Macaya, D., et al., *A synonymous mutation in TCOF1 causes Treacher Collins syndrome due to mis-splicing of a constitutive exon.* Am J Med Genet A, 2009. **149A**(8): p. 1624-7.
204. Clericuzio, C., H.E. Hoyme, and J.M. Aase, *Immune deficient poikiloderma: a new genodermatosis.* Am J Hum Genet, 1991. **49**: p. A661.
205. Erickson, R.P., *Southwestern Athabaskan (Navajo and Apache) genetic diseases.* Genet Med, 1999. **1**(4): p. 151-7.
206. Wang, L.L., et al., *Absence of RECQL4 mutations in poikiloderma with neutropenia in Navajo and non-Navajo patients.* Am J Med Genet A, 2003. **118A**(3): p. 299-301.
207. Van Hove, J.L., et al., *Clericuzio type poikiloderma with neutropenia is distinct from Rothmund-Thomson syndrome.* Am J Med Genet A, 2005. **132A**(2): p. 152-8.
208. Didychuk, A.L., et al., *Usb1 controls U6 snRNP assembly through evolutionarily divergent cyclic phosphodiesterase activities.* Nat Commun, 2017. **8**(1): p. 497.
209. Hilcenko, C., et al., *Aberrant 3' oligoadenylation of spliceosomal U6 small nuclear RNA in poikiloderma with neutropenia.* Blood, 2013. **121**(6): p. 1028-38.
210. Patil, P., T. Uechi, and N. Kenmochi, *Incomplete splicing of neutrophil-specific genes affects neutrophil development in a zebrafish model of poikiloderma with neutropenia.* RNA Biol, 2015. **12**(4): p. 426-34.
211. Colombo, E.A., et al., *A zebrafish model of Poikiloderma with Neutropenia recapitulates the human syndrome hallmarks and traces back neutropenia to the myeloid progenitor.* Sci Rep, 2015. **5**: p. 15814.
212. Tasca, A., et al., *Smad1/5 and Smad4 expression are important for osteoclast differentiation.* J Cell Biochem, 2015. **116**(7): p. 1350-60.
213. Qiao, W., et al., *Hair follicle defects and squamous cell carcinoma formation in Smad4 conditional knockout mouse skin.* Oncogene, 2006. **25**(2): p. 207-17.
214. Yang, L., et al., *Targeted disruption of Smad4 in mouse epidermis results in failure of hair follicle cycling and formation of skin tumors.* Cancer Res, 2005. **65**(19): p. 8671-8.
215. Wimmer, K., et al., *Co-amplification of a novel gene, NAG, with the N-myc gene in neuroblastoma.* Oncogene, 1999. **18**(1): p. 233-8.
216. Scott, D.K., et al., *The neuroblastoma amplified gene, NAG: genomic structure and characterisation of the 7.3 kb transcript predominantly expressed in neuroblastoma.* Gene, 2003. **307**: p. 1-11.
217. Hwang, J. and L.E. Maquat, *Nonsense-mediated mRNA decay (NMD) in animal embryogenesis: to die or not to die, that is the question.* Curr Opin Genet Dev, 2011. **21**(4): p. 422-30.
218. Tarpey, P.S., et al., *Mutations in UPF3B, a member of the nonsense-mediated mRNA decay complex, cause syndromic and nonsyndromic mental retardation.* Nat Genet, 2007. **39**(9): p. 1127-33.
219. Adams, D., et al., *Bloomsbury report on mouse embryo phenotyping: recommendations from the IMPC workshop on embryonic lethal screening.* Dis Model Mech, 2013. **6**(3): p. 571-9.
220. Mork, L. and G. Crump, *Zebrafish Craniofacial Development: A Window into Early Patterning.* Curr Top Dev Biol, 2015. **115**: p. 235-69.
221. Maksimova, N., et al., *Neuroblastoma amplified sequence gene is associated with a novel short stature syndrome characterised by optic nerve atrophy and Pelger-Huet anomaly.* J Med Genet, 2010. **47**(8): p. 538-48.
222. Capo-Chichi, J.M., et al., *Neuroblastoma Amplified Sequence (NBAS) mutation in recurrent acute liver failure: Confirmatory report in a sibship with very early onset, osteoporosis and developmental delay.* Eur J Med Genet, 2015. **58**(12): p. 637-41.
223. Haack, T.B., et al., *Biallelic Mutations in NBAS Cause Recurrent Acute Liver Failure with Onset in Infancy.* Am J Hum Genet, 2015. **97**(1): p. 163-9.

224. Staufner, C., et al., *Recurrent acute liver failure due to NBAS deficiency: phenotypic spectrum, disease mechanisms, and therapeutic concepts.* J Inherit Metab Dis, 2016. **39**(1): p. 3-16.
225. Segarra, N.G., et al., *NBAS mutations cause a multisystem disorder involving bone, connective tissue, liver, immune system, and retina.* Am J Med Genet A, 2015. **167A**(12): p. 2902-12.
226. Balasubramanian, M., et al., *Compound heterozygous variants in NBAS as a cause of atypical osteogenesis imperfecta.* Bone, 2017. **94**: p. 65-74.
227. Riordan, J.D. and J.H. Nadeau, *From Peas to Disease: Modifier Genes, Network Resilience, and the Genetics of Health.* Am J Hum Genet, 2017. **101**(2): p. 177-191.
228. Li, H. and R. Durbin, *Fast and accurate long-read alignment with Burrows-Wheeler transform.* Bioinformatics, 2010. **26**(5): p. 589-95.
229. McKenna, A., et al., *The Genome Analysis Toolkit: a MapReduce framework for analyzing next-generation DNA sequencing data.* Genome Res, 2010. **20**(9): p. 1297-303.
230. Cuccuru, G., et al., *Orione, a web-based framework for NGS analysis in microbiology.* Bioinformatics, 2014. **30**(13): p. 1928-9.
231. Li, M.X., et al., *Predicting mendelian disease-causing non-synonymous single nucleotide variants in exome sequencing studies.* PLoS Genet, 2013. **9**(1): p. e1003143.
232. Pagani, F., et al., *A new type of mutation causes a splicing defect in ATM.* Nat Genet, 2002. **30**(4): p. 426-9.
233. Robinson, L.J., et al., *Gene disruption of the calcium channel Orai1 results in inhibition of osteoclast and osteoblast differentiation and impairs skeletal development.* Lab Invest, 2012. **92**(7): p. 1071-83.
234. Kimmel, C.B., et al., *Stages of embryonic development of the zebrafish.* Dev Dyn, 1995. **203**(3): p. 253-310.
235. Walker, M.B. and C.B. Kimmel, *A two-color acid-free cartilage and bone stain for zebrafish larvae.* Biotech Histochem, 2007. **82**(1): p. 23-8.
236. Gioia, R., et al., *The chaperone activity of 4PBA ameliorates the skeletal phenotype of Chihuahua, a zebrafish model for dominant osteogenesis imperfecta.* Hum Mol Genet, 2017. **26**(15): p. 2897-2911.

10. APPENDIX

ORIGINAL ARTICLE

JBMR®

Buried in the Middle but Guilty: Intronic Mutations in the *TCIRG1* Gene Cause Human Autosomal Recessive Osteopetrosis

Eleonora Palagano,[1,2] Harry C Blair,[3] Alessandra Pangrazio,[1,2] Irina Tourkova,[3] Dario Strina,[1,2] Andrea Angius,[4,5] Gianmauro Cuccuru,[4] Manuela Oppo,[4] Paolo Uva,[4] Wim Van Hul,[6] Eveline Boudin,[6] Andrea Superti-Furga,[7] Flavio Faletra,[8] Agostino Nocerino,[9] Matteo C Ferrari,[10] Guido Grappiolo,[10] Marta Monari,[11] Alessandro Montanelli,[11] Paolo Vezzoni,[1,2] Anna Villa,[1,2] and Cristina Sobacchi[1,2]

[1]UOS/IRGB, Milan Unit, National Research Council (CNR), Milan, Italy
[2]Humanitas Clinical and Research Center, Rozzano, Italy
[3]Veteran's Affairs Medical Center and Department of Pathology, University of Pittsburgh, Pittsburgh, PA, USA
[4]CRS4, Science and Technology Park Polaris, Piscina Manna, Pula, Italy
[5]Institute of Genetic and Biomedical Research (IRGB), National Research Council (CNR), Monserrato, Italy
[6]Department of Medical Genetics, University of Antwerp, Antwerp, Belgium
[7]Department of Pediatrics, Lausanne University Hospital and University of Lausanne, Lausanne, Switzerland
[8]Institute for Maternal and Child Health-IRCCS "Burlo Garofolo", Trieste, Italy
[9]Clinica Pediatrica, Azienda Ospedaliero-Universitaria "S Maria della Misericordia", Udine, Italy
[10]Hip and Prosthetic Replacement Unit, Humanitas Clinical and Research Center, Rozzano, Italy
[11]Clinical Investigation Laboratory, Humanitas Clinical and Research Center, Rozzano, Italy

ABSTRACT

Autosomal recessive osteopetrosis (ARO) is a rare genetic bone disease with genotypic and phenotypic heterogeneity, sometimes translating into delayed diagnosis and treatment. In particular, cases of intermediate severity often constitute a diagnostic challenge and represent good candidates for exome sequencing. Here, we describe the tortuous path to identification of the molecular defect in two siblings, in which osteopetrosis diagnosed in early childhood followed a milder course, allowing them to reach the adult age in relatively good conditions with no specific therapy. No clearly pathogenic mutation was identified either with standard amplification and resequencing protocols or with exome sequencing analysis. While evaluating the possible impact of a 3'UTR variant on the *TCIRG1* expression, we found a novel single nucleotide change buried in the middle of intron 15 of the *TCIRG1* gene, about 150 nucleotides away from the closest canonical splice site. By sequencing a number of independent cDNA clones covering exons 14 to 17, we demonstrated that this mutation reduced splicing efficiency but did not completely abrogate the production of the normal transcript. Prompted by this finding, we sequenced the same genomic region in 33 patients from our unresolved ARO cohort and found three additional novel single nucleotide changes in a similar location and with a predicted disruptive effect on splicing, further confirmed in one of them at the transcript level. Overall, we identified an intronic region in *TCIRG1* that seems to be particularly prone to splicing mutations, allowing the production of a small amount of protein sufficient to reduce the severity of the phenotype usually associated with TCIRG1 defects. On this basis, we would recommend including *TCIRG1* not only in the molecular work-up of severe infantile osteopetrosis but also in intermediate cases and carefully evaluating the possible effects of intronic changes. © 2015 American Society for Bone and Mineral Research.

KEY WORDS: AUTOSOMAL RECESSIVE OSTEOPETROSIS; TCIRG1; EXOME; HYPOMORPHIC MUTATION; SPLICING DEFECT

Introduction

Human osteopetrosis is a genetic bone disease characterized by increased bone density owing to failure in bone resorption by osteoclasts. For a long time, two main forms have been distinguished: an autosomal recessive form, also called malignant infantile, because of its early onset and frequent lethal outcome in the absence of a therapy; and an autosomal dominant form, also termed benign, because of its later presentation and milder course. Since 2000, the molecular

Received in original form November 11, 2014; revised form March 16, 2015; accepted March 22, 2015. Accepted manuscript online March 31, 2015.
Address correspondence to: Cristina Sobacchi, PhD, Humanitas Clinical and Research Center, Via Manzoni 113, 20089 Rozzano (MI), Italy.
E-mail: cristina.sobacchi@humanitasresearch.it
Additional supporting information may be found in the online version of this article.
Journal of Bone and Mineral Research, Vol. 30, No. 10, October 2015, pp 1814–1821
DOI: 10.1002/jbmr.2517

basis of both forms has largely been unraveled, revealing a great genetic heterogeneity.[1] Subsequently, careful clinical characterization and longer follow-up have identified patients who do not fit within either class, documenting a wider variability of phenotypes, some of which escaped molecular characterization, because a responsible mutation could not be identified. In particular, it has become clear that, besides the paradigmatic recessive malignant and dominant benign forms, an intermediate group exists, in which the defect can be inherited as either a recessive or a dominant trait. These intermediate cases often represent a diagnostic challenge but also constitute the opportunity to learn important lessons on the bone biology. On this regard, we have recently reported on a young osteopetrotic patient in which an incomplete splicing defect in the *TCIRG1* gene allowed for the production of the limited amount of wild-type transcript sufficient to dampen the severity of the disease to an almost completely normal lifestyle.[2] However, in that article, we pointed out that a definitive conclusion regarding the prognosis of the pathology was not possible because of the young age of the patient and the extraordinary nature of the mutation.

Exome sequencing is a powerful, high-throughput technique that in few years has greatly improved the discovery of the genetic defect underlying Mendelian disorders.[3] This approach is fundamentally based on the observation that the vast majority of mutations causing inherited diseases are located in coding regions of the genome and, vice versa, a large fraction of rare variants altering a protein structure are predicted to impact on its function. However, current sets of probes for exome capture target not only coding regions but also 5′ and 3′ untranslated regions (5′UTR and 3′UTR, respectively) and stretches of intronic regions, including exon-flanking regions and short introns contained between targeted exons.

Here, we describe the tortuous and, to some extent, serendipitous identification of the molecular defect in the middle of intron 15 of the *TCIRG1* gene in two siblings affected by intermediate recessive osteopetrosis and in three additional patients in which a single mutated allele in the same gene had previously been found.

Materials and Methods

Samples

Clinical data and specimens, including blood and DNA samples, were collected from patients and their relatives after informed consent. This research complies with the standards established by the Independent Ethical Committee of the Humanitas Clinical and Research Centre.

Exome analysis

Exome capture was performed on 1.5 μg of high-quality genomic DNA from patients 1A and 1B and their parents, and the TruSeq Exome Enrichment Kit (Illumina Inc., San Diego, CA, USA) was used. The enriched library was validated by the Agilent DNA 1000 Kit (Agilent Technologies Inc., Santa Clara, CA, USA) and loaded on the cBot Station (Illumina Inc.) to create clonal clusters on the flow cell. Sequencing was performed on the Hiseq2000 Instrument. Reads extracted with the Illumina tools were aligned to the reference genome hg19 by using BWA-MEM[4] and stored in compressed binary files (BAM). Single nucleotide variations, insertions, and deletions were called using the Genome Analysis Toolkit (GATK).[5] All the analyses were performed using the Orione platform.[6] The variants identified were merged in a VariantCallingFormat (VCF) file, annotated by KGGSeq,[7] prioritized, and filtered according to a standard workflow for exome sequencing.

Molecular studies

The molecular analysis of genes known to be responsible for the different types of the disease (*TCIRG1*, *CLCN7*, *PLEKHM1*, *RANKL*, *RANK,* and *SNX10*) was performed by amplification and direct sequencing of exons and intron-exon boundaries as previously described.[8–13] The *TCIRG1* intron 15 was amplified using the forward primer 10271F 5′-TGTTCCTCTTCTCCCACAGC-3′ located in exon 15 and the reverse primer 5R 5′-CATCGGAGCTCCAGC-CATT-3′ in exon 17; sequencing was performed using the 10271F primer. After mRNA isolation from peripheral blood mononuclear cells lysed in Trizol (Invitrogen, Carlsbad, CA, USA) and reverse transcription using the High Capacity cDNA Reverse Transcription kit (Life Technologies, Carlsbad, CA, USA) according to the manufacturers' instructions, the effect of the intronic variants on TCIRG1 transcript processing was investigated with the forward primer 9912F 5′-GCCTGGCTGCCAACCACTTG-3′ in exon 14 and the reverse primer 5R in exon 17. For patient (Pt) 1A and Pt 1B, the PCR product was directly cloned in the TOPO TA Cloning plasmid vector (Life Technologies, Carlsbad, CA, USA), according to the manufacturer's instructions, and individual clones were sequenced using the 9912F forward primer. For Pt 2, a PCR product was obtained from the cDNA with the forward primer 5F 5′-CTGGCCCAGCACACGATGCT-3′ in exon 13 and the reverse primer 5R in exon 17; this product was cloned and individual clones were sequenced using primer 5R. For the confirmation of the variant in the *LRP5* gene, the relevant genomic region was amplified using primers forward 5′-TGGGAGGAAGGAAGGAATGC-3′ and reverse 5′-TCAGTGGCATGGGGATTAGG-3′, whereas primers forward 5′-GGGAGTGAGCACCGTCTATA-3′ and reverse 5′-CTCCTAGGAC-TACGCCCAAG-3′ were used for confirmation of the variant in the *CHKA* gene; in both cases, sequencing was performed using the forward primer.

For all the PCR reactions above, the thermocycling conditions were: initial denaturation step at 94°C for 3 minutes, followed by 34 cycles of denaturation at 94°C for 30 seconds, annealing at 62° C (55°C for the LRP5 variant) for 30 seconds, and amplification at 72°C for 30 seconds.

The effect of the mutations identified in the intron 15 of the *TCIRG1* gene was predicted using the software Human Splicing Finder, Version 2.4.1 (www.umd.be/HSF).[14] The mutation nomenclature conforms to HGVS (www.hgvs.org/mutnomen).[15]

Histological analysis

A bone biopsy specimen of Pt 1A was fixed in 4% paraformaldehyde (PFA), decalcified for 4 hours at 20 °C in 5% HCl (pH ~1), then rinsed in water, paraffin-embedded, and sectioned at 6 μm. Sections were deparaffinized for hematoxylin-eosin staining and for fluorescent antibody labeling as described.[16] For TCIRG1 labeling, a mouse monoclonal (clone 6H3) antibody was used (Sigma Aldrich Co., St. Louis, MO, USA) at 1:100 dilution. For TRAP, a rabbit polyclonal antibody, C-terminal (Abcam PLC, Cambridge, UK) was used at 1:100 dilution. Briefly, sections were blocked in PBS/2% BSA for 2 hours, reacted overnight with antibodies at indicated concentrations in PBS with 0.01% Tween 20, then labeled for fluorescent analysis using Alexa Fluor 488 Donkey Anti-Mouse IgG (H+L) Antibody (green) or Alexa Fluor 594 Donkey Anti-Rabbit IgG (H+L) Antibody (red) antibodies, at

1:1000, both from Life Technologies, for 1 hour. For nuclear labeling, Hoechst 33342 blue (Invitrogen) was used. A Nikon TE2000 inverted microscope was used for imaging, via 14-bit 2048×2048 pixel monochrome CCD and RGB filters to reconstruct color (Spot, Sterling Heights, MI, USA). Green fluorescence (Cy-2) used excitation at 450 to 490 nm, a 510-nm dichroic mirror, and a 500- to 570-nm emission filter. Red fluorescence (Cy3) used excitation at 530 to 560 nm, a 575-nm dichroic mirror, and a 580- to 650-nm emission filter.

Results

Clinical evaluation of patients

Patients 1A and 1B (Pt 1A and Pt 1B) were two affected siblings born from Italian consanguineous parents (third-degree consanguinity). Pt 1A, female, was first evaluated at age 6 years because of visual problems, in particular right amaurosis and divergent strabismus. A radiological investigation of the skull revealed increased bone density, and a skeletal survey confirmed generalized osteopetrosis (Fig. 1*A*). Computed tomography (CT) scan showed bilateral optic and acoustic foramina restriction; analysis of the visual evoked potentials (VEP) confirmed visual impairment on the right eye, whereas brainstem evoked response audiometry (BERA) gave normal results. At that time, her hematological function was normal despite mild hepatosplenomegaly. On these results, a diagnosis of osteopetrosis with low progression was made. The presence of a similar bone phenotype in her younger brother (Pt 1B) at the age of 2 years (Fig. 1*B*), together with the absence of pathological findings in their parents as well as their consanguinity, suggested an autosomal recessive pattern of inheritance. In the following years, the clinical history of both patients was mainly characterized by recurrent fractures (8 in Pt 1A, 11 in Pt 1B) at different skeletal segments, particularly the lower limbs (Fig. 1*C*), and dental problems, with delayed tooth eruption, congenitally missing teeth and, in the elder sibling, dental abscesses, requiring intravenous administration of antibiotics and a surgical intervention. The visual acuity progressively worsened in Pt 1A and was completely lost in the right eye side at the age of 9 years; subsequently, a surgery was performed to preserve the vision of the left eye. In addition, she lost hearing in the left ear starting from age 6 years. Most recent laboratory investigations, performed concomitantly with an orthopedic surgery for total hip replacement after removal of a previous prosthesis, did not show alterations of the evaluated parameters (Table 1). Histological analysis on a bone specimen from Pt 1A demonstrated an incomplete osteopetrosis with some areas displaying mostly retained mineralized cartilage and primary spongiosa, whereas others showing mostly normal lamellar bone in well-formed trabecular bone (Fig. 2). Importantly, several osteoclasts were visualized, thus clearly identifying the disease in this patient as an osteoclast-rich osteopetrosis (Fig. 2). At present, both affected siblings do not receive any specific therapy. Overall, their clinical picture can be considered benign, with Pt 1B displaying no sensorial defects and leading an almost completely normal life at age 32 years.

Patient 2 (Pt 2) was the third child of unrelated, healthy Italian parents. The symptoms of the disease appeared at age 4 years, with a generalized increase in bone density (representative, most recent radiological findings in Fig. 1*D*). He reported 7 nontraumatic fractures and suffered from recurrent osteomyelitis of the jaw. He underwent 3 orthopedic surgeries and several maxilla-facial interventions. No hematological nor sensorial deficits arose, and the patient is alive and reasonably well at age 24 years.

Patient 3 (Pt 3) has been already described (Pt 6 in Mazzolari and colleagues[17]). Briefly, the patient presented with a classical ARO phenotype, with bone defects and secondary hematological and neurological deficits at age 6.5 months. She received hematopoietic stem cell transplantation (HSCT) from a matched unrelated donor (MUD) at age 20.5 months, achieved full engraftment, and was alive and well 7.5 years after transplantation.

Patient 4 (Pt 4) was born from healthy unrelated parents from Southeastern Asia. He presented with bone defects, blindness, and hepatosplenomegaly in neonatal life. He received HSCT but eventually died 4 years after HSCT without engraftment. No further information is available.

Genetic findings

Based on the suspected recessive pattern of inheritance of the disease in Pt 1A and Pt 1B, molecular analysis in this family initially focused on the genes known to cause recessive osteopetrosis (*TCIRG1*, *CLCN7*, *PLEKHM1*, *RANKL*, *RANK,* and *SNX10*); the *OSTM1* gene was not included in the analysis because the two affected siblings did not display the primary neurological defects that are a hallmark of this ARO form. However, no molecular defect could be identified; therefore, we performed exome sequencing on both patients and their parents. This approach achieved an $80\times$ mean coverage over the 62 Mb of exomic sequence, with more than 94% of targeted regions covered. The overall transition to transversion rate (Ti/Tv) was 2.4, which is in line with what was expected for exome sequencing. The analysis identified a total of 191,872 variants that were filtered with dbSNP138 and 1000 Genome Project and according to the pattern of inheritance of the disease and to the parental consanguinity (Table 2).

Among the homozygous variants, we found a single nucleotide change in exon 22 of the *LRP5* gene (Supplementary Fig. 1A) (NG_015835.1:g.138882C>T; NM_002335:c.4574C>T) predicted to cause an amino acid substitution (p.Ala1525Val). Thus far, the so-called "activating mutations" linked with an increased bone density are clustered in the first beta-propeller, at the extracellular N-terminus of the protein, whereas mutations causing low bone density appear to be clustered in the second beta-propeller.[18] Interestingly, the variant c.4574C>T lies in a completely different region of the protein, that is the cytoplasmic tail (Supplementary Fig. 1B), known to interact with axin and FRAT, which are key components in the Wnt/β-catenin signaling pathway.[19,20]

So we confirmed this variant by Sanger sequencing and tested its activity in a classical luciferase reporter assay; however, the activation of the Wnt signaling was comparable in the presence of either the wild-type or the mutant LRP5 construct (Supplementary Fig. 1C). In addition, in this experiment, no difference between the wild-type and mutant LRP5 was observed after cotransfection with sclerostin (Supplementary Fig. 1C), whereas the "activating mutations" in LRP5 are known to result in increased Wnt signaling activity owing to reduced inhibition by sclerostin or dickkopf 1. So, these results did not support the hypothesis of a causative role for the variant in the pathogenesis of the disease. Accordingly, at the time when this article was in preparation, an update of SNP databases included this change in the *LRP5* gene at the homozygous state.

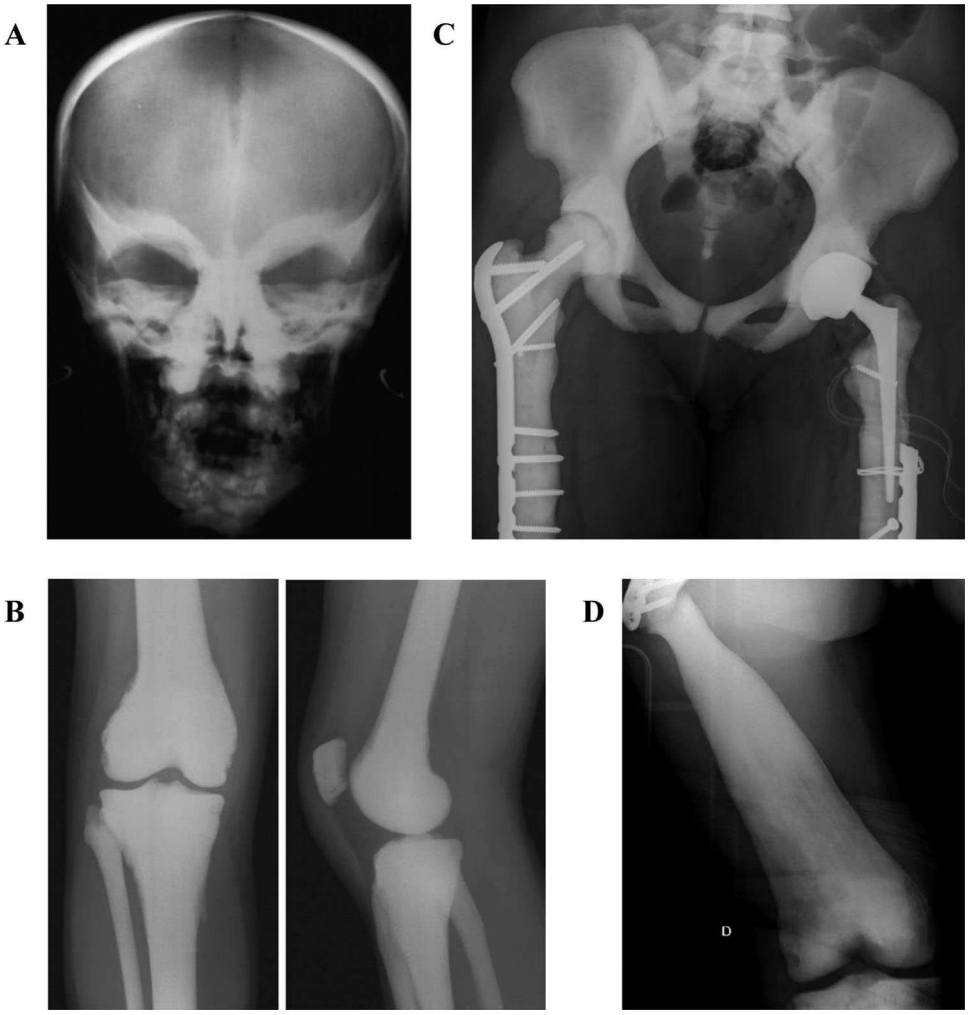

Fig. 1. Representative X-rays of Pt 1A, Pt 1B, and Pt 2, showing a diffuse increase in bone density, the typical harlequin-mask pattern of the sclerotic skull base on the AP cranium, the lack of metaphyseal bone remodeling, and the bone deformities resulting from the remodeling defects and the non-perfect healing and remodeling of fractures. (*A*) Pt 1A at age 6 years; (*B*) Pt 1B at age 2 years; (*C*) Pt 1A at age 35 years; (*D*) Pt 2 at age 22 years. Overall, the radiographs testify for a severe form osteopetrosis.

Table 1. Most Recent Laboratory Data in Pt 1A andPt 1B

	Pt 1A	Pt 1B	Ref. range
Age (years)	37	33	
Erythrocytes ($\times 10^6/\mu L$)	3.79	5.10	4.2–5.4
Hemoglobin (g/dL)	11.2	14.5	12–16
Hematocrit (%)	34.5	43.9	37–47
Serum calcium (mmol/L)	2.38	2.48	2.10–2.60
Serum phosphorus (mmol/L)	1.22	1.40	0.80–1.50
Serum iron ($\mu g/dL$)	98	123	50–170
Serum ferritin (ng/mL)	23	288	10–120
Serum alkaline phosphatase (U/L)	44	65	40–150
Serum bone ALP isoenzyme ($\mu g/L$)	6.2	10.9	6–26
Serum osteocalcin (ng/mL)	21	18	6.5–42.3
Serum PTH (pg/mL)	37.6	27.1	14.5–87.1
Serum calcitonin (pg/mL)	3.8	4	0–5.5
Serum $25(OH)D_3$ (ng/mL)	10.4	23.2	8.6–54.8

Therefore, we returned to the list of variants identified by exome sequencing. No additional noteworthy variants in coding regions were present, so we focused our attention on variants in 3′ untranslated regions (3′UTR) because they are known to influence gene expression.[21] A single nucleotide change was annotated in the 3′UTR of the choline kinase alpha (*CHKA*) gene (NM_001277; *327T>C), at the homozygous state in patients 1A and 1B and at the heterozygous state in their parents. Interestingly, *CHKA* maps to chromosome 11q13.2 on the reverse strand and immediately downstream to the *TCIRG1* gene. Because of the close proximity of the two genes, we asked whether the *327T>C variant might affect the expression of the *TCIRG1* gene. Investigation at the cDNA level through semi-quantitative RT-PCR did not show reduced expression; however, at least two unexpected bands in the two affected siblings by RT-PCR spanning exons 14 to 17 were observed (Fig. 3A), suggesting a splicing aberration. Therefore, we sequenced the corresponding genomic region, including also the whole of the three introns, and identified a single nucleotide change in the middle of intron 15 (g.10466G>A, c.1884+146G>A), which was

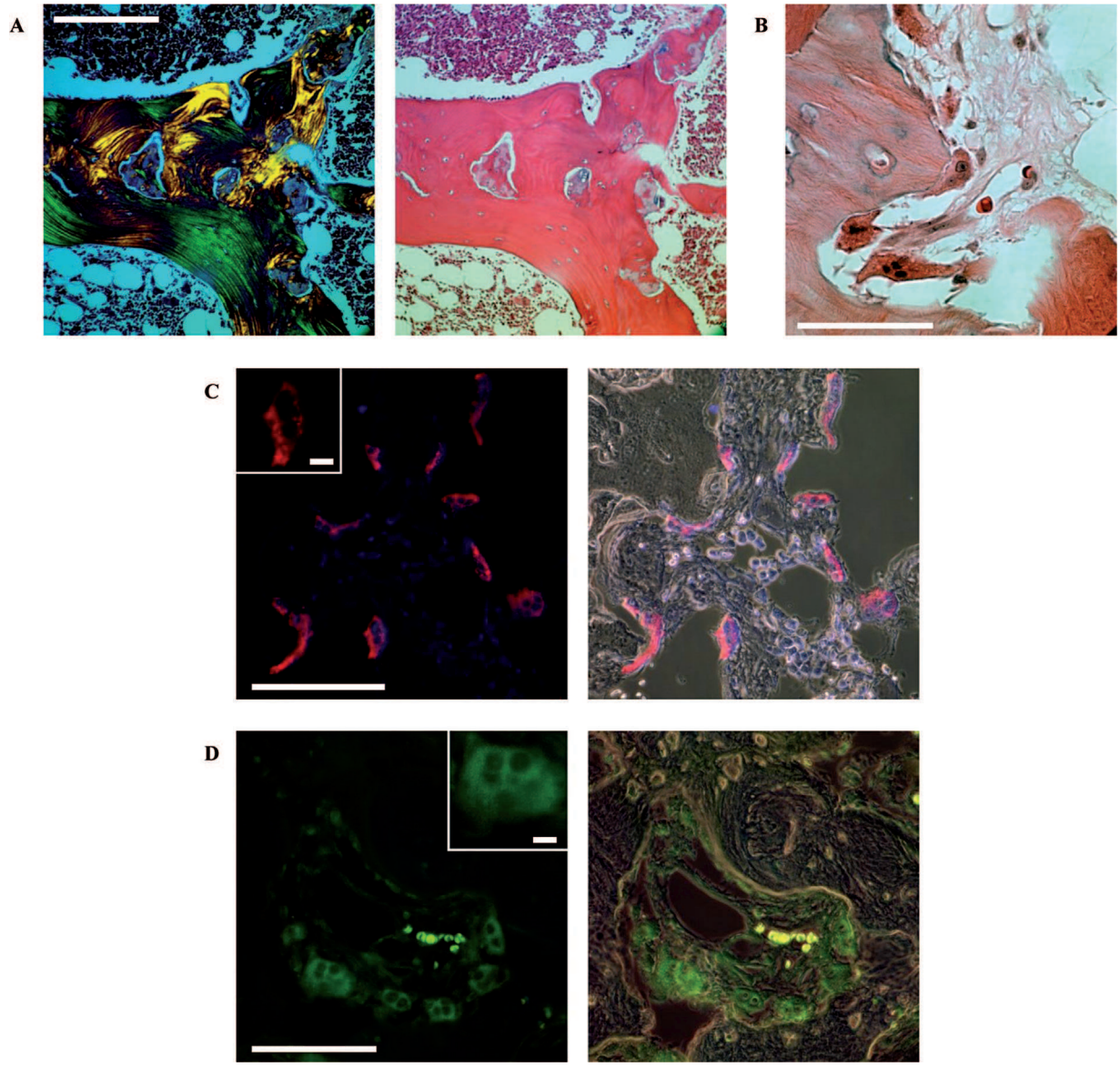

Fig. 2. Representative histological sections of a bone specimen from Pt 1A at age 35 years. (*A*) Visualization in polarized light and hematoxilin-eosin staining. Scale bar = 200 μm. The mature cortical bone shows lamellae in polarized light; the defects within the bone are islands of retained mineralized cartilage. (*B*) Higher magnification of hematoxilin-eosin staining showing several multinucleated osteoclasts. Scale bar = 100 μm. (*C*) TRAP fluorescent antibody labeling (red) and phase contrast with the fluorescence image overlaid; nuclei are stained with Hoechst (blue). The inset shows a single osteoclast at twice the magnification. Scale bar = 100 μm; inset = 10 μm. (*D*) TCIRG1 fluorescent antibody labeling (green) and phase contrast with the fluorescence overlaid (right). Scale bar = 100 μm; inset = 10 μm.

not reported in dbSNP and was present at the homozygous state in Pt 1A and Pt 1B and at the heterozygous state in their parents but absent in 100 control chromosomes from a matched population (Fig. 3*B* and data not shown). Despite this change being far from both the donor of exon 15 and the acceptor of exon 16, in silico analysis suggested a potential detrimental effect on the splicing process, by altering the strength of alternative splice sites compared with the wild-type sequence. As a confirmation of this prediction, when we cloned the cDNA PCR product spanning exons 14 to 17 and sequenced 73 independent clones, we found that few clones displayed the wild-type sequence (4/73 clones), whereas at least 8 diverse aberrant transcripts were produced, the most abundant being clones retaining 144 nucleotides of intron 15 (22/73 clones) and clones in which the first 183 nucleotides of exon 15 were skipped and 144 nucleotides of intron 15 retained (30/73 clones) (Fig. 3*C*). These data clearly supported the hypothesis of a pathogenetic role of the variant.

Prompted by these findings, we sequenced *TCIRG1* intron 15 in 26 osteopetrotic patients not yet assigned to any subgroup because of the absence of mutations in known genes, as well as in 7 ARO patients in which we had previously identified only a single mutated *TCIRG1* allele[17,22] (unpublished data). Although no mutation was found in the 26 unclassified patients, in 3 of the 7 patients harboring a single mutated *TCIRG1* allele, we found 3 additional, heterozygous single nucleotide changes in intron 15,

Table 2. Number of Variants/Genes Identified in Pt 1A and Pt 1B Through Exome Sequencing

Total variants	191,872
Shared variants after variant-quality filtering	157,065
Variant with MAF <0.05	19,170
Nonsynonymous/indel/splice sites/UTR variants	1319/98/506/5149
Homozygous variants	32
Novel variants (dbSNP138/1000GP queried)	2
Genes with plausible disease association	1 (LRP5)

close to that carried by Pt 1A and Pt 1B, namely g.10462T>A (c.1884+142T>A) in Pt 2 (mutation confirmed at the heterozygous state in Pt 2's healthy mother and in one unaffected brother; data not shown), g.10452T>C (c.1884+132T>C) in Pt 3, and g.10469C>T (c.1884+149C>T) in Pt 4 (Fig. 3*B* and Table 3. In silico analysis was performed also on these variants, obtaining a similar prediction of potential disruptive effects on the splicing process. A cell sample suitable for expression studies was available only for Pt 2, and we could confirm also in this case by RT-PCR followed by cloning and sequencing, the presence of a residual amount of wild-type transcript (5/75 clones, 6.7%) and the same pattern of aberrant transcripts previously found in Pt 1A and Pt 1B, namely 12/75 clones retaining 143 nucleotides of intron 15, 20/75 clones skipping the first 183 nucleotides of exon

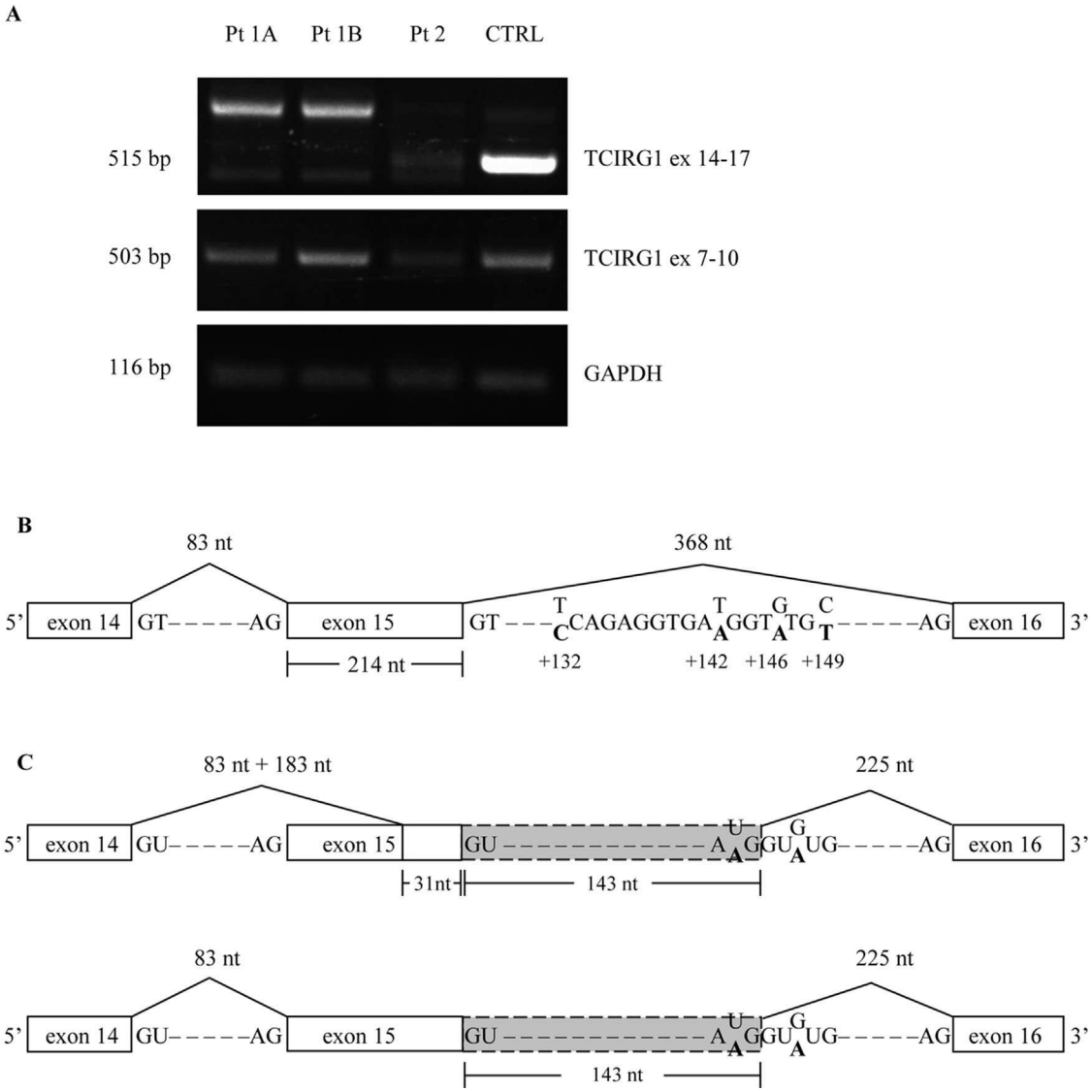

Fig. 3. (*A*) Semi-quantitative RT-PCR spanning exons 14 to 17 (upper panel), showing the presence of at least two abnormal bands in the patients (the normal band seen in Pt 2 is from the other mutated allele), or exons 7 to 10 (middle panel), showing only the presence of the expected band in all the samples. (*B*) Schematic representation of the relevant region of the TCIRG1 gene, highlighting the position of the mutations identified in intron 15; the nucleotide change found in each patient is in bold in the lower line. (*C*) Structure of the most frequent aberrant transcripts found in Pt 1A, Pt 1B and Pt 2: i) clones in which only the last 31 nucleotides of exon 15 are retained, followed by 143 nucleotides of intron 15, and ii) clones retaining 143 nucleotides of intron 15. The nucleotide change found in each patient is in bold in the lower line, as in panel B.

Table 3. Molecular Findings

Patient	Genomic change[a]	Location	cDNA change[b]	Effect
1A and 1B	g.10466G>A	Intron 15	c.1887+146G>A	Putative aberrant splicing
	g.10466G>A	Intron 15	c.1887+146G>A	Putative aberrant splicing
2	g.9909G>A	Exon 14	c.1559G>A	p.Trp520X
	g.10462T>A	Intron 15	c.1887+142T>A	Putative aberrant splicing
3	g.11622T>C	Exon 19	c.2345T>C	p.Met782Thr
	g.10452T>C	Intron 15	c.1887+132T>C	Putative aberrant splicing
4	g.8600T>C	Intron 11	c.1305+2T>C	Putative aberrant splicing
	g.10469C>T	Intron 15	c.1887+149C>T	Putative aberrant splicing

[a]Accession number genomic sequence of the *TCIRG1* gene: AF033033.
[b]Accession number of the TCIRG1variant1 cDNA: NM_006019; the numbering used starts with nucleotide +1 for the A of the ATG-translation initiation codon.

15 and retaining 143 nucleotides of intron 15, 20/75 clones skipping the first 183 nucleotides of exon 15 and retaining 141 nucleotides of intron 15, plus other less frequent species. Sequence analysis of individual clones showed that loss of large part of exon 15 was due to the usage of an internal, cryptic acceptor site, while retention of 143 nucleotides of intron 15 was due to the usage of an intronic, cryptic donor site (Supplementary Fig. 2).

Discussion

Fifteen years of genetic dissection of human osteopetrosis have greatly extended our understanding of the physiopathology of this disease and, more in general, of the bone tissue. At present, an exact classification is obtained in most cases of the extreme phenotypes: on one hand, autosomal recessive forms with a very severe and early presentation; on the other, adult, benign forms mildly impacting on the patients' life. This allows the identification of the most appropriate therapy. On the contrary, intermediate, atypical forms are more difficult to solve and manage; therefore, these are often addressed by next-generation sequencing technologies or require an adaptation of commonly used protocols.

We recently reported the identification of an incomplete splicing defect in the *TCIRG1* gene leading to benign, recessive osteopetrosis in a young girl.[2] At that time, we thought that this kind of phenotype owing to the *TCIRG1* gene was extremely rare because no other similar finding was present in either our cohort of more than 300 patients or in the literature, to the best of our knowledge. However, our present data suggest that this is not the case; in fact, we report here the identification of 4 different single nucleotide changes in intron 15 predicted to impact on the splicing process of the neighboring exons. For 2 of 4 novel mutations, the effect was demonstrated at the cDNA, showing that these genetic defects were hypomorphic and allowed for the production of a small amount of wild-type transcript. In addition, bone histology in Pt 1A allowed us to clearly document osteoclast-rich osteopetrosis, in the presence of areas of well-formed, mature trabecular bone. Interestingly, the mutations herein described are located in close proximity to one another and probably identify a hot spot region for mutation within intron 15. Moreover, they are found in the middle of a 368-nucleotide-long intron, quite far from the canonical splice sites, so our standard molecular analysis of the *TCIRG1* gene initially failed to identify them. Due to their localization, we were not able to exactly define the pathogenic mechanism; however, a careful sequence analysis of the alternative transcripts revealed the usage of cryptic splicing sites, namely an acceptor in exon 15 and a donor in intron 15. Deep intronic mutations, leading to the formation of cryptic splice sites which compete with the canonical ones during RNA processing, have been recently reported also in different diseases, such as Stargardt disease, Gorlin syndrome, optic atrophy, Marfan syndrome and others.[23–26] In the field of skeletal diseases, a deep intronic mutation in the TMEM165 gene has been reported to cause the congenital disorder of glycosylation type II with bone dysplasia.[27] At present this type of defects is likely underestimated, since the genetic tests are still mainly focused on coding genomic sequences and transcript analysis is rarely performed; however, these data clearly highlight the importance of the noncoding genome and the need to assess the functional impact of remote intronic variants in potential disease-genes.

The patients described in the present study displayed a different level of severity of the disease. Whereas in Pt 3 and Pt 4 the diagnosis was made in early life and their osteopetrosis was treated with HSCT, in Pt 1A and Pt 2 the bone defects became apparent at school age and the disease progression was slow and overall benign, thus representing typical intermediate cases. Moreover, Pt 1B was diagnosed at an asymptomatic early stage because of the previous identification of his elder affected sister, Pt 1A. In this regard, the difference between these two siblings is interesting; whereas the elder showed important secondary neurological deficits, these were completely absent in her younger brother, who seemed to be more mildly affected. This is reminiscent of what is commonly observed in autosomal dominant osteopetrosis, in which phenotypic variations can be observed in the presence of the very same genetic defect, even within the same family. A role for variants in modifier genes has been often suggested. Intriguingly, we noticed that Pt 1A and Pt 1B carried an almost completely different set of single-nucleotide polymorphisms (SNPs) in the *CLCN7* gene (only 2 shared SNPs out of 30 genotyped, data not shown). Among these, Pt 1B, but not his sister, bore 2 SNPs within exon 15 (rs12926089 and rs12926669) at the heterozygous state, which have been associated with low bone mineral density in different populations.[28,29] Similarly, it could be hypothesized that additional variants in other genes influencing bone metabolism are present in one or the other affected sibling and modulated their phenotype. Moreover, in adolescence and adult life, sexual hormones might have further impacted on the disease manifestation.

In conclusion, our results depict an even wider spectrum of mutations and phenotypes in TCIRG1-dependent osteopetrosis and suggest the analysis of this gene is appropriate not only in

the molecular work-up of severe patients but also of intermediate cases. Based on these findings, standard protocols for gene amplification and sequencing, focused on exons and exon-intron boundaries, are likely to be revised. In particular, intron 15 should be included in the routine sequencing of the *TCIRG1* gene; more in general, intronic changes in genes associated with osteopetrosis, even deeply embedded in introns, should be considered and their effect carefully evaluated.

Disclosures

All authors state that they have no conflicts of interest.

Acknowledgments

We are grateful to the patients and their relatives for their cooperation. This work was partially supported by the Telethon Foundation (grant GGP12178 to CS); by PRIN Project (20102M7T8X_003 to AV); by Giovani Ricercatori from Ministero della Salute (grant GR-2011-02348266 to CS); by Ricerca Finalizzata from Ministero della salute (RF-2009-1499,542 to AV); by the European Community's Seventh Framework Program (FP7/2007-2013, SYBIL Project to AV and WVH); by PNR-CNR Aging Program 2012–2014 to PV and AV; by the Leenaards Foundation Lausanne and the Swiss National Foundation to AS-F; by the National Institutes of Health USA (R01 AR065407-01 to HCB), and by the Department of Veteran's Affairs USA (BX002490-01 to HCB); by the Research Foundation-Flanders (FWO grant G.0197.12N to WVH); and by a TOP grant to WVH. EB holds a postdoctoral fellowship of the Research Foundation-Flanders.

Author's roles: Molecular studies: EP, AP, and DS. Patient evaluation: ASF, FF, AN, MCF, and GG. Laboratory investigation: MM and AM. Exome sequencing and bioinformatics analysis: AA, GC, MO, and PU. Histological analysis: HCB and IT. Luciferase assay on LPR5: WVH and EB. Study design: PV, AV, and CS. Drafting manuscript and revising manuscript content: all authors.

References

1. Sobacchi C, Schulz A, Coxon FP, Villa A, Helfrich MH. Osteopetrosis: genetics, treatment and new insights into osteoclast function. Nat Rev Endocrinol. 2013;9:522–536.
2. Sobacchi C, Pangrazio A, López AG, et al. As little as needed: the extraordinary case of a mild recessive osteopetrosis due to a novel splicing hypomorphic mutation in the TCIRG1 gene. J Bone Miner Res. 2014;29:1646–1650.
3. Rabbani B, Tekin M, Mahdieh N. The promise of whole-exome sequencing in medical genetics. J Hum Genet. 2014;59:5–15.
4. Li H, Durbin R. Fast and accurate long-read alignment with Burrows-Wheeler transform. Bioinformatics. 2010;26:589–595.
5. McKenna A, Hanna M, Banks E, et al. The genome analysis toolkit: a MapReduce framework for analyzing next-generation DNA sequencing data. Genome Res. 2010;20:1297–303.
6. Cuccuru G, Orsini M, Pinna A, et al. Orione, a web-based framework for NGS analysis in microbiology. Bioinformatics. 2014;30:1928–1929.
7. Li M-X., Kwan JSH, Bao S-Y, et al. Predicting Mendelian disease-causing non-synonymous single nucleotide variants in exome sequencing studies. PLoS Genet. 2013;9:e1003143.
8. Frattini A, Orchard PJ, Sobacchi C, et al. Defects in the TCIRG1-encoded 116kD subunit of the vacuolar proton pump are responsible for a subset of human autosomal recessive osteopetrosis. Nat Genet. 2000;25:343–346.
9. Frattini A, Pangrazio A, Susani L, et al. Chloride channel ClCN7 mutations are responsible for severe recessive, dominant and intermediate osteopetrosis. J Bone Miner Res. 2003;18:1740–1747.
10. Van Wesenbeeck L, Odgren PR, Coxon FP, et al. Involvement of PLEKHM1 in osteoclastic vesicular transport and osteopetrosis in incisors absent rats and humans. J Clin Invest. 2007;117:919–930.
11. Sobacchi C, Frattini A, Guerrini M, et al. Osteoclast-poor human osteopetrosis due to mutations in RANKL. Nat Genet. 2007;39:960–962.
12. Guerrini MM, Sobacchi C, Cassani B, et al. Human osteoclast-poor osteopetrosis with hypogammaglobulinemia due to TNFRSF11A (RANK) mutations. Am J Hum Genet. 2008;83:64–76.
13. Pangrazio A, Fasth A, Sbardellati A, et al. SNX10 mutations define a subgroup of human autosomal recessive osteopetrosis with variable clinical severity. J Bone Miner Res. 2013;28:1041–1049.
14. Desmet FO, Hamroun D, Lalande M, Collod-Béroud G, Claustres M, Béroud C. Human Splicing Finder: an online bioinformatics tool to predict splicing signals. Nucl Acids Res. 2009;37:e67.
15. den Dunnen JT, Antonarakis SE. Mutation nomenclature extensions and suggestions to describe complex mutations: a discussion. Hum Mutat. 2000;15:7–12.
16. Robinson LJ, Mancarella S, Songsawad D, et al. Gene disruption of the calcium channel Orai1 results in inhibition of osteoclast and osteoblast differentiation and impairs skeletal development. Lab Invest. 2012;92:1071–1083.
17. Mazzolari E, Forino C, Razza A, Porta F, Villa A, Notarangelo LD. A single-center experience in 20 patients with infantile malignant osteopetrosis. Am J Hematol. 2009;84:473–479.
18. Balemans W, Van Hul W. The genetics of low-density lipoprotein receptor-related protein 5 in bone: a story of extremes. Endocrinology. 2007;148:2622–2629.
19. Zeng X, Tamai K, Doble B, et al. A dual-kinase mechanism for Wnt co-receptor phosphorylation and activation. Nature. 2005;438:873–877.
20. Katoh M, Katoh M. WNT signaling pathway and stem cell signaling network. Clin Cancer Res. 2007;13:4042–4045.
21. Michalova E, Vojtesek B, Hrstka R. Impaired pre-mRNA processing and altered architecture of 3′ untranslated regions contribute to the development of human disorders. Int J Mol Sci. 2013;14:15681–15694.
22. Sobacchi C, Frattini A, Orchard P, et al. The mutational spectrum of human malignant autosomal recessive osteopetrosis. Hum Mol Genet. 2001;10:1767–1773.
23. Bax NM, Sangermano R, Roosing S, et al. Heterozygous deep-intronic variants and deletions in ABCA4 in persons with retinal dystrophies and one exonic ABCA4 variant. Hum Mutat. 2015;36:43–47.
24. Bholah Z, Smith MJ, Byers HJ, Miles EK, Evans DG, Newman WG. Intronic splicing mutations in PTCH1 cause Gorlin syndrome. Fam Cancer. 2014;13:477–480.
25. Bonifert T, Karle KN, Tonagel F, et al. Pure and syndromic optic atrophy explained by deep intronic OPA1 mutations and an intralocus modifier. Brain. 2014;137:2164–2177.
26. Gillis E, Kempers M, Salemink S, et al. An FBN1 deep intronic mutation in a familial case of Marfan syndrome: an explanation for genetically unsolved cases? Hum Mutat. 2014;35:571–574.
27. Zeevaert R, de Zegher F, Sturiale L, et al. Bone Dysplasia as a Key Feature in Three Patients with a Novel Congenital Disorder of Glycosylation (CDG) Type II Due to a Deep Intronic Splice Mutation in TMEM165. JIMD Rep. 2013;8:145–152.
28. Pettersson U, Albagha OME, Mirolo M, et al. Polymorphisms of the CLCN7 gene are associated with BMD in women. J Bone Miner Res. 2005;20:1960–1967.
29. Chu K, Snyder R, Econs MJ. Disease status in autosomal dominant osteopetrosis type 2 is determined by osteoclastic properties. J Bone Miner Res. 2006;21:1089–1097.
30. Gong Y, Slee RB, Fukai N, et al. LDL receptor related protein 5 (LRP5) affects bone accrual and eye development. Cell. 2001;107:513–523.
31. Balemans W, Devogelaer JP, Cleiren E, Piters E, Caussin E, Van Hul W. Novel LRP5 missense mutation in a patient with a high bone mass phenotype results in decreased DKK1-mediated inhibition of Wnt signaling. J Bone Miner Res. 2007;22:708–716.

ORIGINAL ARTICLE

JBMR®

Synonymous Mutations Add a Layer of Complexity in the Diagnosis of Human Osteopetrosis

Eleonora Palagano,[1,2] Lucia Susani,[1,3] Ciro Menale,[1,3] Ugo Ramenghi,[4] Massimo Berger,[5] Paolo Uva,[6] Manuela Oppo,[6,7] Paolo Vezzoni,[1,3] Anna Villa,[1,3] and Cristina Sobacchi[1,3]

[1]Humanitas Clinical and Research Institute, Rozzano, Italy
[2]Department of Medical Biotechnologies and Translational Medicine, University of Milan, Milan, Italy
[3]National Research Council–Institute of Genetics and Biomedical Research (CNR-IRGB), Milan Unit, Milan, Italy
[4]Department of Public Health and Pediatric Sciences, University of Turin, Turin, Italy
[5]Pediatric Onco-Hematology and Stem Cell Transplant Division, Regina Margherita Children Hospital, City of Health and Science, Turin, Italy
[6]CRS4, Science and Technology Park Polaris, Pula, Italy
[7]Department of Biomedical Sciences, University of Sassari, Sassari, Italy

ABSTRACT

Autosomal recessive osteopetroses (AROs) are rare, genetically heterogeneous skeletal diseases with increased bone density that are often lethal if left untreated. A precise molecular classification is relevant for the patient's management, because in some subgroups hematopoietic stem cell transplantation (HSCT), which is the only curative therapy, is contraindicated. In two unrelated ARO patients, the molecular analysis revealed the presence of a synonymous variant in known ARO genes, namely in the *TCIRG1* gene in one patient and in the *CLCN7* in the other patient, predicted to impact on the splicing process. In the latter case, sequencing of the transcript confirmed the splicing defect, whereas in the former, for whom an RNA sample was not available, the defect was reconstructed in vitro by the minigene technology. These results strongly suggest that these synonymous changes were responsible for the disease in our patients. Our findings are novel with respect to ARO and add to the few reports in literature dealing with different diseases, underlining the importance of cDNA analysis for the correct assessment of exonic changes, even when exome sequencing is performed. In particular, we highlight the possibility that at least in some cases ARO is due to synonymous changes, erroneously considered clinically silent, in the genes already described in literature, and suggest carefully reevaluating the sequencing results of these genes when mutations are not found at a first analysis. In addition, with respect to the *CLCN7* gene, we suggest that synonymous variants might also contribute to the large spectrum of severity typical of *CLCN7*-dependent osteopetrosis through more subtle, but not negligible, effects on protein availability and functionality. © 2016 American Society for Bone and Mineral Research.

KEY WORDS: OSTEOPETROSIS; *TCIRG1*; *CLCN7*; SYNONYMOUS MUTATION; MINIGENE

Introduction

Autosomal recessive osteopetroses (AROs) are rare inherited skeletal diseases characterized by increased bone density due to failure in bone resorption by the osteoclasts and secondary hematological and neurological defects.[1] ARO is genetically heterogeneous; mutations in the *TCIRG1* gene encoding the osteoclast specific a3 subunit of the vacuolar proton pump, responsible for the acidification of the resorption lacuna, account for more than 50% of ARO cases.[2,3] About 100 different mutations in this gene have been reported in the literature, comprising missense and nonsense mutations, splicing defects, and small insertions or deletions[2–4] (http://structure.bmc.lu.se/idbase/).[5] Moreover, our group has recently identified four different deep intronic mutations affecting the splicing process of *TCIRG1*, thus highlighting the possibility that nucleotide changes in intronic regions far from those with a well-recognized function can also be responsible for the disease.[6]

The second most frequently affected gene in human ARO (about 13% of cases) is *CLCN7*,[7] encoding a $2Cl^-/1H^+$ antiporter involved in the acidification process. A great variety of mutations have been reported for this gene too, in association with a range of severities of the disease.[8,9]

To the best of our knowledge, no synonymous mutation in the *TCIRG1* and *CLCN7* genes (or in the other ARO genes) has been attributed a causative role in human osteopetrosis.

Synonymous mutations are nucleotide changes in the coding region of a gene that do not lead to a modification in the amino acid sequence of the encoded protein because of the degeneracy of the genetic code. These mutations have long been considered silent, that is with no functional effects,

Received in original form April 29, 2016; revised form July 25, 2016; accepted July 27, 2016. Accepted manuscript online September 7, 2016.
Address correspondence to: Cristina Sobacchi, CNR-IRGB, Humanitas Clinical and Research Institute, via Manzoni 113, 20089 Rozzano, Italy.
E-mail: cristina.sobacchi@humanitasresearch.it

Journal of Bone and Mineral Research, Vol. 32, No. 1, January 2017, pp 99–105
DOI: 10.1002/jbmr.2929

because of the assumption that the structure, and hence the function, of a protein is dictated by the amino acid sequence which is identical to the wild type in the presence of a synonymous change.[10] This paradigm became a matter of discussion in recent years because of evidence from disease genes suggesting that even translationally silent mutations could be able to impact on gene functionality.[11] Indeed, accumulating data in literature pointed to a non-neutral effect of at least some synonymous changes through different mechanisms, including alterations of the splicing process, of the RNA structure, of transcription factor binding, or rate of translation due to different codon usage.[12] This means that synonymous mutations may actually be involved in human health and disease.

In the present work we report for the first time synonymous mutations in the *TCIRG1* and *CLCN7* genes responsible for the disease in two ARO patients.

Patients and Methods

Patients and samples

Samples were collected from the patients and their parents after informed consent. This research complies with the World Medical Association Declaration of Helsinki–Ethical Principles for Medical Research Involving Human Subjects, and with the standards established by the Independent Ethical Committee of the Humanitas Clinical and Research Centre.

The clinical description of patient 1 (Pt1 in this work, carrying the synonymous variant in the *TCIRG1* gene) has been already published (as Pt14 in Mazzolari and colleagues[13]). Briefly, the patient was diagnosed at 2 months of age and presented a severe osteopetrotic phenotype; in the absence of a matched donor, hematopoietic stem cell transplantation (HSCT) was not performed and the patient died because of septic shock at 18 months of age.

Patient 2 (Pt2, carrying the synonymous variant in the *CLCN7* gene) is reported here for the first time. He was born from an Italian mother and a Moroccan father, through Caesarean section at week 39 of gestation because of bradycardia. The amniotic fluid was stained by meconium, but the clinical general condition was good (Apgar score 9/9; birth weight 2900 g). On the third day of life he developed a bacterial sepsis treated with antibiotics. The newborn was discharged after 3 weeks with mild thrombocytopenia (platelet count 70×10^9/L) ascribed to bone marrow late toxicity. At 2 months of age the infant was referred to the Pediatric Hematology Unit for splenomegaly (splenic edge 1 cm below the umbilical line); he also displayed anemia (hemoglobin 7.7 g/dL) and thrombocytopenia (platelet count 30×10^9/L) and was transfused. Bone marrow (BM) aspiration revealed reduced cellularity without abnormal cells. In the workup for differential diagnosis, Juvenile myelomonocytic leukemia, familial hemophagocytic lymphohistiocytosis, and Gaucher disease were ruled out by the appropriate assays.[14–16] Chest radiograph performed before insertion of a central vein catheter, showed increased bone intensity and aftereffects of fractures in both humeri. Total body radiographs revealed the typical diffuse bone sclerosis (Fig. 1*A*). In addition, light reflex was absent and CT scan showed narrow optical foramina and optical nerve atrophy. All these findings led to the diagnosis of osteopetrosis. No specific biochemical evaluations, such as tartrate resistant acid phosphatase and creatine kinase brain isoenzyme serum levels,[17] were performed nor was a bone biopsy taken from the patient.

Fig. 1. Representative radiographs of Pt2 showing: (*A*) diffuse increase in bone density and aftereffects of humeral fracture, and (*B*) complete restoration of bone phenotype and marrow cavity after transplantation.

At 7 months of age he received BM transplantation from a fully matched unrelated donor, according to the guidelines of the European Society for Immunodeficiencies (ESID) and the European Society for Blood and Marrow Transportation (EBMT) Working Party (WP) on Inborn Errors. He achieved full engraftment, and 3 months after transplantation hemoglobin and platelet levels were in the normal range. One year after transplantation, the bone defect was completely corrected (Fig. 1*B*). The patient is alive and well at 5.6 years; impaired vision persists, but light reflex is present and the child can follow objects nearby.

Sanger sequencing

PCR amplification and direct Sanger sequencing of the *TCIRG1*, *CLCN7*, *RANKL*, *RANK*, and *SNX10* genes was performed as described[4,8,18–20] in Pt1, whereas *OSTM1*, *CAII*, and *PLEKHM1* were not directly analyzed because the clinical signs in this patient were not in accordance to the typical presentation of OSTM1-dependent ARO, CAII deficiency, or PLEKHM1-dependent ARO. In Pt2 only *TCIRG1* and *CLCN7* genes were analyzed, because the evaluations at the transcript level of the two mutations found in the *CLCN7* gene strongly supported the hypothesis regarding their pathogenicity, so further genetic investigations were not deemed necessary.

The effect of the identified mutations was predicted using the following software: Berkeley Drosophila Genome Project (http://www.fruitfly.org/seq_tools/splice.html) and Human Splicing Finder, Version 3.0 (http://www.umd.be/HSF3/HSF.html).

The mutation nomenclature conforms to the Human Genome Variation Society (HGVS; http://varnomen.hgvs.org/).[21]

Exome analysis

Exome capture, sequencing, and analysis was performed on a DNA sample of Pt1 and his parents, according to a previously reported protocol.[6]

Minigene construct for splicing analysis in Pt1

The pTB hybrid minigene vector used here to investigate the putative splicing defect in the *TCIRG1* gene of Pt1 has been described.[22] The *TCIRG1* genomic region spanning exons 11 to 13 was amplified from the paternal DNA using forward primer 5′-TTTTCATATGctgtgcctggctgctaagtg-3′ in intron 10 and reverse primer 5′-CCCCTCGACCATATGcccactcccagctgccttca-3′ in intron 13; upper case indicates the nucleotides added to obtain the NdeI enzyme restriction site; thermocycling conditions are available upon request.

The PCR product was cloned in the TA cloning vector (Life Technologies, Carlsbad, CA, USA), according to the manufacturer's instructions. Independent clones carrying either the wild-type or the mutated variant were identified by direct Sanger sequencing using the M13R primer, digested with the NdeI enzyme (New England Biolabs, Ipswich, MA, USA) and inserted into the pTB minigene vector. HeLa cells were transfected with 4 μg of each construct DNA using Lipofectamine 2000 (Life Technologies). RNA was extracted after 48 hours using the TRIzol reagent (Thermo Fisher Scientific, Waltham, MA, USA) and retrotranscribed with the High-capacity cDNA Reverse Transcription Kit (Applied Biosystems, Waltham, MA, USA). Finally, PCR was carried out as described with primers 2-3α (forward) and B2 (reverse) specific for the pTB vector.[23]

Transcript cloning and sequencing in Pt2

RNA was extracted from peripheral blood mononuclear cells (PBMCs) using the TRIzol reagent and retrotranscribed as described in the previous section. Primers and conditions for all the RT-PCR described in the text are available upon request.

Each PCR product was separately cloned in the TA cloning vector, according to the manufacturer's instructions; about 50 independent clones for each cloning reaction were sequenced using the M13R primer.

In addition, for the amplification of the *CLCN7* cDNA region containing both the paternally and the maternally inherited mutations, a forward primer in exon 11 and a reverse primer in exon 18, were specifically designed. The PCR product was cloned as described in the previous section; 62 independent clones were tested for the length of the cDNA amplicon and nine of them were sequenced, including the only three clones with apparently normal size.

Results

In Pt1, molecular analysis through Sanger sequencing of the known ARO genes did not identify obvious mutations in the investigated regions, nor did exome sequencing detect evident candidate variants for further confirmation after application of common filters to exclude low-quality, common, and synonymous variants. However, a number of occurrences on the synonymous variant c.1371C>A, p. (Thr457=) found in the patient in the exon 12 of the *TCIRG1* gene attracted our attention: the nucleotide variant was present at the homozygous state in the proband and at the heterozygous state in his parents, as expected based on parental consanguinity, whereas it was not found in SNP databases nor in our in-house database or in the TCIRG1-dependent patients of our cohort. The threonine residue in that position was highly conserved throughout evolution, but interestingly the adenosine nucleotide in the third position of the corresponding codon was never present (Fig. 2*A*). In addition, in silico prediction with different software suggested a pathogenetic role. In the absence of an RNA sample from the patient or his parents, we tested this prediction using the minigene technology, as we have already done in the past for other mutations suspected to affect the splicing process.[22] The minigene assay is a functional splicing assay based on hybrid constructs that, when transfected into eukaryotic cell lines, are able to reproduce the splicing pattern of a specific genomic sequence inserted therein.[23] For the present purpose, we cloned the wild-type and mutant *TCIRG1* genomic region spanning exons 11 to 13 into the pTB minigene vector (Fig. 2*B*), and analyzed the pattern of transcripts produced from the obtained hybrid after transfection in HeLa cells. By this means we confirmed that the variant c.1371C>A caused aberrant splicing, namely loss of 67 nucleotides (Δ67nt) of exon 12, due to the usage of the internal acceptor site created by the variant (Fig. 2*C*, *D*). Because of the inherent artificial nature of this system, it is expected that a variety of transcripts is also generated in the clones carrying the wild-type sequence; however, the keynote is the complete absence of the splicing aberration Δ67nt in these wild-type clones (Fig. 2*C*). At the protein level this nucleotide loss was predicted to result in frameshift and premature termination (p.Ile436AlafsX70).

A similar finding occurred in Pt2, who was found to be a compound heterozygote for two different changes in the *CLCN7* gene: the paternally-inherited allele carried a transition (c.1098G>A) at the last nucleotide of exon 12, constituting a synonymous substitution p. (Glu366=), not previously reported in any database to the best of our knowledge; on the maternal allele a deletion of two nucleotides in intron 17 (c.1617+6_1617+7delTG), close to the canonical acceptor splice site, was present. In this case we could directly verify the effect of each mutation on the cDNA of the patient and confirm that both changes led to splicing aberration (Fig. 3*A*). In fact, we amplified the two relevant cDNA regions separately, spanning exons 11 to 16 and 16 to 20, respectively, cloned the RT-PCR product, and sequenced about 50 independent clones; in this way, we found

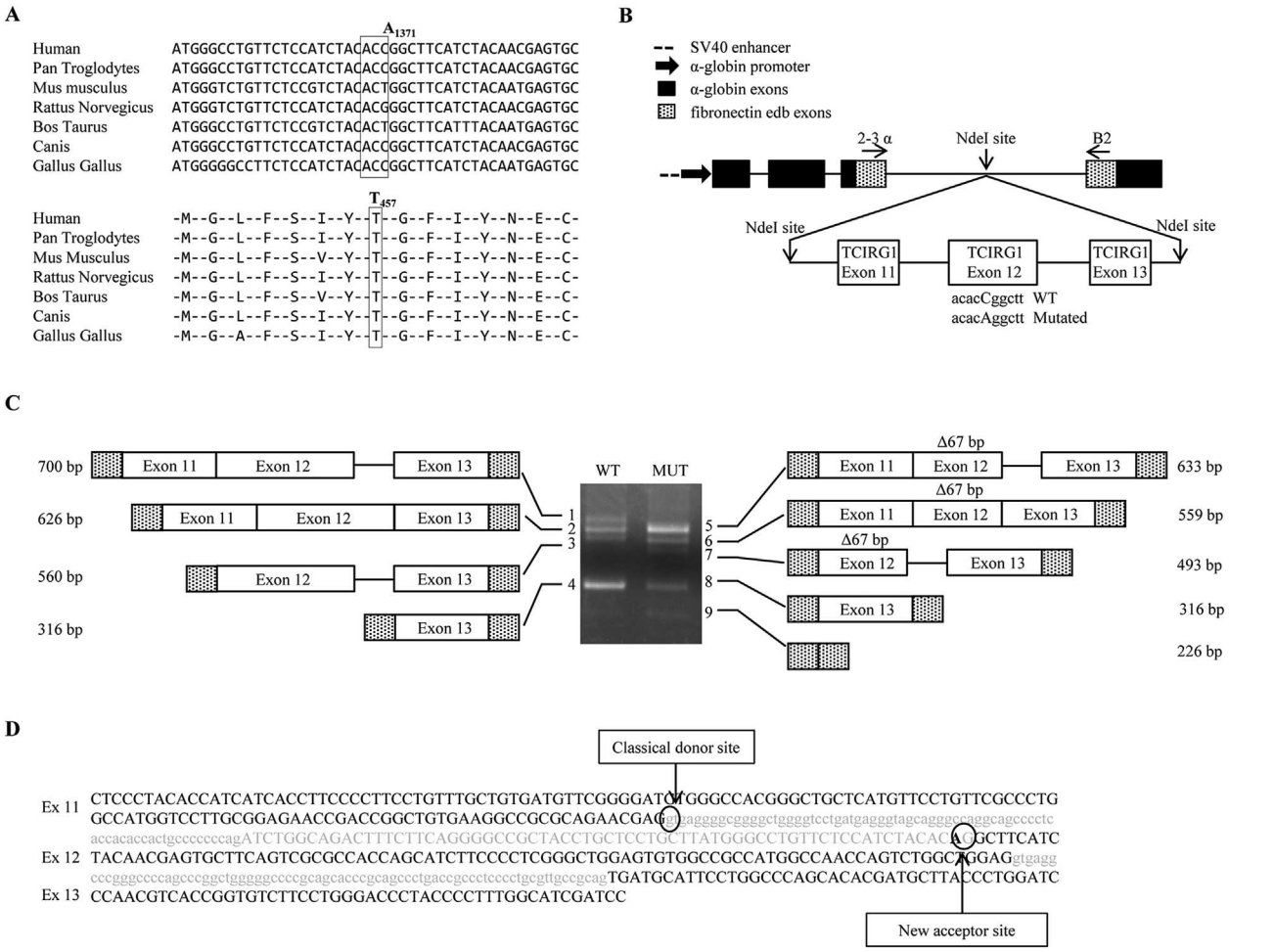

Fig. 2. (*A*) Sequence alignment of the *TCIRG1* gene and protein in the relevant region in different species, showing absence of the adenosine residue (A1371) in the last position of codon 457 (only numbering of the human sequence is reported) and evolutionary conservation of the Threonine residue. (*B*) Schematic representation of the minigene constructs; the sequences relevant for the assay are the alpha-globin promoter region with the SV40 enhancer, a genomic region spanning exons 1 to 3 of the human alpha-globin gene, a portion of the fibronectin gene inserted into exon 3 of the previous gene, and an NdeI cloning site used to insert either the normal or mutated *TCIRG1* genomic sequence spanning exons 11 to 13. (*C*) Analysis of the processed transcripts derived from the minigene constructs carrying the normal or the mutant *TCIRG1* sequence; the composition of the corresponding bands (determined by sequence analysis) is represented respectively on the left and on the right. (*D*) Sequence of the *TCIRG1* gene spanning exons 11 to 13; upper case indicates exonic regions, lower case intronic ones. The creation of a new acceptor site in exon 12, possibly used instead of the canonical one, is highlighted.

that the c.1098G>A transition caused in-frame skipping of exon 12, thus demonstrating a non-neutral effect (Fig. 3*B*, left panel). On the other allele, the deletion of two nucleotides in intron 17 gave rise to at least three aberrant transcripts, respectively showing retention of 230 nucleotides of intron 17 or complete skipping of exon 17, both predicted to cause frameshift, or deletion of 93 nucleotides of exon 17, predicted to cause in-frame loss of 31 amino acids (Fig. 3*B*, right panel). Then, using ad hoc–defined PCR conditions and primer pair, we also obtained a larger *CLCN7* cDNA product spanning exons 11 to 18, thus containing both mutations. Also in this case, we cloned the RT-PCR product and sequenced independent clones, and we never found the wild-type transcript (Fig. 3*C*). In fact, even the band that migrated as expected for the normal transcript, once sequenced, turned out to lack 13 nucleotides as compared to the wild-type. Overall these data strongly suggested that both mutations were completely disruptive and did not allow any residual normal splicing.

Discussion

A precise molecular diagnosis has become an essential part of a patient's management, strongly influencing therapeutic decisions in many inherited disorders. In recent years, an important contribution has been provided by next-generation sequencing approaches[24]; in particular, exome sequencing, investigating the coding fraction of the genome where the large majority of mutations responsible for inherited disease are found, has become widely used because it has lower costs and

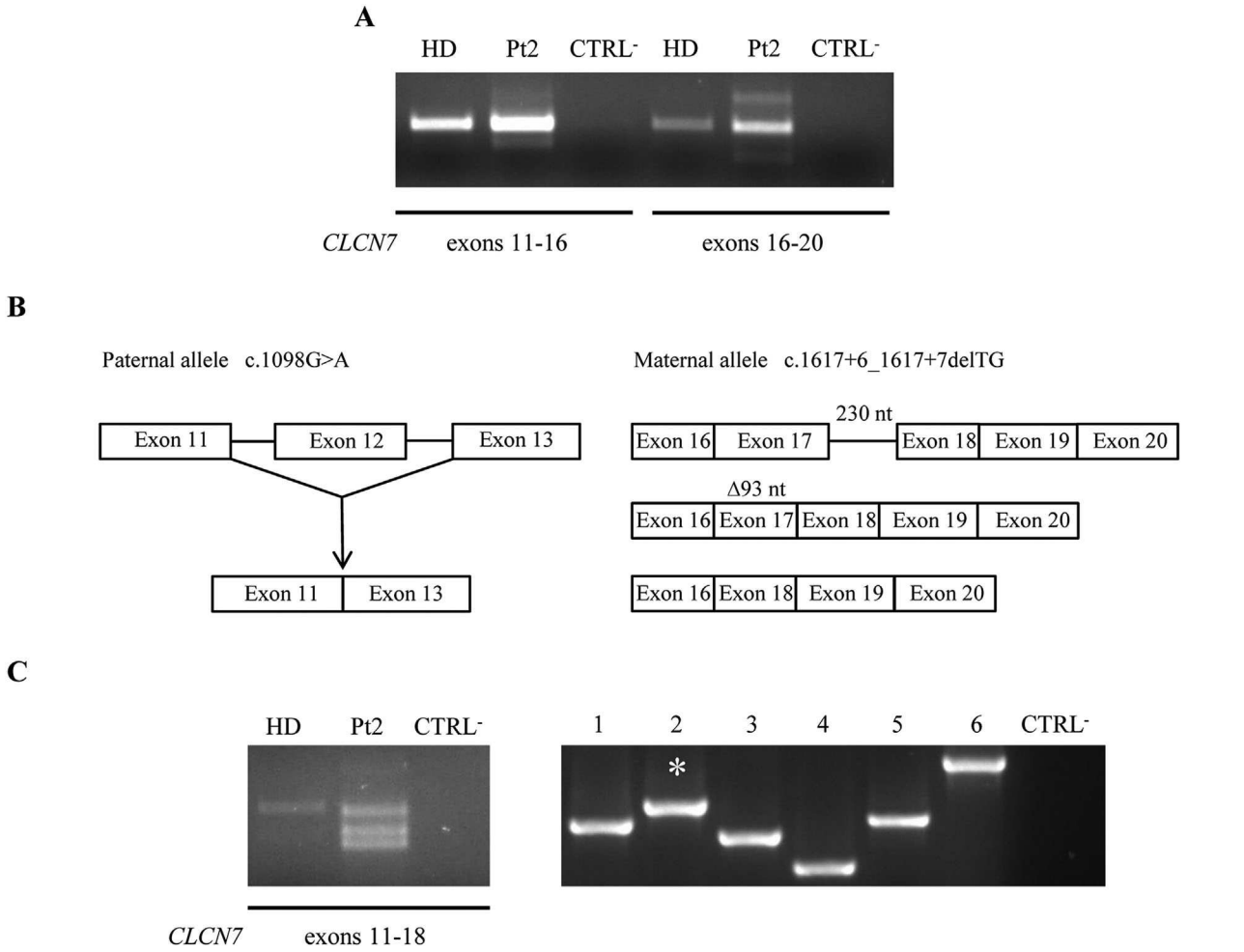

Fig. 3. (*A*) RT-PCR of the *CLCN7* gene in Pt2. (*B*) Schematic representation of the relevant region of the aberrant *CLCN7* transcript produced in Pt2 from the paternal allele, showing skipping of exon 12 (on the left), and from the maternal allele, showing at least 3 different sequences (on the right). (*C*) RT-PCR spanning exons 11 to 18 of the *CLCN7* gene on the Pt2 cDNA (on the left) and PCR amplification of 6 independent clones of this product (on the right). The asterisk indicates the apparently normal transcript lacking 13 nucleotides as compared to the wild type. HD = healthy donor; CTRL– = negative control.

produces a more manageable amount of data as compared to whole-genome sequencing.[25] Independent of the approach, the most challenging step is the filtering of the called variants and the functional validation of those possibly damaging based on software prediction and suspected to be disease-causing. In this process synonymous variants are actually most often filtered out, based on the common assumption that they do not have an impact on the protein product; on the other hand, this is probably the case for many, but not all of them.

Our results strongly suggest the causative role of deleterious synonymous mutations in the pathogenesis of human ARO. In fact the patients herein reported carried synonymous substitutions in the *TCIRG1* and *CLCN7* genes, respectively, leading to the production of aberrant transcripts with a causative role in the pathogenesis of their disease. Protein sequencing, performed for example through mass spectrometry, would strengthen the results obtained at the cDNA level and confirm in silico predictions; on the other hand, this is not a routine procedure. In addition, when the synonymous mutation causes a splicing defect with frameshift, it is likely that no protein or a lower amount of the normal protein is produced due to nonsense-mediated RNA decay, thus limiting the utility of protein sequencing.

Similar findings have been reported in other disorders,[26–32] also including skeletal defects[33–35]; nonetheless, the contribution of synonymous mutations to human pathologies is likely highly underestimated at present. Although performing functional evaluations of all the synonymous changes in an individual exome is not cost-effective, it might be worth assessing the effect of those located in genes already known to be associated with diseases.

With particular respect to human ARO, seven genes have been involved in the pathogenesis of this disease, and the presence of mutations in additional genes is likely in the non-classified patients, who represent about 20% of cases. The data reported in the present work support the hypothesis that at least in some cases ARO is due to synonymous changes erroneously regarded as silent, in the genes already described in the literature. Therefore, based on our experience, we would suggest carefully reevaluating the sequencing results of the known ARO genes,

when mutations are not found at a first analysis. In addition, with particular respect to the *CLCN7* gene, our result can raise the hypothesis that synonymous but not silent changes may contribute to the spectrum of severity typical of CLCN7-dependent osteopetrosis. Specifically pertaining to the Pt2 described herein, no wild-type transcript from both mutated alleles was produced, which could be in agreement with the severe presentation, requiring HSCT in early life. On the other hand, by eliciting different effects on transcription and translation, synonymous variants might also constitute at least one of the long-sought, elusive elements responsible for phenotypic differences reported in different individuals carrying the same mutations, if they only mildly impact CLCN7 protein function.

Disclosures

All authors state that they have no conflicts of interest.

Acknowledgements

This work was partially supported by Giovani Ricercatori from Ministero della Salute (grant GR-2011-02348266 to CS), by the European Community's Seventh Framework Program (FP7/2007-2013, SYBIL Project to AV), by the Programma Nazionale per la Ricerca-Consiglio Nazionale delle Ricerche Aging Project to AV and PV, and by Ricerca Finalizzata from Ministero della Salute (grant PE-2011-02347329) to PV. We are grateful to the patients and their relatives for their cooperation. We thank Dr. Franco Pagani for providing us the pTB minigene vector.

Authors' roles: Molecular studies: EP, LS, and CM. Patient evaluation: UR and MB. Exome sequencing and bioinformatics analysis: EP, PU, and MO. Study design: PV, AV, and CS. Drafting manuscript and revising manuscript content: All authors.

References

1. Sobacchi C, Schulz A, Coxon FP, Villa A, Helfrich MH. Osteopetrosis: genetics, treatment and new insights into osteoclast function. Nat Rev Endocrinol. 2013;9(9):522–36.
2. Frattini A, Orchard PJ, Sobacchi C, et al. Defects in TCIRG1 subunit of the vacuolar proton pump are responsible for a subset of human autosomal recessive osteopetrosis. Nat Genet. 2000;25(3):343–6.
3. Pangrazio A, Caldana ME, Lo Iacono N, et al. Autosomal recessive osteopetrosis: report of 41 novel mutations in the TCIRG1 gene and diagnostic implications. Osteoporos Int. 2012;23(11):2713–8.
4. Sobacchi C, Frattini A, Orchard P, et al. The mutational spectrum of human malignant autosomal recessive osteopetrosis. Hum Mol Genet. 2001;10(17):1767–73.
5. Piirilä H, Väliaho J, Vihinen M. Immunodeficiency mutation databases (IDbases). Hum Mutat. 2006;27(12):1200–8.
6. Palagano E, Blair HC, Pangrazio A, et al. Buried in the middle but guilty: intronic mutations in the TCIRG1 gene cause human autosomal recessive osteopetrosis. J Bone Miner Res. 2015;30(10):1814–21.
7. Kornak U, Kasper D, Bösl MR, et al. Loss of the ClC-7 chloride channel leads to osteopetrosis in mice and man. Cell. 2001;104(2):205–15.
8. Frattini A, Pangrazio A, Susani L et al. Chloride channel ClCN7 mutations are responsible for severe recessive, dominant, and intermediate osteopetrosis. J Bone Miner Res. 2003;18(10):1740–7.
9. Pangrazio A, Pusch M, Caldana E, et al. Molecular and clinical heterogeneity in CLCN7-dependent osteopetrosis: report of 20 novel mutations. Hum Mutat. 2010;31(1):E1071–80.
10. Anfinsen CB. Principles that govern the folding of protein chains. Science. 1973;181:223–30.
11. Cartegni L, Chew SL, Krainer AR. Listening to silence and understanding nonsense: exonic mutations that affect splicing. Nat Rev Genet. 2002 Apr;3(4):285–98.
12. Sauna ZE, Kimchi-Sarfaty C. Understanding the contribution of synonymous mutations to human disease. Nat Rev Genet. 2011;12(10):683–91.
13. Mazzolari E, Forino C, Razza A, Porta F, Villa A, Notarangelo LD. A single-center experience in 20 patients with infantile malignant osteopetrosis. Am J Hematol. 2009;84(8):473–9.
14. Mistry PK, Cappellini MD, Lukina E, et al. A reappraisal of Gaucher disease–diagnosis and disease management algorithms. Am J Hematol. 2011;86(1):110–5.
15. Hoyoux C, Dresse MF, Forget P, et al. Osteopetrosis mimicking juvenile myelomonocytic leukemia. Pediatr Int. 2014;56(5):779–82.
16. Erlacher M, Strahm B. Missing cells: pathophysiology, diagnosis, and management of (pan)cytopenia in childhood. Front Pediatr. 2015;3:64.
17. Waguespack SG, Hui SL, White KE, Buckwalter KA, Econs MJ. Measurement of tartrate-resistant acid phosphatase and the brain isoenzyme of creatine kinase accurately diagnoses type II autosomal dominant osteopetrosis but does not identify gene carriers. J Clin Endocrinol Metab. 2002;87(5):2212–7.
18. Sobacchi C, Frattini A, Guerrini MM, et al. Osteoclast-poor human osteopetrosis due to mutations in the gene encoding RANKL. Nat Genet. 2007;9(8):960–2.
19. Guerrini MM, Sobacchi C, Cassani B, et al. Human osteoclast-poor osteopetrosis with hypogammaglobulinemia due to TNFRSF11A (RANK) mutations. Am J Hum Genet. 2008;83(1):64–76.
20. Pangrazio A, Fasth A, Sbardellati A, et al. SNX10 mutations define a subgroup of human autosomal recessive osteopetrosis with variable clinical severity. J Bone Miner Res. 2013;28(5):1041–9.
21. den Dunnen JT, Antonarakis SE. Mutation nomenclature extensions and suggestions to describe complex mutations: a discussion. Hum Mutat. 2000;15(1):7–12.
22. Susani L, Pangrazio A, Sobacchi C, et al. TCIRG1-dependent recessive osteopetrosis: mutation analysis, functional identification of the splicing defects, and in vitro rescue by U1 snRNA. Hum Mutat. 2004;24(3):225–35.
23. Pagani F, Buratti E, Stuani C, et al. Splicing factors induce cystic fibrosis transmembrane regulator exon 9 skipping through a non-evolutionary conserved intronic element. J Biol Chem. 2000;275(28):21041–7.
24. Stranneheim H, Wedell A. Exome and genome sequencing: a revolution for the discovery and diagnosis of monogenic disorders. J Intern Med. 2016;279(1):3–15.
25. Tetreault M, Bareke E, Nadaf J, Alirezaie N, Majewski J. Whole-exome sequencing as a diagnostic tool: current challenges and future opportunities. Expert Rev Mol Diagn. 2015;15(6):749–60.
26. Fu XJ, Nozu K, Eguchi A, et al. X-linked Alport syndrome associated with a synonymous p.Gly292Gly mutation alters the splicing donor site of the type IV collagen alpha chain 5 gene. Clin Exp Nephrol. Forthcoming. Epub 2015 Nov 18. DOI:10.1007/s10157-015-1197-9.
27. Ho CK, Musa FR, Bell C, Walker SW. LDLR gene synonymous mutation c.1813C<T results in mRNA splicing variation in a kindred with familial hypercholesterolaemia. Ann Clin Biochem. 2015;52(Pt 6):680–4.
28. Nuzzo F, Bulato C, Nielsen BI, et al. Characterization of an apparently synonymous F5 mutation causing aberrant splicing and factor V deficiency. Haemophilia. 2015;21(2):241–8.
29. Pizzo L, Iriarte A, Alvarez-Valin F, Marín M. Conservation of CFTR codon frequency through primates suggests synonymous mutations could have a functional effect. Mutat Res. 2015;775:19–25.
30. Ferri L, Dionisi-Vici C, Taurisano R, Vaz FM, Guerrini R, Morrone A. When silence is noise: infantile-onset Barth syndrome caused by a synonymous substitution affecting TAZ gene transcription. Clin Genet. Forthcoming. Epub 2016 Feb 8. DOI:10.1111/cge.12756.
31. Tonin R, Caciotti A, Funghini S, et al. Clinical relevance of short-chain acyl-CoA dehydrogenase (SCAD) deficiency: exploring the role of new variants including the first SCAD-disease-causing allele carrying a synonymous mutation. BBA Clin. 2016;5:114–9.

32. Corrado L, Magri S, Bagarotti A, et al. A novel synonymous mutation in the MPZ gene causing an aberrant splicing pattern and Charcot-Marie-Tooth disease type 1b. Neuromuscul Disord. 2016 Aug; 26(8):516–20.
33. Macaya D, Katsanis SH, Hefferon TW, et al. A synonymous mutation in TCOF1 causes Treacher Collins syndrome due to mis-splicing of a constitutive exon. Am J Med Genet A. 2009;49A(8):1624–7.
34. Richards AJ, Fincham GS, McNinch A, et al. Alternative splicing modifies the effect of mutations in COL11A1 and results in recessive type 2 Stickler syndrome with profound hearing loss. J Med Genet. 2013;50(11):765–71.
35. Fenwick AL, Goos JA, Rankin J, et al. Apparently synonymous substitutions in FGFR2 affect splicing and result in mild Crouzon syndrome. BMC Med Genet. 2014;15:95.

Bone 97 (2017) 126–129

Contents lists available at ScienceDirect

Bone

journal homepage: www.elsevier.com/locate/bone

Case Report

Hematopoietic stem cell transplantation corrects osteopetrosis in a child carrying a novel homozygous mutation in the *FERMT3* gene

Eleonora Palagano [a,b], Mary A. Slatter [c,d], Paolo Uva [e], Ciro Menale [a,f], Anna Villa [a,f], Mario Abinun [c,d,*], Cristina Sobacchi [a,f]

[a] Humanitas Clinical and Research Institute, Rozzano, Italy
[b] Department of Medical Biotechnologies and Translational Medicine, University of Milan, Milan, Italy
[c] Bone Marrow Transplantation Unit, Great North Children's Hospital, The Newcastle upon Tyne Hospitals NHS Foundation Trust, Newcastle upon Tyne, UK
[d] Primary Immunodeficiency Group, Institute of Cellular Medicine, Newcastle University, Newcastle upon Tyne, UK
[e] CRS4, Science and Technology Park Polaris, Pula, Italy
[f] CNR-IRGB, Milan Unit, Milan, Italy

ARTICLE INFO

Article history:
Received 7 November 2016
Revised 22 December 2016
Accepted 13 January 2017
Available online 14 January 2017

Keywords:
Integrin
Osteoclast
Bleeding

ABSTRACT

Osteopetrosis (OPT) is a rare skeletal disorder with phenotypic and genotypic heterogeneity: a variety of clinical features besides the bony defect may be present, and at least ten different genes are known to be involved in the disease pathogenesis. In the framework of this heterogeneity, we report the clinical description of a neonate, first child of consanguineous parents, who had osteoclast-rich osteopetrosis and bone marrow failure in early life, but no other usual classical features of infantile malignant OPT, such as visual or hearing impairments. Because of the severe presentation at birth, the patient received Hematopoietic Stem Cell Transplantation (HSCT) at 2 months of age with successful outcome. Post-HSCT genetic investigation by means of exome sequencing identified a novel homozygous mutation in the Fermitin Family Member 3 (*FERMT3*) gene, which was predicted to disrupt the functionality of its protein product kindlin 3. Our report provides information relevant to physicians for recognizing patients with one of the rarest forms of infantile malignant OPT, and clearly demonstrates that HSCT cures kindlin 3 deficiency with severe phenotype.

1. Introduction

Osteopetrosis refers to a group of genetically heterogeneous, rare skeletal diseases characterized by increased bone density due to failure in bone resorption and a variety of associated clinical phenotypes [1]. Hematological (bone marrow failure, hepatosplenomegaly) and neurological defects (cranial nerves compression, blindness, deafness, developmental delay, hydrocephalus) are frequent, particularly in the severe end of the spectrum of infantile malignant osteopetrosis [1]. Some features are mainly present in association with mutations in specific genes (e.g. renal tubular acidosis and cerebral calcifications with carbonic anhydrase 2 deficiency, skin manifestations with *NEMO* or *SLC29A3* mutations, and spontaneous bleeding with kindlin 3 deficiency) [2–5]. Others, such as primary hypothyroidism, structural brain abnormalities, poikiloderma and neutropenia, juvenile xantogranuloma, congenital aural atresia, are sporadic and due to as yet undefined molecular defects [6–10], thus at present it is not known whether they are incidental findings due to the co-occurrence of different diseases in the same patient [11], or whether they are caused by mutations in specific genes responsible for both the skeletal defect and the extraskeletal manifestation. In most cases Hematopoietic Stem Cell Transplantation (HSCT) is the only curative treatment option and should be performed early to prevent progressive visual and hearing impairment, bone marrow failure and growth retardation.

2. Materials and methods

Clinical data and specimens (peripheral-blood for DNA isolation) were collected from the patient and her parents after informed consent. This research complies with the standards established by the Independent Ethical Committee of the Humanitas Clinical and Research Centre, Rozzano (Milan), Italy.

Based on the clinical data and presence of osteoclasts in the bone marrow trephine biopsy, only genes known to cause the different types of osteoclast-rich OPT (*TCIRG1*, *CLCN7*, *OSTM1* and *SNX10*) were initially analyzed by amplification and direct Sanger sequencing of exons and intron-exon boundaries as previously described [12–15]. Based on our recent report [16], the *CTSK* gene was as well included in the analysis. Since no mutation was found in the above mentioned

* Corresponding author at: Bone Marrow Transplantation Unit, Great North Children's Hospital, The Newcastle upon Tyne Hospitals NHS Foundation Trust, Queen Victoria Road, NE1 4LP Newcastle upon Tyne, UK.
E-mail address: Mario.Abinun@nuth.nhs.uk (M. Abinun).

http://dx.doi.org/10.1016/j.bone.2017.01.012
8756-3282/

genes, for a more comprehensive molecular analysis we decided to proceed with exome sequencing.

Exome capture, sequencing and data analysis of DNA collected from the patient and her parents was performed as previously described [17].

3. Results

3.1. Patient

A female newborn, the only child of Pakistani consanguineous parents (first degree consanguinity), presented at birth with widespread purpuric/petechial rash, hepatomegaly (+3 cm), limited bleeding of the scalp (where electrodes were placed), severe anemia (hemoglobin 5.5 g/dL, normal range 10.5–13.5), thrombocytopenia (platelet count 33×10^9/L, normal range 150-450 $\times 10^9$/L), and leucocytosis (white cell count 30.7 $\times$ 10^9/L, normal range 6.0–17.5 $\times$ 10^9/L) with leucoerythroblastic picture on peripheral blood smear, and normal blood clotting tests. Although initially these features were suggestive for neonatal leukemia, the morphology and immunophenotyping of peripheral blood, and bone marrow aspirate showed no features of malignant cells. The borderline and clinically asymptomatic hypocalcaemia and hypophosphatemia (serum calcium 1.8 mmol/L, normal range 2.2–2.6 mmol/L; phosphate 1.06 mmol/L, normal range 1.4–2.5 mmol/L), pale optic discs and very dense bones noted on initial abdominal radiography (Fig. 1A) suggested infantile malignant osteopetrosis. This was confirmed by subsequent iliac crest bone marrow trephine biopsy showing strikingly abnormal architecture with profuse overgrowth of bone around cartilage in an expanded network encroaching on the marrow space, strikingly increased large osteoclasts, and reduced residual hematopoiesis, the appearances typical of osteoclast-rich osteopetrosis (Fig. 1B). There were no signs of pulmonary hypertension; brain MRI and electroencephalography showed no abnormalities, CT scan of the skull base showed no obstruction of optic or auricular canals, and functional assessment of hearing and vision (evoked potentials, electroretinography), revealed no major abnormalities suggestive of the exceptionally severe forms of infantile malignant OP with progressive neurodegeneration [18].

Despite somewhat surprising absence of visual or hearing impairments usually present in infantile malignant osteopetrosis, our patient's clinical presentation was deemed particularly severe already at birth, suggesting in utero onset. At 2 months of age she underwent allogeneic HSCT from a matched unrelated umbilical cord (HLA 10/10) (0.9×10^6/kg $CD34^+$ stem cell dose) donor after conditioning with fludarabine (150 mg/m^2), treosulfan (36 mg/m^2), thiotepa (5 mg/kg) and rabbit anti T cell globulin (ATG) (6 mg/kg, dose reduced due to cytomegalovirus viremia), with cyclosporine and mycophenolate mofetil for graft versus host disease (GvHD) prophylaxis. The early post-transplant period was complicated by prolonged but transient acute GvHD of skin (grade 3) and liver, cytomegalovirus (CMV) reactivation, candida pneumonitis, and hypertrophic cardiomyopathy, which all resolved. She was discharged to home after 6 months hospital stay with full and stable engraftment (100% donor chimerism in myeloid, T and B cells) since 2 months post-HSCT, and good immune reconstitution with normal peripheral blood lymphocyte markers, serum immunoglobulin levels and specific vaccine antibody responses.

Two and a half years post-HSCT an irregular osteolytic lesion of unknown etiology with sclerotic borders within the proximal metaphysis of the left fibula (Fig. 1C) was found on knee radiography performed during investigation of the cause of limping and mild flexion contracture of the left knee; however, gait was improved by physiotherapy. Three years post-HSCT she developed Grave's thyrotoxicosis (TSH 0.07 mIU/L, normal range 0.3–4.7; free thyroxine 47.6 pmol/L, normal range 9.5–21.5; free T3 19.5 pmol/L, normal range 3.5–6.5; thyroid peroxidase antibodies 30 IU/mL, normal value <35, but increased thyrotropin receptor antibodies 16.6 U/L, normal value <1.8), for which she remains on carbimazole treatment [19].

At the last follow-up at 5.5 year of age she was well, in school full time, with no visual, hearing or developmental problems, growing nicely with weight on the 75th and height on the 9th centile for age, under dentist follow up because of secondary dentition formation problems, which are a common complication of OPT even after successful HSCT [1].

3.2. Molecular studies

The analysis of the genomic sequence of the *TCIRG1*, *CLCN7*, *OSTM1*, *SNX10* and *CTSK* gene revealed no mutations, indicating the involvement of a different gene in the pathogenesis of the disease in this family. Therefore, trio-based exome sequencing was performed at CRS4 (Science and Technology Park Polaris, Pula, Italy) and achieved an 80× mean coverage over the 62 Mb of exomic sequence, with >94% of targeted regions covered. The analysis identified a total of 10,166 variants with a minor allele frequency lower than 0.05 (MAF <0.05); among them, there were 7815 variants in untranslated regions (UTRs), 2137 nonsynonymous, 180 indel and 34 splice site variants. They were further filtered based on known parental consanguinity, yielding 316 homozygous variants, comprising 68 novel ones. In this group, we found a novel single nucleotide deletion in the Fermitin Family Member 3 (*FERMT3*) gene (c.1802delA). The mutation, confirmed by Sanger sequencing to be present at the homozygous state in the affected

Fig. 1. (A) Representative radiographies demonstrating osteopetrotic phenotype before HSCT (B) Iliac crest bone marrow trephine biopsy, paraffin-embedded sections stained with hematoxylin-eosin showing abnormal bone architecture (light blue) with cartilage remnants (bright pink), numerous large multinucleated osteoclasts (indicated by arrows) and limited residual hematopoiesis. Magnification: 10× (C) Radiography (left knee) performed at the time of limping, showing restoration of normal bone density 2.5 years after HSCT.

child and at the heterozygous state in her parents, was predicted to cause a frameshift (p.Asn603Thrfs*?) affecting the F3 domain, which is involved in integrin binding [20]. Unfortunately, it was not possible to evaluate the presence or absence of a mutant protein by Western blot; however, based on its position the mutation could be predicted to severely impact on the protein function and was considered as responsible of the disease in the patient.

4. Discussion

The *FERMT3* gene is mainly expressed in hematopoietic cells and codes for kindlin-3 protein, which plays a crucial role in integrin inside-out activation, a mechanism required for platelet aggregation, leukocyte adhesion and extravasation and osteoclast adhesion and spreading, as demonstrated in the *kindlin3*$^{-/-}$ mouse model [21]. Mutations in the *FERMT3* gene impair integrin activation and cause a rare disease named leukocyte adhesion deficiency type III (LAD III), characterized by severe bleeding, recurrent infections and (in some patients) osteopetrosis [5,22,23]. To the best of our knowledge, so far 22 patients (of Turkish, Maltese and Middle-Eastern origin, and more recently an Afro-American and a Thai patient), have been described in literature carrying loss of function mutations in the *FERMT3* gene [5, 22–28]. Recurrent infections and bleeding were common features, whilst osteopetrosis was clearly apparent in only 9 out of 22 patients [5,22,25,28]; in additional 9 it was defined as not a prominent feature [22]. HSCT was reported to cure the disease in 7 out of 13 transplanted patients [5,22,23,25–27].

Ten different mutations have been identified in this small cohort of patients, including mainly truncating mutations (p.Arg509Ter, which is the most frequent; p.Trp229Ter; p.Arg513Ter, p.Gln533Ter, p.Arg573Ter; and p.Trp16Ter, the latter suggested to allow for the production of a shorter protein product starting from a downstream transcription start site at codon 181), a single nucleotide substitution (c.1683-2A > G) causing aberrant splicing, a single nucleotide deletion (c.1287delT) predicted to lead to frame shift and premature termination of the protein product (p.Glu430ArgfsTer3) and two missense mutations (p.Gly308Arg and p.Gln595Pro). As reported above with respect to our newly identified mutation, the majority of those reported in literature affect the C-terminus of the protein, namely the F3 domain, suggesting loss of integrin binding as likely pathogenetic mechanism; in addition, in some patients complete absence of the protein product has been demonstrated by Western blot analysis [23,25,26]. On the other hand, a few mutations lie in domains with no specific function recognized thus far, so in these cases the exact pathological mechanism still has to be clarified. So far, no correlation between the specific *FERMT3* mutation and clinical presentation has been defined, in part due to the limited number of reported patients, and interestingly our patient did not have recurrent bleeding and infections, possibly due to very early presentation and HSCT.

Allogeneic HSCT is curative for most forms of infantile malignant osteoclast-rich osteopetrosis, except for those associated with progressive neurodegeneration [1]. Whilst knowing the genetic mutation is helpful when making the decision about HSCT (mutations in *OSTM1* are always 'a contraindication'), the ultimate decision is almost always based on clinical grounds for two main reasons: first, there is phenotype heterogeneity (some patients do present with more severe neurological features questioning the indication for HSCT), and second, obtaining results of genetic mutation analysis usually (still) takes too long as infantile malignant OPT is a progressive disease HSCT should be undertaken as an emergency procedure [1].

Our report of a patient bearing a homozygous novel mutation in the *FERMT3* gene widens the clinical and molecular features of this rare disease. Early-onset bone marrow failure and osteoclast-rich osteopetrosis, in spite of absence of visual impairment otherwise expected in infantile malignant osteopetrosis, and of severe neurological impairment suggestive of progressive neurodegenerative form of the disease, influenced the decision to perform HSCT even before reaching a defined molecular diagnosis which was subsequently identified as homozygous *FERMT3* gene mutation. Finally, we confirm the curative outcome of HSCT for the severe phenotype of kindlin3 deficiency.

Conflict of interest

All authors state that they have no conflict of interest.

Acknowledgements

We are grateful to the patient and her parents for their cooperation. We thank Prof S Kinsey for referring the patient for HSCT and Dr. P Carey for providing the bone marrow biopsy slide in Fig. 1. This work was partially supported by Giovani Ricercatori from Ministero della Salute (grant GR-2011-02348266 to CS), by the European Community's Seventh Framework Program (FP7/2007-2013, SYBIL Project to AV), by the Programma Nazionale per la Ricerca-Consiglio Nazionale delle Ricerche Aging Project to AV, and by Ricerca Finalizzata from Ministero della Salute (grant PE-2011-02347329).

References

[1] C. Sobacchi, A. Schulz, F.P. Coxon, A. Villa, M.H. Helfrich, Osteopetrosis: genetics, treatment and new insights into osteoclast function, Nat. Rev. Endocrinol. 9 (2013) 522–536.
[2] M.P. Whyte, Carbonic anhydrase II deficiency, Clin. Orthop. Relat. Res. 294 (1993) 52–63.
[3] S. Dupuis-Girod, N. Corradini, S. Hadj-Rabia, J.C. Fournet, L. Faivre, F. Le Deist, P. Durand, R. Döffinger, A. Smahi, A. Israel, G. Courtois, N. Brousse, S. Blanche, A. Munnich, A. Fischer, J.L. Casanova, C. Bodemer, Osteopetrosis, lymphedema, anhidrotic ectodermal dysplasia, and immunodeficiency in a boy and incontinentia pigmenti in his mother, Pediatrics 109 (2002), e97. .
[4] P.M. Campeau, J.T. Lu, G. Sule, M.M. Jiang, Y. Bae, S. Madan, W. Högler, N.J. Shaw, S. Mumm, R.A. Gibbs, M.P. Whyte, B.H. Lee, Whole-exome sequencing identifies mutations in the nucleoside transporter gene SLC29A3 in dysosteosclerosis, a form of osteopetrosis, Hum. Mol. Genet. 21 (2012) 4904–4909.
[5] N.L. Malinin, L. Zhang, J. Choi, A. Ciocea, O. Razorenova, Y.Q. Ma, E.A. Podrez, M. Tosi, D.P. Lennon, A.I. Caplan, S.B. Shurin, E.F. Plow, T.V. Byzova, A point mutation in KINDLIN3 ablates activation of three integrin subfamilies in humans, Nat. Med. 15 (2009) 313–318.
[6] A. Pangrazio, A. Frattini, R. Valli, E. Maserati, L. Susani, P. Vezzoni, A. Villa, W. Al-Herz, C. Sobacchi, A homozygous contiguous gene deletion in chromosome 16p13.3 leads to autosomal recessive osteopetrosis in a Jordanian patient, Calcif. Tissue Int. 91 (2012) 250–254.
[7] Z. Stark, A. Pangrazio, G. McGillivray, A.M. Fink, Association of severe autosomal recessive osteopetrosis and structural brain abnormalities: a case report and review of the literature, Eur. J. Med. Genet. 56 (2013) 36–38.
[8] S. Migliaccio, M. Luciani, A. Taranta, G. De Rossi, S. Minisola, M. El Hachem, C. Bosman, L. De Felice, R. Boldrini, A. Corsi, P. Bianco, A. Teti, Association of intermediate osteopetrosis with poikiloderma, J. Bone Miner. Res. 14 (1999) 834–836.
[9] S. Almarzooqi, S. Reed, B. Fung, D.R. Boué, V. Prasad, D. Pietryga, Infantile osteopetrosis and juvenile xanthogranuloma presenting together in a newborn: a case report and literature review, Pediatr. Dev. Pathol. 14 (2011) 307–312.
[10] R. Verma, M. Jana, A.S. Bhalla, A. Kumar, R. Kumar, Diagnosis of osteopetrosis in bilateral congenital aural atresia: Turning point in treatment strategy, World J. Clin. Pediatr. 5 (2016) 228–233.
[11] J.E. Posey, T. Harel, P. Liu, J.A. Rosenfeld, R.A. James, Z.H. Coban Akdemir, M. Walkiewicz, W. Bi, R. Xiao, Y. Ding, F. Xia, A.L. Beaudet, D.M. Muzny, R.A. Gibbs, E. Boerwinkle, C.M. Eng, V. Reid Sutton, C.A. Shaw, S.E. Plon, Y. Yang, J.R. Lupski, Resolution of disease phenotypes resulting from multilocus genomic variation, N. Engl. J. Med. (2016).
[12] C. Sobacchi, A. Frattini, P. Orchard, O. Porras, I. Tezcan, M. Andolina, R. Babul-Hirji, I. Baric, N. Canham, D. Chitayat, S. Dupuis-Girod, I. Ellis, A. Etzioni, A. Fasth, A. Fisher, B. Gerritsen, V. Gulino, E. Horwitz, V. Klamroth, E. Lanino, M. Mirolo, A. Musio, G. Matthijs, S. Nonomaya, L.D. Notarangelo, H.D. Ochs, A. Superti Furga, J. Valiaho, J.L. van Hove, M. Vihinen, D. Vujic, P. Vezzoni, A. Villa, The mutational spectrum of human malignant autosomal recessive osteopetrosis, Hum. Mol. Genet. 10 (2001) 1767–1773.
[13] A. Frattini, A. Pangrazio, L. Susani, C. Sobacchi, M. Mirolo, M. Abinun, M. Andolina, A. Flanagan, E.M. Horwitz, E. Mihci, L.D. Notarangelo, U. Ramenghi, A. Teti, J. Van Hove, D. Vujic, T. Young, A. Albertini, P.J. Orchard, P. Vezzoni, A. Villa, Chloride channel ClCN7 mutations are responsible for severe recessive, dominant, and intermediate osteopetrosis, J. Bone Miner. Res. 18 (2003) 1740–1747.
[14] A. Pangrazio, P.L. Poliani, A. Megarbane, G. Lefranc, E. Lanino, M. Di Rocco, F. Rucci, F. Lucchini, M. Ravanini, F. Facchetti, M. Abinun, P. Vezzoni, A. Villa, A. Frattini, Mutations in OSTM1 (grey lethal) define a particularly severe form of autosomal recessive osteopetrosis with neural involvement, J. Bone Miner. Res. 21 (2006) 1098–1105.

[15] A. Pangrazio, A. Fasth, A. Sbardellati, P.J. Orchard, K.A. Kasow, J. Raza, C. Albayrak, D. Albayrak, O.M. Vanakker, B. De Moerloose, A. Vellodi, L.D. Notarangelo, C. Schlack, G. Strauss, J.S. Kühl, E. Caldana, N. Lo Iacono, L. Susani, U. Kornak, A. Schulz, P. Vezzoni, A. Villa, C. Sobacchi, SNX10 mutations define a subgroup of human autosomal recessive osteopetrosis with variable clinical severity, J. Bone Miner. Res. 28 (2013) 1041–1049.
[16] A. Pangrazio, A. Puddu, M. Oppo, M. Valentini, L. Zammataro, A. Vellodi, B. Gener, I. Llano-Rivas, J. Raza, I. Atta, P. Vezzoni, A. Superti-Furga, A. Villa, C. Sobacchi, Exome sequencing identifies CTSK mutations in patients originally diagnosed as intermediate osteopetrosis, Bone 59 (2014) 122–126.
[17] E. Palagano, H.C. Blair, A. Pangrazio, I. Tourkova, D. Strina, A. Angius, G. Cuccuru, M. Oppo, P. Uva, W. Van Hul, E. Boudin, A. Superti-Furga, F. Faletra, A. Nocerino, M.C. Ferrari, G. Grappiolo, M. Monari, A. Montanelli, P. Vezzoni, A. Villa, C. Sobacchi, Buried in the middle but guilty: Intronic mutations in the TCIRG1 Gene cause human autosomal recessive osteopetrosis, J. Bone Miner. Res. 30 (2015) 1814–1821.
[18] M. Abinun, T. Newson, P. Rowe, T.J. Flood, A.J. Cant, Importance of neurological assessment before bone marrow transplantation for osteopetrosis, Arch. Dis. Child. 80 (1999) 273–274.
[19] A. Sinha, M. Abinun, A.R. Gennery, D. Barge, M. Slatter, T. Cheetham, Graves' immune reconstitution inflammatory syndrome in childhood, Thyroid 23 (2013) 1010–1014.
[20] E. Rognoni, R. Ruppert, R. Fässler, The kindlin family: functions, signaling properties and implications for human disease, J. Cell Sci. 129 (2016) 17–27.
[21] S. Schmidt, I. Nakchbandi, R. Ruppert, N. Kawelke, M.W. Hess, K. Pfaller, P. Jurdic, R. Fässler, M. Moser, Kindlin-3-mediated signaling from multiple integrin classes is required for osteoclast-mediated bone resorption, J. Cell Biol. 192 (2011) 883–897.
[22] A. Mory, S.W. Feigelson, N. Yarali, S.S. Kilic, G.I. Bayhan, R. Gershoni-Baruch, Kindlin-3: a new gene involved in the pathogenesis of LAD-III, Blood 112 (2008) 2591.
[23] L. Svensson, K. Howarth, A. McDowall, I. Patzak, R. Evans, S. Ussar, M. Moser, A. Metin, M. Fried, I. Tomlinson, N. Hogg, Leukocyte adhesion deficiency-III is caused by mutations in KINDLIN3 affecting integrin activation, Nat. Med. 15 (2009) 306–312.
[24] T.W. Kuijpers, E. van de Vijver, M.A. Weterman, M. de Boer, A.T. Tool, T.K. van den Berg, M. Moser, M.E. Jakobs, K. Seeger, O. Sanal, S. Unal, M. Cetin, D. Roos, A.J. Verhoeven, F. Baas, LAD-1/variant syndrome is caused by mutations in FERMT3, Blood 113 (2009) 4740–4746.
[25] K. Jurk, A.S. Schulz, B.E. Kehrel, D. Räpple, H. Schulze, D. Möbest, W.W. Friedrich, H. Omran, E. Deak, R. Henschler, J.S. Scheele, B. Zieger, Novel integrin-dependent platelet malfunction in siblings with leukocyte adhesion deficiency-III (LAD-III) caused by a point mutation in FERMT3, Thromb. Haemost. 103 (2010) 1053–1064.
[26] A. McDowall, L. Svensson, P. Stanley, I. Patzak, P. Chakravarty, K. Howarth, H. Sabnis, M. Briones, N. Hogg, Two mutations in the KINDLIN3 gene of a new leukocyte adhesion deficiency III patient reveal distinct effects on leukocyte function in vitro, Blood 115 (2010) 4834–4842.
[27] R. Crazzolara, K. Maurer, H. Schulze, B. Zieger, J. Zustin, A.S. Schulz, A new mutation in the KINDLIN-3 gene ablates integrin-dependent leukocyte, platelet, and osteoclast function in a patient with leukocyte adhesion deficiency-III, Pediatr. Blood Cancer 62 (2015) 1677–1679.
[28] N. Suratannon, P. Yeetong, C. Srichomthong, P. Amarinthnukrowh, P. Chatchatee, D. Sosothikul, P.M. van Hagen, M. van der Burg, M. Wentink, G.J. Driessen, K. Suphapeetiporn, V. Shotelersuk, Adaptive immune defects in a patient with leukocyte adhesion deficiency type III with a novel mutation in FERMT3, Pediatr. Allergy Immunol. 27 (2016) 214–217.